Soils and Rocks
An International Journal of Geotechnical and Geoenvironmental Engineering
www.soilsandrocks.com
ISSN 1980-9743
ISSN-e 2675-5475

The 8th Victor de Mello lecture: role played by viscosity on the undrained behaviour of normally consolidated clays

Ian Schumann Marques Martins[1#]

Lecture

Keywords
Strain-rate effects
Soft clay
Creep
Stress relaxation
Stress-strain-strain-rate relationships

Abstract

Phenomena that do not obey Terzaghi's principle of effective stress (PES) are related to strain rate and time effects. This issue led the author to refer to early articles in soil mechanics, which used to consider the shear resistance of clays as a combination of two components: a frictional and a viscous one. In these articles the viscous component was assigned to the distortion of highly viscous adsorbed water layer in the contact points between grains along the plane where shearing takes place. Assuming the shear resistance of plastic soils comprises frictional and viscous resistance components, a shear stress equation can be added to the PES. It is shown that Mohr's circle of effective stress is the sum of two ellipses: the viscosity and the friction ellipses. The ordinates of the viscosity and the friction ellipses represent the viscous and the frictional components of shear resistance in different planes, respectively. This approach leads to a failure criterion considering strain rate, according to which failure takes place whenever the friction ellipse touches the strength envelope, which is the ϕ'_e sloped straight line passing through the origin, ϕ'_e being the Hvorslev's true angle of friction. By adding such shear stress equation to the PES, a model that explains strain rate and time effects is developed. Predictions of the proposed model are compared to results from tests carried out on San Francisco Bay Mud specimens.

1. Professor Victor de Mello as perceived by the author

Differently from those who have preceded the author towards the honourable task of writing the eighth Victor de Mello Lecture, he belongs to a subsequent generation, the same of his son, his friend Luiz Guilherme de Mello. Our fathers were born in the very year of 1926, with a difference of a month and a half. For this reason, he thinks his way of perceiving Professor Victor F. B. de Mello may be different and more distant from those ways posed by the previous de Mello lecturers. Such a distance should be taken as a measure of the author's respect and admiration since the time he was a student at the Polytechnic School of the Federal University of Rio de Janeiro and trainee at the Geotechnical Laboratory of COPPE/UFRJ at the end of the seventies. The author perceived Professor Victor Froilano Bachmann de Mello as a live legend, as a shining and unreachable sun of knowledge rising from the horizon…

The author has heard about his critical mind several times. In fact, the author has been introduced to his critical way of behaving even before meeting him in person. This happened when the author read the preface of the book *Soil Testing for Engineers* (Lambe, 1951), in which the acknowledgements end with: "*To Dr. Victor F. B. de Mello, a former member of the soil mechanics staff at the Massachusetts Institute of Technology, especial thanks are due for his sharp but constructive criticisms based on a careful study of the manuscript.*" (Lambe, 1951, pp. v-vi).

The practice of criticism is usually taken with reservation among Latins. Many times the Latin spirit takes criticism as a personal attack. Perhaps, for this reason, when practicing criticism, Victor de Mello may often have been misunderstood in the country he chose to live in. The biographical notes posed by Moreira & Décourt (1989) for the *de Mello Volume* suggest that, as regards Victor de Mello, who was born in a family in which education was always taken into high account, the practice of criticism used to be a natural consequence of the act of thinking, with ideas fighting against each other. Criticism as the exercise of ever trying to improve what is being criticized. Criticism in the very analytical meaning of the word. Criticism addressed to opinions and ideas, never to persons.

Perhaps this gift to criticism has even more been developed in the soul of the young man who, having left Goa, an old Portuguese province on the west coast of India, had to triumph by using merit as the main weapon within the competitive environment of the Massachusetts Institute of Technology (MIT), as Christian & Baecher (2015) suggest. If he had not imposed himself, neither would he have become

#Corresponding author. E-mail address: ian@coc.ufrj.br
[1]Universidade Federal do Rio de Janeiro, Departamento de Engenharia Civil, Rio de Janeiro, RJ, Brasil.

Submitted on May 18, 2023; Final Acceptance on May 18, 2023; Discussion open until November 30, 2023.
https://doi.org/10.28927/SR.2023.006123

the eventual substitute of Professor Taylor [de Mello, L.G. (2021). Personal communication.] nor would he have deserved the comment made by Moreira & Décourt (1989) in his biographical notes: "*Back at MIT his academic past had left one mark. It has been heard that Taylor often mentioned him as the best student to have gone through the department, and that for a couple of decades the challenge to the new staff was to hear from the older faculty "how de Mello would have handled the problem*" (Moreira & Décourt, 1989, p. xiii). The Italians would say: "*se non è vero è bene trovato*", because vestiges of this admiration appear at Taylor's (1955) acknowledgements in his ultimate report: "*Review of Research on Shearing Strength of Clay*". Part of the acknowledgements says: "*Especially valuable contributions were made by V.F.B. de Mello and R.H.Clough.*" (Taylor, 1955, p. 2). This happened about 6 years after Victor de Mello had left MIT on his way to Brazil, showing that Victor and Don Taylor were still connected.

The author, who was also educated within an environment in which the practice of criticism was always carried out, deeply understood that way of behaving because he apprehended its aims. An illustrative example of Victor de Mello's critical attitude appears in the outline of his potential book (de Mello, 2014), where he presented a list of items which should be reviewed. One of these items is, for instance, the void ratio (e) versus vertical effective stress (σ'_v, log scale) relationship in the one-dimensional compression, which, if represented by a straight line, leads to the mistake of obtaining a void ratio equal to zero (and even negative ones). By the way, the author (Martins, 1983; Martins & Lacerda, 1994) also discussed such subject.

Despite the author had maintained brief contacts with Professor Victor de Mello, usually during conferences and meetings' intervals, he always tried to draw closer to him to listen to the soil mechanics stories he witnessed. These stories, which were always told in a picturesque way and with a special pleasure, were usually "painted" with the colours of his vernacular palette.

Marzionna (2014), a close friend and colleague of his son Luiz Guilherme at the Polytechnic School of the University of São Paulo, managed, in the author's opinion, to capture by the adjectives *passionate*, *unresigned* and *perfectionist* the essence of the man who, even being aware that many things inside his soul were utopian, knew that dreams, although unreachable, have just one purpose in life: to keep everyone walking forward. Nevertheless, according to Burland (2008) his way of saying that was more poetical: "*Choose your love and love your choice*" (Burland, 2008, p. 116). That was what he did throughout his life.

2. Philosophical spirit of this lecture

As regards science, the soul of things is in the fundamentals. The birth of any science is in man's creative ability to observe and imagine how things work. To make science means to explain how things operate in our universe and to establish links between causes and effects, thus following the so-called scientific method. Several texts have been written about the scientific method, but none of them teaches neither how to observe nor how to proceed in order to make ideas spring out concerning a given phenomenon. Such ideas are "creation blows" and nobody knows where they come from … they are the "soul of science".

Costa (2005) quotes the following passage from Lobo Carneiro's study about Galileu's investigation method: "*his scientific investigation method consists in a suitable combination of experiment with mathematics, a deductive logical tool. Considering some experimental facts, a first hypothesis or theory is built in order to interpret them. Certain conclusions are deductively drawn from that theory; then the validity of those conclusions is submitted to experiment, which the last word always correspond to. The hypothesis should be replaced or improved if the tests do not corroborate it. The final verdict is based on the truth criterion, which is always given by the experimental results.*" (Costa, 2005, p. 139).

Philosophically speaking, the first step of that method consists in something that cannot be taught: in the observation of a phenomenon and of ideas concerning why and how that phenomenon occurs. (Where do the ideas come from and how do they spring into our thoughts?) That is a mystery, which is in the birth of all sciences. The idea becomes a working hypothesis regardless of how it has appeared. By means of sequential reasoning or deductive logic, that working hypothesis leads to forecasts regarding the studied phenomenon. If forecasts are confirmed by means of tests whose results are repeated, then the hypothesis becomes a principle, a postulate, an axiom or a law. So to speak, theories that allow predicting phenomena concerning that science are developed based on those laws. Therefore, every science is supported by a principle or a set of principles. The word *principle* is used because it means the beginning of things. As regards soil mechanics, it is not different; it is built upon the Principle of Effective Stress (Terzaghi, 1936).

Being a postulate, a principle cannot be demonstrated. After being accepted as a truth, it is strengthened every time its validity is checked by an experimental result. However, despite a principle may many times have its validity confirmed, the repeatability of experimental results indicating the principle's validity does not turn such repeatability into proof. On the contrary, just one example that does not follow a principle (called a counterexample) is enough to show the validity of that principle is restricted.

Irrespective of a principle having a chance of being of restricted validity (a common thing in science), "to make science" follows no other path than that of the idea that evolves into a working hypothesis, which, after confirming experimental results, reaches the status of a principle.

Understanding, examining, reexamining and pondering about what a principle establishes is also a role of science. For this reason, it is necessary to deeply understand the statements of the established principles to correctly apply them but also to adequately check their validity.

If the process of managing to have an idea cannot be taught, perhaps to exercise thinking may be a way of opening the doors of mind to let the ideas come in. [Saramago, R.P. (2021). Personal communication.] reminded that Lobo Carneiro, the creator of the "*Brazilian Test*" (used to measure tensile strength of concrete), of whom the author is also proud of having been a pupil, used to say that, before writing any mathematical equation to describe a phenomenon, "*it is necessary to conceive a mental model explaining how and why the phenomenon occurs, no matter how rudimentary the model can be*". Another important task is to identify the variables on which the studied phenomenon depends and to identify any other already known phenomenon with which an analogy may be established, a parallel may be drawn. We must think about the subject and let ideas flow. [Santa Maria, P.E.L.(2000). Personal communication.] posed to the author the following thought about the matter: "*... so that ideas may arise from our minds, time is necessary to think about them, to appraise them...and thus brain must be "idle" and free from daily tasks, otherwise ideas shall take another way...*".

In these modern times, when lack of time predominates, the profusion of published papers leads to the reflection that much more time has been spent in writing rather than in thinking about things that would be worth writing. In short: producing papers has become more important than producing knowledge. One of the reasons for that can be found in a statement made by Lambe (1981) when he referred to one aspect of the geotechnical engineering history of MIT: "*One outstanding paper can contribute far more than five mediocre papers; unfortunately five mediocre papers can carry more weight in the [university] promotion process than one outstanding paper.*" (Lambe, 1981, p. 56).

Similarly, de Mello's thought "*We professionals beg less rapid novelties, more renewed reviewing of what is already there*" also seems to express his concern about the rapid and abundant way by which most new papers have been written, without taking into consideration a deeper analysis of the subjects. Since Taylor was the sole soil mechanics professor at MIT from the mid thirties up to 1945 (Christian & Baecher, 2015), it is not difficult to imagine how much de Mello and Lambe, both Taylor's pupils at that period, have been influenced by his careful way of thinking, rethinking and understanding the phenomena, mainly as regards the fundamental concepts. Christian & Baecher (2015) realized that part of the cause for the bad treatment dispensed to Taylor by the group led by Terzaghi was related to Taylor's way of being. The following quotation illustrates this point of view: "*Neither MIT nor his Professional colleagues treated Taylor well. The reasons are hard to grasp at this remove, but part of the problem seems to be that he often worked on problems that were supposed to have already been solved and he discovered previously unappreciated complexities. He was a careful and thorough experimentalist, a strength that lay behind many of his successes. He had actually looked at the data and understood mechanics.*" (Christian & Baecher, 2015, p. 16).

The author heard from Professor Victor F. B. de Mello that "*Fundamentals of Soil Mechanics*" could be considered one of the five major books ever written about soil mechanics. The author also shares this opinion. Christian & Baecher (2015) still went further and added: "*Fundamentals of Soil Mechanics remains today a seminal text on soil mechanics and influenced generations of geotechnical engineers. In many ways, it is as contemporary as texts written fifty years later, and it may be as influential to the modern field of soil Mechanics as the books of Terzaghi. The presentation is clear and reflects careful thought.*".

Again, the author not only agrees with the above mentioned comments but also intends to show the ideas presented herein came from Terzaghi (1936) and Terzaghi & Frölich (1936). Those ideas grew up with the special care Taylor (1942, 1948) used to carry out research: observing phenomena, creating a mechanism to explain them, translating them into a mathematical language, solving the equations assumed as representative of the phenomena and comparing their results to the experimental data obtained. Just the same path followed by Galileu.

As the name suggests, "*Fundamentals of Soil Mechanics*" was written with a focus on fundamentals. The author learned from Carneiro & Battista (1975) and studying Taylor (1948) that the soul of science is in the fundamentals. This lecture also concerns fundamentals and was written inspired by de Mello's spirit of thought: "*We professionals beg less rapid novelties, more renewed reviewing of what is already there*" (Jamiolkowski, 2012, p. 117) (or pursuant to the author's perception). That is why the number of references is not so large. After all, the task of reviewing already settled issues in a renewed way requires deeper and more intensive work rather than extensive. That is what the author tried to do.

3. The principle of effective stress (PES)

3.1 PES statement and its fundamental equation

Very usually, the PES is only presented by means of its fundamental equation. However, as the PES has a status of law, besides its fundamental equation, it has a statement that is as important as its equation. Instead of presenting the PES statement just as it was presented by Terzaghi (1936), the PES will be presented split up into two parts, as Atkinson & Bransby (1978) did. This statement "version" uses a more up-to-date terminology and makes the PES statement easier to be understood.

The first part of the PES statement defines the effective stress:

> *The stresses in any point of a section through a mass of soil can be computed from the total principal stresses* σ_1,σ_2 *and* σ_3 *which act at this point. If the voids of the soil*

> *are filled with water under a stress u, the total principal stresses consist of two parts. One part u acts in the water and in the solid in every direction with equal intensity. It is called the neutral stress (or the pore pressure). The balance* $\sigma'_1 = \sigma_1 - u$, $\sigma'_2 = \sigma_2 - u$ *and* $\sigma'_3 = \sigma_3 - u$ *represents an excess over the neutral stress u and it has its seat exclusively in the solid phase of the soil. This fraction of the total principal stress will be called the effective principal stress*. (Atkinson & Bransby, 1978, p. 21).

Hence, the fundamental effective stress equation is given by Equation 1.

$$\sigma' = \sigma - u \tag{1}$$

The second part of the PES statement gives the role played by effective stresses on the behaviour of soils:

> *All measurable effects of a change of stress, such as compression, distortion and a change of shearing resistance, are exclusively due to changes in the effective stress*es. (Atkinson & Bransby, 1978, p. 21).

3.2 Role played by effective stresses on the behaviour of soils

Considering the way the PES was stated, the second part only assures that volume change, distortion and a change of shearing resistance are effects caused by a change in the effective stress state. Nevertheless, rigorously speaking, according to the way it was stated, the second part of the PES does not ensure that changes in the effective stress state necessarily cause volume variation, distortion or change of shearing resistance. However, that is the way how soil mechanics interprets and uses the PES. Thus, as far as volume change and distortion are concerned, the second part of the PES might be summarized, without loss of its essence, in the following bidirectional mathematical sentence:

change in effective stress ↔ volume change or distortion

The above mathematical sentence is then interpreted as follows

→ the "going"

Whenever there is a change in the state of effective stress, there will be either a change of volume or distortion (or both).

The connective *or* in the right side of the PES second part sentence makes the sentence true when at least one of the two statements (volume change *or* distortion) is true and false only when both are false.

← the "converse"

Whenever there is a change of volume or distortion (it is enough that one of them occurs) or both, the change(s) was (were) caused by a change in the state of effective stress.

To illustrate the PES meaning according to classical soil mechanics, Atkinson & Bransby (1978) state the three following corollaries:

> *Corollary 1: The engineering behaviour of two soils with the same structure and mineralogy will be the same if they have the same effective stress.*
>
> *Corollary 2: If a soil is loaded or unloaded without any change of volume and without any distortion there will be no change of effective stress.*
>
> *Corollary 3: Soil will expand in volume (and weaken) or compress (and strengthen) if the pore pressure alone is raised or lowered*. (Atkinson & Bransby, 1978, pp. 21-24).

The above-mentioned corollaries are illustrations of how the PES is interpreted and used in classical soil mechanics. Nevertheless, it is possible to present counterexamples which show that these corollaries have no general validity.

As regards corollary 1, one knows that two specimens of the same soil subjected to $\overline{\text{CIU}}$ (isotropically consolidated, undrained) triaxial tests starting from the same state of effective stress, but sheared with different axial strain rates $\left(\dot{\varepsilon}_a = d\varepsilon_a / dt\right)$, show different behaviour. This effect was identified a long time ago [see, for instance, Taylor (1948)]. Such effect is illustrated in Figure 1 by $\overline{\text{CIU}}$ test results carried out by Lacerda (1976) on San Francisco Bay Mud samples.

It is possible to present counterexamples which show that the second corollary also has no general validity. In this case, it is enough to observe what happens during an undrained stress relaxation test. As far as this kind of test is concerned, the procedure is almost the same followed during a conventional $\overline{\text{CIU}}$ triaxial test. The specimen is subjected to a constant axial strain rate $\left(\dot{\varepsilon}_a\right)$ and led up to a determined deviator stress without necessarily being led to failure. Then, at a given axial strain, the load frame motor is switched off and the specimen behaviour is observed over time. It is the so-called stress relaxation test (or stage).

Provided the soil is saturated, there will be no volume change in a $\overline{\text{CIU}}$ triaxial test during the shearing phase but only distortion. When the load frame motor is switched off, there will be no variation of distortion at all. However, even with no change in volume and distortion, there is a substantial variation of the effective stress state (see Figure 2).

Finally, it is possible to present counterexamples showing that the third corollary does not have general validity. Suppose that a soil specimen has been isotropically consolidated to some stress in the normally consolidated range. If after dissipation of the excess pore pressure drainage is closed and the total stress is kept constant, it is observed that pore pressure increases over time (Figure 3). According to corollary 3, if a soil specimen is kept under a constant isotropic state of total stress and pore pressure increases over time, the effective stress decrease should make the specimen to expand, but this cannot occur since drainage is closed.

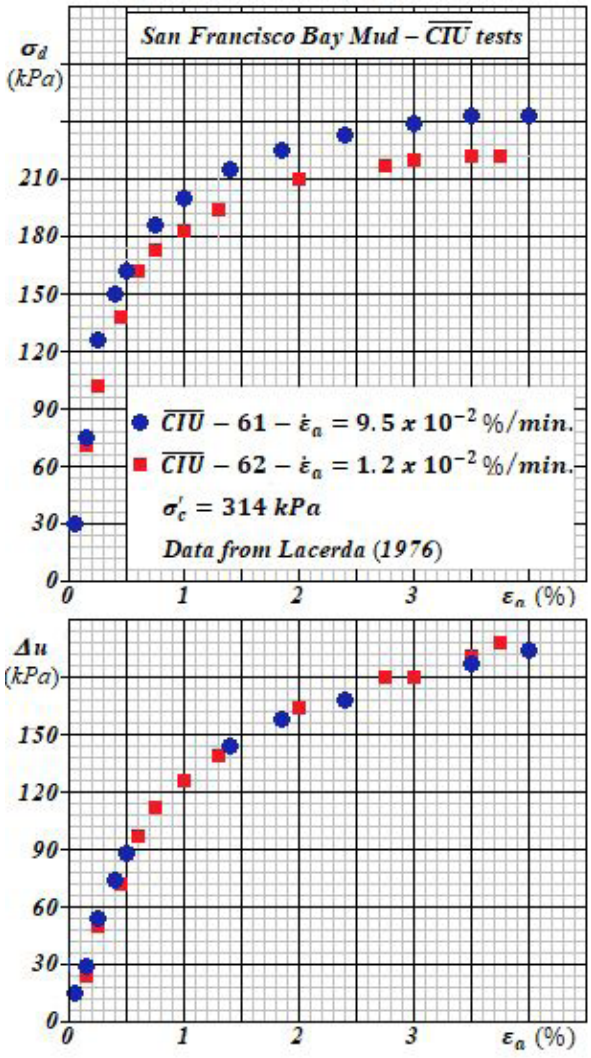

Figure 1. Example of strain rate effect on consolidated-undrained tests [after Lacerda (1976)].

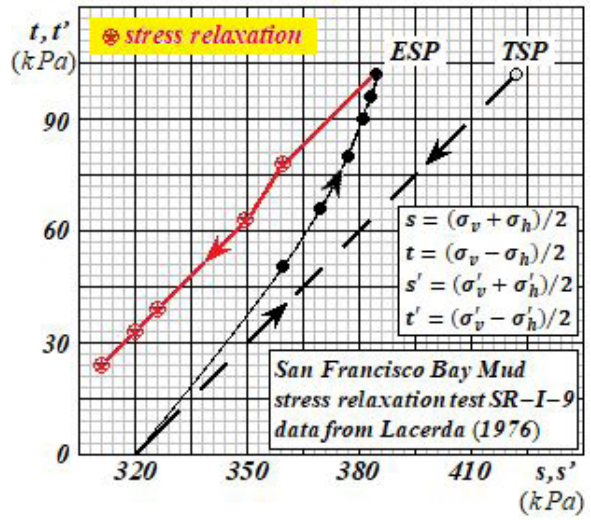

Figure 2. Example of effective stress path (ESP) and total stress path (TSP) during stress relaxation [after Lacerda (1976)].

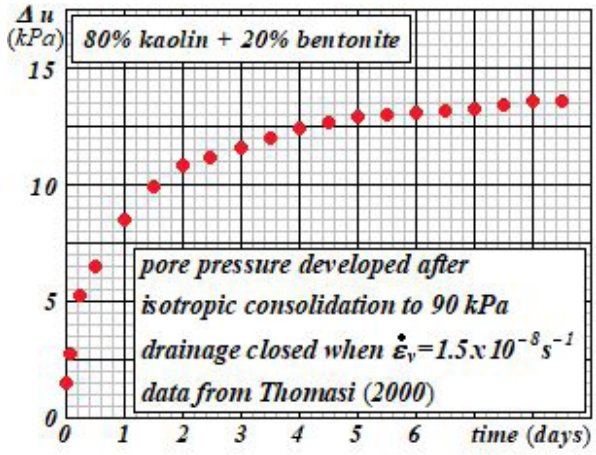

Figure 3. Pore pressure increase after closing drainage after isotropic consolidation (Thomasi, 2000).

The counterexamples relating to the three aforementioned corollaries serve to raise important issues regarding the PES validity. After the advent of critical state soil mechanics, a relevant evolution towards theoretical soil mechanics approach took place, mainly as regards the introduction of plasticity theory concepts. As far as the above-mentioned counterexamples are concerned, time and strain rate effects are present in all of them. Thus, it is natural the attempt to create behavioural models into which concepts that deal with such effects may be introduced. Nevertheless, in view of the theoretical difficulties to deal with phenomena such as creep, stress relaxation and secondary consolidation, the usual approach is to preserve the PES essence and develop tools to tackle one of these specific phenomena, considering each one out of the PES validity domain. A typical example of such an approach is the assumption $C_\alpha / C_c = \text{constant}$ (Mesri & Godlewski, 1977) to handle secondary consolidation.

Computer-aided numerical analyses have made sophisticated stress-strain-strength models feasible. However, those approaches often become so tricky that the feeling of the physical phenomenon sometimes is lost in the midst of the mathematical approach.

As the main purpose of this paper is to study the causes and effects of strain rate on the undrained behaviour of clays, the focus will be on fundamentals. Thus, one will only study here saturated isotropic normally consolidated clays, without cementation among grains, subjected to undrained axi-symmetric stress states, similar to those found in $\overline{\text{CIU}}$ triaxial tests.

This paper follows a different approach from those usually found. The original PES is extended so that phenomena which escape from its validity domain, such as strain rate effects, undrained creep and stress relaxation, may naturally result from the extended PES version. Concepts that allow such PES extension are already presented in classic texts. Many of these concepts can be found in Terzaghi & Frölich (1936),

Terzaghi (1941), Taylor (1942), Taylor (1948), Hvorslev (1960), Bjerrum (1973) and Leroueil et al. (1985), once more illustrating de Mello's thought: "*We professionals beg less rapid novelties, more renewed reviewing of what is already there.*" (Jamiolkowski, 2012, p. 117).

3.3 Strain rate effects on the undrained strength of clays – a brief discussion

The expression *strain rate effects* as used in this article means the effects of speed of shear as defined by Taylor (1948, p. 377). In his own words: "*...all plastic materials exhibit a resistance to shearing strain that varies with the speed at which the shearing strain occurs. The plastic structural resistance to distortion in clays, called herein the plastic resistance, is an example.*".

From now on the acronym $\overline{\text{CIUCL}}$ (consolidated isotropically undrained compression loading) will be used to denote $\overline{\text{CIU}}$ triaxial tests carried out keeping the radial stress σ_r constant and increasing the axial stress σ_a. This is to say that during the undrained shear stage of a $\overline{\text{CIUCL}}$ test, $\sigma_r = \sigma_2 = \sigma_3$ and $\sigma_a = \sigma_1$.

The shear strain rate can be defined by Equation 2

$$\dot{\gamma} = d\gamma / dt = d\left(\varepsilon_a - \varepsilon_r\right) / dt \tag{2}$$

where γ is the distortion $\left(\gamma = \varepsilon_a - \varepsilon_r\right)$ and ε_a and ε_r are respectively the axial and radial strains. During the shear stage of a $\overline{\text{CIUCL}}$ test, $\varepsilon_r = \varepsilon_2 = \varepsilon_3$ and $\varepsilon_a = \varepsilon_1$, causing distortions to occur except for horizontal planes.

When ε_a and $_r$ are small, volumetric strain $\left(\varepsilon_v\right)$ can be written as $\varepsilon_v = \varepsilon_a + 2\varepsilon_r$. During the shear stage of a $\overline{\text{CIUCL}}$ test $\varepsilon_v = 0$ and $\gamma = \varepsilon_a - \varepsilon_r$. Therefore, $\varepsilon_r = -\varepsilon_a / 2$, $\gamma = \frac{3}{2}\varepsilon_a$ and $\dot{\gamma} = \frac{3}{2}\dot{\varepsilon}_a$. Thus, $\dot{\gamma}$ can be written as shown in Equation 3.

$$\dot{\gamma} = d\gamma / dt = d\left(\varepsilon_a - \varepsilon_r\right) / dt = \frac{3}{2}\dot{\varepsilon}_a \tag{3}$$

According to Equation 3, the shear strain rate $\left(\dot{\gamma}\right)$ effects on $\overline{\text{CIUCL}}$ test results can also be studied by observing axial strain rate $\left(\dot{\varepsilon}_a\right)$ effects. One of these effects is the dependency of the undrained shear strength of clays on the axial strain rate $\left(\dot{\varepsilon}_a\right)$.

In this article the undrained shear strength $\left(S_u\right)$ is defined by

$$S_u = \frac{\left(\sigma'_{af} - \sigma'_{rf}\right)}{2} \tag{4}$$

where σ'_{af} and σ'_{rf} are respectively the axial and radial effective stresses at failure (condition indicated by the use of the subscript *f*).

The strain rate effect on the undrained strength of clays may be illustrated by the results of a $\overline{\text{CIUCL}}$ test carried out in a normally consolidated specimen of Sarapuí II Clay [for a detailed description of this clay, see Danziger et al. (2019)]. Such a test has been carried out using an intact sample and lubricated ends technique so that the specimen could be led to a high axial strain, maintaining the cylindrical format. Different axial strain rates $\left(\dot{\varepsilon}_a\right)$ have been imposed to the specimen during the test. Photos of such specimen taken at the end of the test $\left(\varepsilon_a = 17\%\right)$ are shown in Figure 4.

Figure 5 shows the $\left(\sigma'_a - \sigma'_r\right) / 2 \times \varepsilon_a$ plot for the $\overline{\text{CIUCL}}$ test carried out on the specimen shown in Figure 4. Initially, the specimen was sheared with the strain rate $\dot{\varepsilon}_a = 0.02$ % / min.up to $\varepsilon_a \cong 10\%$, when failure occurred with $S_u \cong 68.5$ kPa Then, the strain rate was increased to 0.2 % / min. causing S_u to increase to 76.0 kPa. The strain rate was then reduced to 0.002 % / min. obtaining $S_u \cong 62.0$ kPa . Finally, the strain rate was reduced to 0.0002 % / min., showing $S_u \cong 56.5$ kPa. The deviator stress drops observed in Figure 5 are due to the stress relaxation stages carried out before the strain rate was changed.

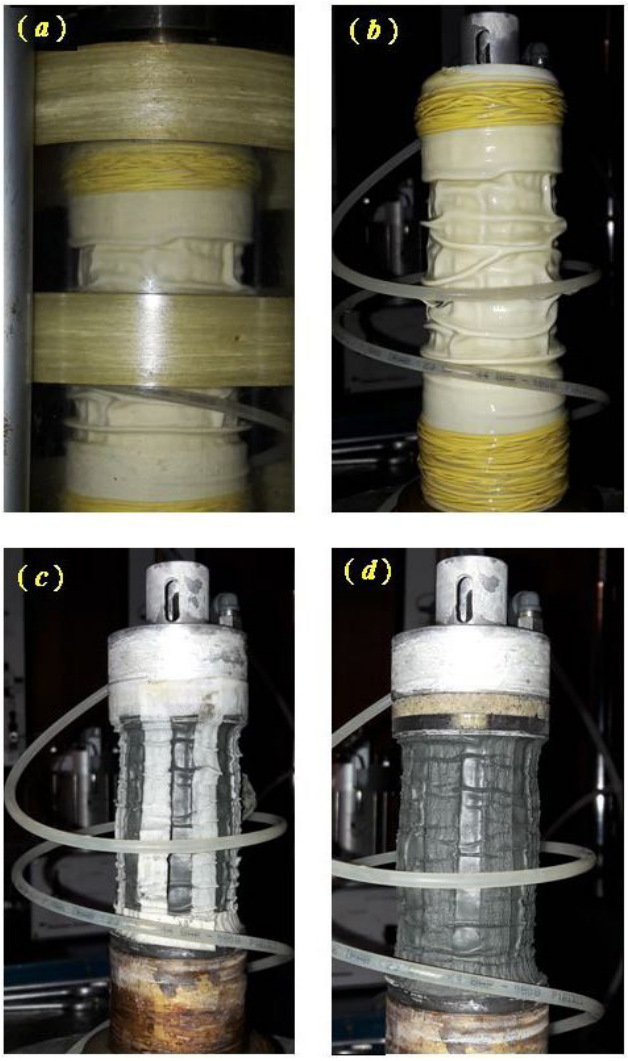

Figure 4. Sarapuí II Clay specimen after a $\overline{\text{CIUCL}}$ test with lubricated ends: (a) Inside the triaxial chamber $\left(\varepsilon_a = 17\%\right)$; (b) Outside the triaxial chamber with the rubber membrane; (c) Without the rubber membrane and with the lateral filter paper; (d) Without the filter paper.

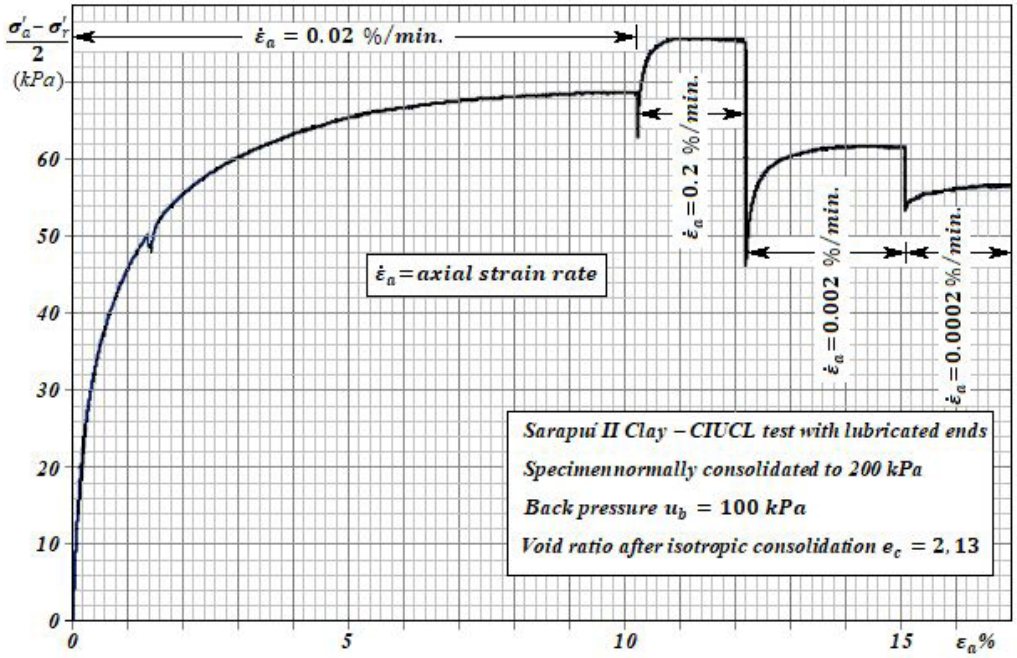

Figure 5. Strain rate effect on the undrained strength of Sarapuí II Clay.

An attempt to estimate the undrained shear strength (S_u) as a function of strain rate is given by Equation 5 [see, for example, Schnaid et al. (2021)].

$$S_u = S_{u,ref}\left[1+\mu log\frac{\dot{\gamma}}{\dot{\gamma}_{ref}}\right] \quad (5)$$

where $\dot{\gamma}_{ref}$ is a reference distortion rate, taken as 1%/hour or 0.017%/min. As in a $\overline{\text{CIUCL}}$ test $\dot{\gamma} = \frac{3}{2}\dot{\varepsilon}_a$ (see Equation 3), Equation 5 can be rewritten as:

$$S_u = S_{u,ref}\left[1+\mu log\frac{\dot{\varepsilon}_a}{\dot{\varepsilon}_{aref}}\right] \quad (6)$$

being $\dot{\varepsilon}_{aref} = \frac{2}{3}\dot{\gamma}_{ref} \cong 0.01\,\%/\,\text{min}$.

Figure 6 presents S_u values as a function of $\dot{\varepsilon}_a$ from the test results shown in Figure 5. Using Equation 6 and $S_{u,ref} = 66.5\,\text{kPa}$, corresponding to $\dot{\varepsilon}_{aref} = 0.01\%/\,\text{min.}$, a $\mu \cong 0.10$ is obtained. The fitted curve is also shown in Figure 6.

Figures similar to Figure 6 were firstly presented by Taylor (1948, p. 378) and afterwards by several authors [as for instance Berre & Bjerrum (1973) and Sheahan et al. (1996)]. Although Equations 5 and 6 provide good fitting curves, one can observe that, in general, the curve $S_u \times \dot{\varepsilon}_a\,(log\ scale)$ shows an upward concavity, thereby suggesting that S_u might have a lower bound as $\dot{\varepsilon}_a$ approaches 0.

The dependence of S_u on $\dot{\varepsilon}_a$ leads to the idea of multiple state boundary surfaces, each one corresponding to a given $\dot{\varepsilon}_a$ value. This would mean that for clayey soils the critical state line (CSL) is dependent on $\dot{\varepsilon}_a$. Therefore, the CSL could not be considered a clay property. This idea was qualitatively presented by Leroueil et al. cited by Jamiolkowski et al. (1991) and is reproduced in Figure 7.

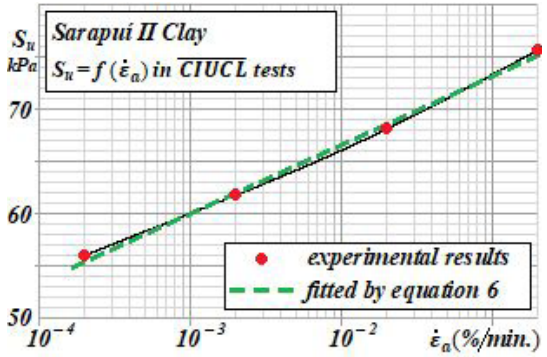

Figure 6. Values of S_u as a function of $\dot{\varepsilon}_a$ for Sarapuí II Clay measured in a $\overline{\text{CIUCL}}$ test.

As concerns the existence of multiple state boundary surfaces, Figure 7 would also indicate the dependence of the virgin oedometric compression line on the axial strain rate $(\dot{\varepsilon}_a)$. This would be in full accordance with the results of Leroueil et al. (1985), showing that in one-dimensional compression there is a unique relationship between effective vertical stress (σ'_v), vertical strain (ε_a) and axial (vertical) strain rate $(\dot{\varepsilon}_a)$. The following natural question would be what is to happen in this case to the coefficient of earth pressure at rest (K_0). This question, raised by Schmertmann (1983) and discussed by several

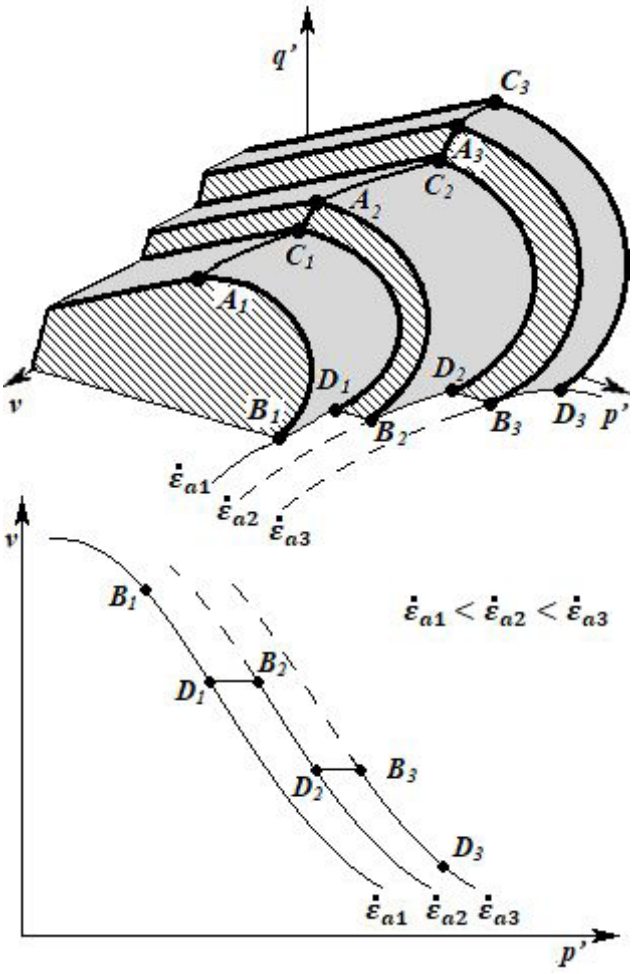

Figure 7. Influence of strain rate $\left(\dot{\varepsilon}_a\right)$ on state boundary surface [adapted from Leroueil et al. cited by Jamiolkowski et al. (1991)].

authors (Lacerda, 1977; Kavazanjian Junior & Mitchell, 1984; Holtz & Jamiolkowski, 1985; Lacerda & Martins, 1985; Leonards, 1985; Kavazanjian Junior & Mitchell, 1985; Mesri & Castro, 1987, 1989), has also remained without a final verdict up to now. Nevertheless, this is a discussion that is beyond the scope of this paper.

According to Bjerrum (1973), who refers to the strain rate effect on the shear strength of clays as "effect of time" (the shorter the time to failure, the greater the strain rate), the referred effect aroused interest from Terzaghi, who discussed it in deep detail in a paper from 1931. According to Bjerrum (1973), the mentioned paper would led Hvorslev to include in his test program the "effect of time" on shear strength of Little Belt plastic remoulded clay.

Henceforth, instead of using the expression "effect of time", it will be used the expression "strain rate effects" since it is an expression which better translates the mechanics of the phenomenon. According to Bjerrum (1973), who was one of the authors that have most deeply studied strain rate effects on the shear strength of clays, there are many evidences which show that strain rate effects are associated with the cohesive component of shear strength, as defined by Hvorslev (1960). Notwithstanding, as discussed by Schofield (1999, 2001) and assumed in critical state soil mechanics, soils do not possess cohesion in the sense used by Coulomb, or rather, they do not resist to effective tensile stresses. How can this impasse be solved? After all, what is cohesion? Do soils have or do not have cohesion? That is what will be discussed in the next section.

4. What is cohesion?

4.1 On the true (Coulomb) cohesion and how the materials fail

> *When I use a word, Humpty Dumpty said in a rather scornful tone, it means just what I choose it to mean – neither more nor less. The question is, said Alice, whether you can make words mean so many different things* (*Lewis Carroll, Through The Looking Glass*).

This seems to be the case of the word cohesion, which in soil mechanics has assumed different meanings, thereby bringing about a lot of confusion [see, for instance, Schofield (1999)]. In order to discuss this subject, it will be necessary to make a brief review of the Mohr failure criterion.

Mohr's failure criterion, for a given material, can be stated as follows: there is a shear stress expressed as a function f of the normal stress σ with the following property: if a couple (σ, τ) which satisfies the function $\tau = f(\sigma)$ is acting on a plane passing through a point ***P*** of the material, then there will be failure at that point ***P*** along the referred plane.

One of the functions used to express the failure criterion in rocks and natural materials is the so-called Mohr-Coulomb envelope, gathering Mohr criterion and Coulomb law. The Mohr-Coulomb envelope can be written as:

$$\tau_{ff} = c' + \sigma'_{ff} . tan\phi' \tag{7}$$

where τ_{ff} and σ'_{ff} are respectively the shear stress and the normal effective stress on the failure plane at failure, ϕ' is the *angle of internal friction* and c' is the *cohesion*. Plotting Equation 7, taking into account just the positive values of τ_{ff}, Figure 8 is obtained.

Solid materials such as concrete and rocks have a strength which cannot be assigned to any applied stress state which can be perceived by human eyes. This kind of strength can be described as a consequence of an "*imaginary pressure*", called "*intrinsic pressure*" (Taylor, 1948), denoted by σ_i', which remains from the formation of those materials and which awards a certain tensile strength to those materials. This "*intrinsic pressure*" corresponds to the segment $\overline{O'O_P}$ in Figure 8. This occurs, for example, in the case of an igneous rock that, after being formed by magma cooling, presents

this type of strength. Similar thing happens in the formation of a sedimentary rock, when a cementation agent by means of a process called diagenesis gradually links grains of a sedimentary soil. A similar phenomenon happens as regards concrete, when cement connects the aggregates. Cementation makes such materials present a tensile strength (σ'_t) when subjected to tensile effective stresses. This type of strength can be quantified by segment $\overline{OpC} = \sigma'_i \tan\phi'$, as shown in Figure 8. Such strength is denoted by c' and defined as *true cohesion* or *Coulomb cohesion*.

An alternative way of writing the envelope in Figure 8 would be to introduce the "*intrinsic pressure*", denoted by σ'_i, shifting the origin of the graph in Figure 8 to point ***O'***. Thus,

$$\tau_{ff} = c' + \sigma'_{ff} \tan\phi' = \left(\sigma'_i + \sigma'_{ff}\right) \tan\phi' \quad (8)$$

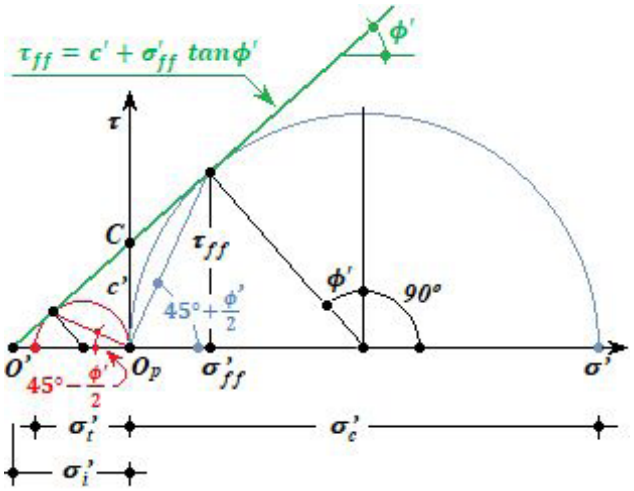

Figure 8. Mohr-Coulomb envelope for soils and rocks.

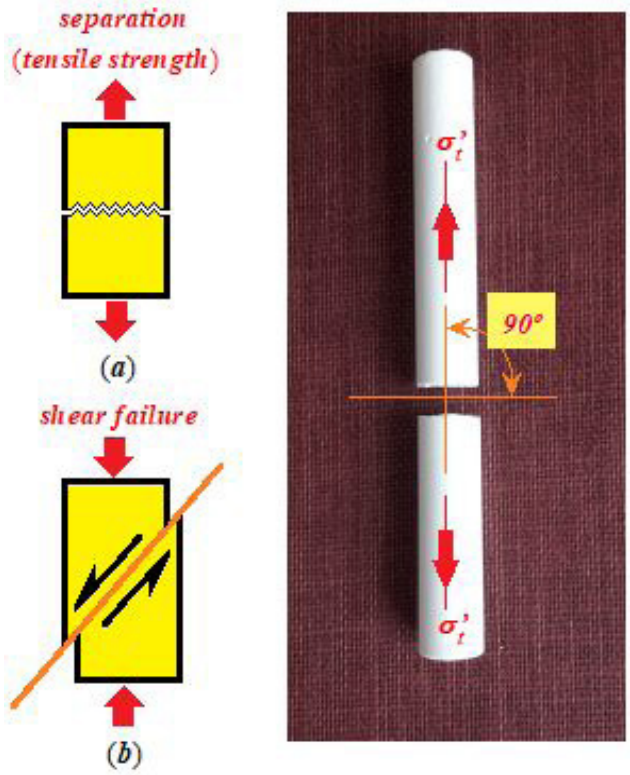

Figure 9. Failure modes: (a) By separation in a tensile test (see the piece of chalk after failure by separation at the right side of Figure 9); (b) By shear during an unconfined compression test.

According to Figure 8, being O_p the pole of Mohr circles at failure under unconfined compression and simple tension tests, the angles of failure planes in compression and in simple tension would be $45° + \phi'/2$ and $45° - \phi'/2$ respectively (see Figure 8). Nevertheless, in a homogeneous and isotropic material subjected to a simple tension test, failure planes occur orthogonally to the tensile stress direction, as shown in Figure 9. It is the failure by separation. So, there are two failure modes: by shear and by separation [Carneiro, F.L.L.B.(2021). Private communication].

As in the separation failure mode the failure plane is orthogonal to the tensile stress direction, the strength envelope must necessarily be a vertical tangent to the Mohr circle at failure under simple tension at its leftmost point, or rather, at the point of abscissae σ'_t, on the left side of the effective stresses axis, as shown in Figure 10a. This kind of strength envelope is illustrated in Figure 10b for a residual soil. In this case, the true cohesion given by *c'* in Figure 10b can be assigned to grain cementation remaining from the mother rock, which have not yet been destroyed by the weathering process in its inexorable march of transforming rocks into soils. A way of evaluating *c'* of a residual soil was used by Rodriguez (2005) carrying out a drained Brazilian Test on a submerged specimen, as shown in Figure 10c.

One can say that weathering, a process by means of which rocks are transformed into residual soils, occurs due to loss of true cohesion (grain cementation) existing in the mother rock. Concerning the inverse process, called diagenesis, in which sedimentary soils suffer a litification process and have their grains cemented, there is a gain in true cohesion. This process is illustrated in Figure 11. The assumption that during weathering/litification the strength envelope suffers a displacement keeping the friction angle ϕ' constant and reducing/increasing the true cohesion is admittedly an oversimplification to better explain the phenomenon.

4.2 Hvorslev's "true cohesion", cohesive soils, plasticity and viscosity

Figure 12 gathers figures from Terzaghi (1938) and Gibson (1953), summing up the results obtained by Hvorslev (1960) as regards a set of drained direct shear tests carried out on saturated remoulded clay specimens.

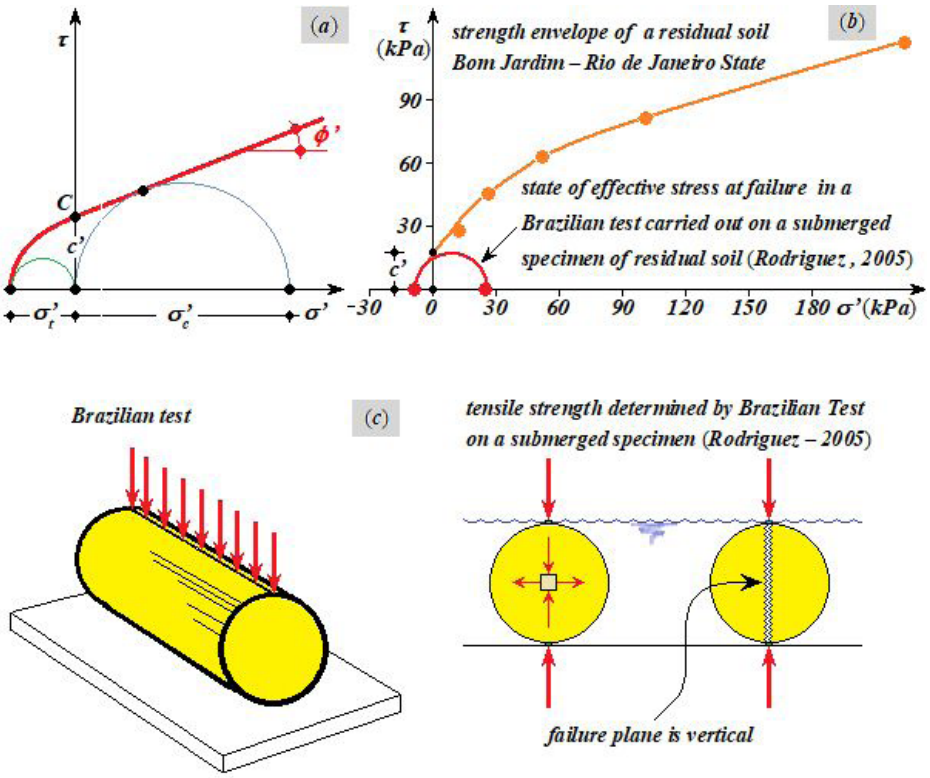

Figura 10. (a) Curved strength envelope showing true cohesion c'; (b) Strength envelope of a residual soil showing true cohesion c' [adapted from Rodriguez (2005)]; (c) Sketch of a Brazilian test carried out on a submerged specimen of residual soil.

In Figure 12, $A_0B_0C_0D_0$ represents the virgin one-dimensional (oedometric) compression line followed by a rebound $D_0E_0F_0G_0H_0I_0$. When the normally consolidated specimens represented by A_0, B_0, C_0 and D_0 are subjected to a drained direct shear test, they decrease in volume during shear and fail respectively with the void ratios of points A, B, C and D. At the lower part of Figure 12, it is shown the strength envelope $OABCD$, corresponding to the normally consolidated condition: a straight line with slope $tan\,\phi'$ passing through the origin. This means that, under the normally consolidated condition, the clay does not have true cohesion in the physical sense given by Coulomb, or rather, it does not have shear strength under effective stress minor than or equal to zero or tensile strength conferred by cementation, as discussed in section 4.1.

When testing the specimens represented by D_0, E_0, F_0, G_0 and H_0, the last four ones being overconsolidated, the void ratios at failure are given by D, E, F, G and H. In the lower part of Figure 12 it is shown the corresponding overconsolidated strength envelope $DEFGH$. The strength envelope $DEFGH$ depends upon two variables: the normal effective stress on the failure plane at failure σ'_{ff} (which is equal to σ'_v in a drained direct shear test) and the void ratio at failure. However, Hvorslev (1937) observed that a straight line strength envelope of equation $\tau_{ff} = c_e(e) + \sigma'_{ff}\,tan\,\phi'_e$ could be drawn provided the specimens had the same void ratio at failure. Hvorslev (1937) also noted that the linear coefficient c_e of these

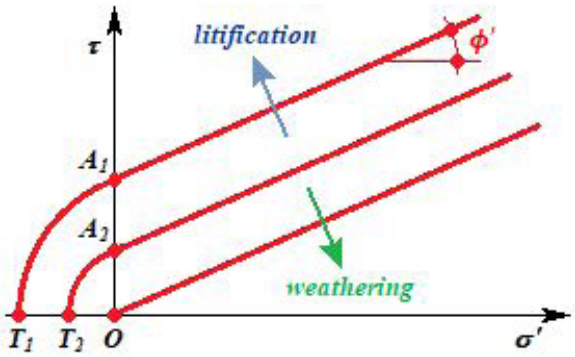

Figure 11. Weathering/litification as a loss/gain in true cohesion of rocks/soils.

straight lines was a function of the void ratio at failure and that the slope $tan\,\phi'_e$ was a constant. One of these straight lines, as shown at the lower part of Figure 12, is the line XHB, whose τ_{ff} axis intercept is $c_e(e_1)$, associated with the void ratio e_1 at failure. All points of straight line XHB have the same void ratio at failure equal to e_1. Another straight line, which represents failure of specimens with void ratios at failure equal to e_2, is the straight line YFC, whose τ_{ff} axis intercept is $OY = c_e(e_2)$. Thus, it is possible to express the shear strength of a clay as:

$$\tau_{ff} = c_e(e) + \sigma'_{ff}\,tan\,\phi'_e \qquad (9)$$

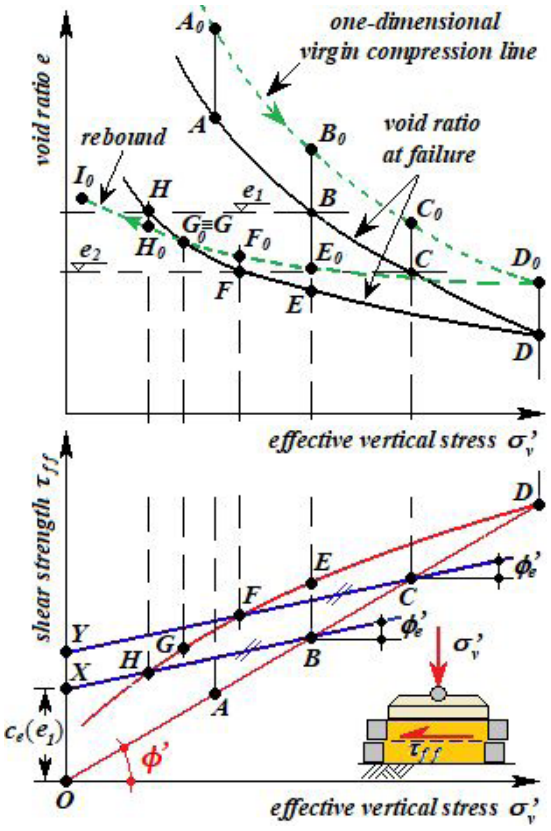

Figure 12. Determination of c_e and ϕ_e' from drained direct shear tests.

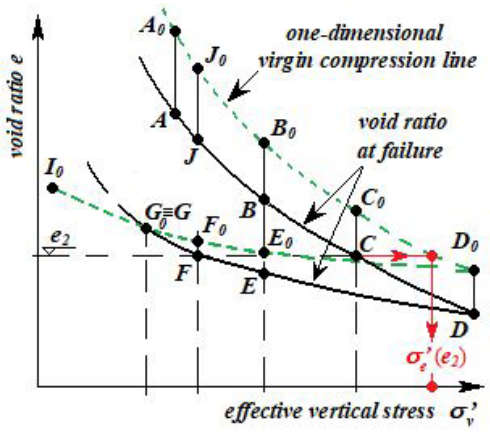

Figure 13. Definition of the equivalent stress σ_e'.

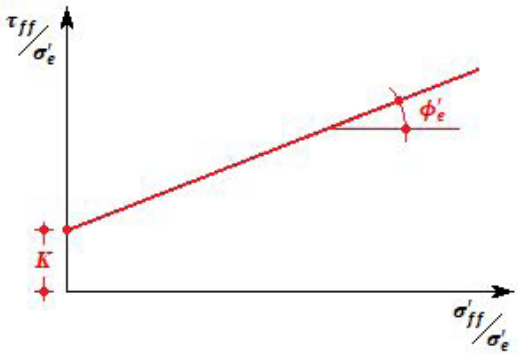

Figure 14. Relationship between normalized shear stress on failure plane at failure $\left(\tau_{ff} / \sigma_e'\right)$ and effective stress on failure plane at failure $\left(\sigma_{ff}' / \sigma_e'\right)$.

In Equation 9, τ_{ff} is the shear stress on the failure plane at failure, is denominated "*effective cohesion*" or "*true cohesion*", a function of the void ratio and soil structure at failure, σ_{ff}' is the effective normal stress on the failure plane at failure, and ϕ_e' is called "*effective angle of internal friction*" or "*true angle of internal friction*".

If the clay is saturated, $e = G \cdot w$, being e the void ratio, G the specific gravity and w the water content. As $G =$ constant for a given soil, there is a one-to-one correspondence between void ratio and water content. Thus, the parameter c_e can be expressed as a function of either the void ratio or the water content, provided that both correspond to the failure condition.

In order that Equation 9 can be dimensionally homogeneous, $c_e\left(e\right)$ must have the physical dimension of a stress. To write $c\ \left(e\right)$ expressing it as a stress [see Terzaghi (1938)], the equivalent stress σ_e' has been used. As for direct shear tests, σ_e' is defined as the effective vertical stress, taken on the one-dimensional (oedometric) virgin compression line (see Figure 13), corresponding to the void ratio at failure.

Tests carried out by Hvorslev (1937) on remoulded saturated clay specimens showed that $c_e\left(e\right)$ was a linear function of the equivalent stress σ_e' corresponding to the void ratio of the specimen at failure. Thus, $c_e\left(e\right)$ can be written as:

$$c_e\left(e\right) = K\,\sigma_e' \tag{10}$$

where K is a non-dimensional constant.

Then, the shear strength of a saturated clay would be given by

$$\tau_{ff} = K.\sigma_e' + \sigma_{ff}'\,tan\phi_e' \tag{11}$$

Dividing both members of Equation 11 by σ_e', Equation 12 is obtained

$$\tau_{ff} / \sigma_e' = K + \left(\sigma_{ff}' / \sigma_e'\right) tan\phi_e' \tag{12}$$

According to Terzaghi (1938), if the results of direct shear tests are plotted in a $\left(\sigma_{ff}' / \sigma_e'\right) \times \left(\tau_{ff} / \sigma_e'\right)$ graph, the straight line shown in Figure 14 will be obtained.

As previously told, Terzaghi (1938) and Hvorslev (1937, 1960) called the product $K\,\sigma_e' = c_e\left(e\right)$ as "*cohesion*", "*true*

cohesion" or "*effective cohesion*" and the product $\sigma'_{ff}\ tan\phi'_e$ as "*effective friction component*". Considering what has been discussed, the following question arises: if the clays studied by Hvorslev were remoulded, there would not be cementation among the grains and, therefore, according to the true cohesion concept established by Coulomb [see Schofield (1999, 2001)], as discussed in section 4.1, none of the three terms (cohesion, true cohesion and effective cohesion) would be adequate in this case. Then, what would be the physical meaning of the term $c_e(e)$ in Equation 9? This is the major discussion posed in this section.

Going ahead on the discussion, all the points on the straight line segment ***HB*** in Figure 12 have the same void ratio e_1 at failure. Therefore, in a $\tau_{ff} \times \sigma'_v$ plot, points ***H*** and ***B*** define a straight line envelope, with slope $tan\phi'_e$, for which the Hvorslev "*true cohesion*" is constant and has magnitude equal to ***OX***. Then, along the envelope ***XHB*** there is only variation of the friction component $\sigma'_v\ tan\phi'_e$. In a similar way, the points on the straight line segment ***FC*** in Figure 12 have void ratio at failure equal to e_2 (with $e_2 < e_1$). Thus, points ***F*** and ***C*** define another strength envelope, with the same slope $tan\phi'_e$, but with a Hvorslev "*true cohesion*" of magnitude ***OY***.

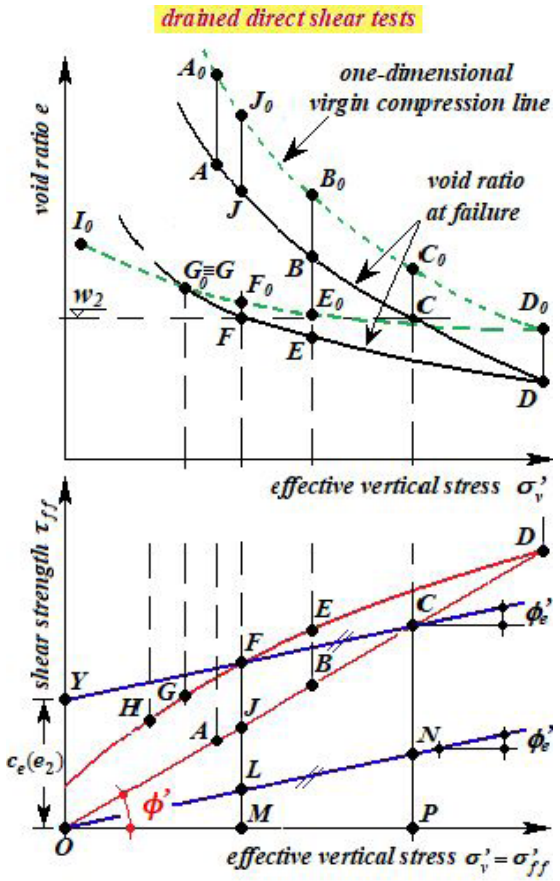

Figure 15. Comparison between Hvorslev (1937) strength envelope for an overconsolidated clay and Mohr-Coulomb strength envelope for the same clay in the normally consolidated condition.

Now, it is worth comparing a strength envelope of the type obtained by Hvorslev (1937) for an overconsolidated clay with the envelope obtained from normally consolidated specimens of the same clay. This is presented in Figure 15.

The straight line ***OAJBCD***, at the lower part of Figure 15, is the strength envelope corresponding to the normally consolidated condition, where the shear stress at failure $\tau_{ff} = \sigma'_{ff}\ tan\phi'$. On the other hand, the same strength envelope can be written as $\tau_{ff} = c_e(e) + \sigma'_{ff}\ tan\phi'_e$. However, in this case, $c_e(e)$ varies along the envelope ***OAJBCD*** because the void ratio also varies. The difference between the ordinates of the straight lines ***OAJBCD*** and ***OLN*** is a linear function of σ'_{ff} (or σ'_v), that is:

$$c_e(e) = \sigma'_{ff}\ tan\phi' - \sigma'_{ff}\ tan\phi'_e = C.\sigma'_{ff} \tag{13}$$

where C is a constant. This means that the shear strength τ_{ff} of a normally consolidated clay can be written as:

$$\tau_{ff} = \sigma'_{ff}\ tan\phi' = c_e(e) + \sigma'_{ff}\ tan\phi'_e = C.\sigma'_{ff} + \sigma'_{ff}\ tan\phi'_e \tag{14}$$

Dividing Equation 14 by σ'_{ff}, Equation 15 is obtained:

$$tan\phi' = C + tan\phi'_e \tag{15}$$

Equation 15 reveals that the friction angle ϕ' of a normally consolidated clay is "contamined" by a portion C. In other words, within the shear strength of a normally consolidated clay, which does not have cohesion in the physical sense used by Coulomb, there is a portion C which is not due to friction. Shearing of a normally consolidated clay produces decrease in volume. Being so, C cannot be assigned to the work done to dilate the specimen since, being normally consolidated, the specimen presents a contractile behaviour. Then, once more, a question is asked: which physical phenomenon does the portion $c_e(e) = C\,\sigma'_{ff}$ come from, since it cannot be attributed neither to cohesion (cementation), as conceived by Coulomb, nor to additional dilating work? After all, what does exist behind the "*effective cohesion*" as inappropriately defined by Hvorslev and Terzaghi? This is the discussion that follows.

What the author believes that exists behind Hvorslev's (1937) "*effective cohesion*" is the "softness" sensation when one rubs between the fingers an amount of clay with a water content between the liquid limit and the plastic limit. It is also the sensation of something "sticky" which is found in clays, because of its *plasticity*. Possibly, owing to such sensation, clays have begun to be improperly called "*cohesive soils*".

According to the author's understanding, the expression "*cohesive soil*" leads to plastic soils. As regards soil mechanics, plastic soils are those soils that present liquid and plastic limits. After all, where does the "sticky" sensation come from when a moist clayey soil is rubbed between the fingers?

A mechanistic picture given by Terzaghi (1941) throws some light on this question.

According to Terzaghi (1941), clay particles are surrounded by an adsorbed water layer. On the clay particles surface, adsorbed water is in the solid state and is strongly adhered to it. As the distance from the particle surface increases, the adsorbed water viscosity decreases. For distances greater than a limiting value, viscous water becomes free water. This means that in a clay the interactions among grains are influenced by the adsorbed water layer that involves them. Since the viscosity of the adsorbed water decreases as the distance from the particle surface increases, it is expected that in a saturated clay the greater the water content (or the void ratio) the smaller the relative displacement resistance between neighbouring particles. In this case, "*true cohesion*" or "*effective cohesion*" to which Hvorslev (1937, 1960) and Terzaghi (1938) refer should be called *viscous resistance*, as explicitly written in a passage by Terzaghi & Frölich (1936). To avoid loss of fidelity, this passage is transcribed below:

> "*Les résultats des expériences entreprises pour trouver la relation entre l'indice des vides et le coefficient de perméabilité des argiles, imposaient déjà il y a quelques années, l'hipothése que chaque particule d'argile est séparée de l'eau interstitielle par une couche séparatrice dont la constitution diffère de celle de l'eau ordinaire. L'épaisseur de cette couche est une fraction d'un micron (1/1000 mm).*
> *A l'intérieur de cette couche séparatrice, la viscosité de l'eau tombe d'une valeur élevée (surface de la particule solide) à sa valeur normale (surface extérieure de la couche séparatrice). Les avis relatifs aux forces attractives qui provoquent la couche séparatrice sont trés partagés.*
> *La* Figure 7 *représente trois coupes à travers deux particules voisines. A l'intérieur de la zone hachurée, la viscosité augmente beaucoup à mesure que l'on s'approche de la surface solide. Par suite de l'application d'une surcharge, les grains sont serrés les uns contre les autres et les couches d'eau séparatrices entourant les corpuscules solides s'embrassent (*fig. 7a*). Comme à pression constante, la viscosité de l'eau comprise dans la zone hachurée n'augmente au cours du temps qu'avec une vitesse décroissante, un rapprochement plus poussée des elements solides devient de plus en plus difficile et il se passe parfois des années et des dizaines d'années avant que les grains ne se touchent (*fig. 7b*). Dans une couche d'argile qui reste pendant des milliers d'années sous l'influence de son poids propre constant, ce contact devient inévitable. La resistance au glissement des particules n'est pas produite uniquement par la résistance de frottement mais aussi par la viscosité des couches séparatrices, entourant la zone de frottement.*
> *Dans cet état, l'argile doit forcément présenter les propriétés élastiques d'un amas des grains dont les pointes de contact sont reliés rigidement les uns aux autres.*
> *Aprés le glissement (*fig. 7c*), les particules sont de nouveau séparées par une couche de fluide visqueux. La mobilité des particules augmente avec l'épaissseur de cette couche; le coefficient de compressibilité, par contre diminue*." (Terzaghi & Frölich, 1936, pp. 18-19).

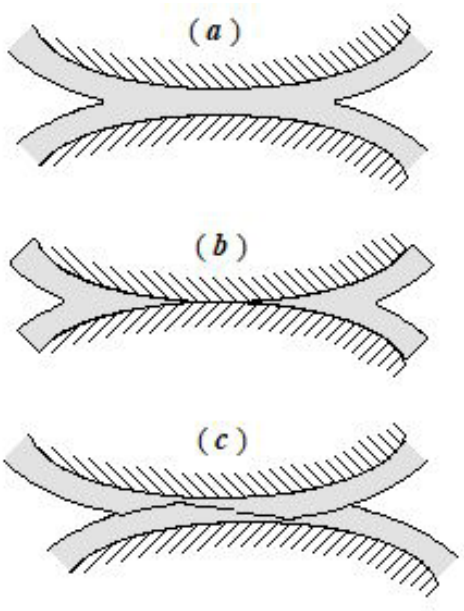

Figure 16. Action of the adsorbed water layer during the relative displacement between two neighbour particles. (a) Clay particles are separated by a thin water layer of high viscosity or (b) Clay particles are in direct touch. (c) Sliding resistance between clay particles is made up of frictionplus viscosity. After relative displacement, clay particles can be separated by a water viscous layer again. [adapted from Terzaghi & Frölich (1936), p.19].

An adaptation of Figures 7a, 7b and 7c as mentioned by Terzaghi & Frölich (1936) in the above quotation is reproduced in this article as Figure 16a, 16b and 16c, as follows:

From the passage transcribed above, it seems clear that the "*cohesion*" to which Terzaghi (1938) refers and the "*effective cohesion*"and "*true cohesion*" referred by Hvorslev (1937, 1960) and Gibson (1953) are all of them from viscous nature. This seems to be Bjerrum's (1973) understanding as well. As a matter of fact, it is the viscous nature of "*cohesion*" which is behind the Bjerrum's (1973) correction factor to be applied to the undrained shear strength $\left(S_u\right)$ measured in the vane test (measured in a vane test is higher because it is obtained with higher shear speed). It is believable that, viewing "*cohesion*" as being of a viscous nature, Bjerrum (1973) proposed the correction factor as a function of the plasticity index. After all, the more plastic the clay the greater its "*cohesion*" (or viscous resistance). Therefore, the higher the plasticity index the higher the influence of viscous resistance on the measured undrained shear strength. What is not appropriate is the use of the expression "*time effect*" to describe the phenomenon. Although Bjerrum (1973) had used the expression "*time effect*", it is clear that, according to his own understanding, the effect in question can be more properly called "*strain rate effect*".

In a re-appraisal of his 1937 work, Hvorslev (1960) highlights three components of shear strength τ_{ff} of a

"*cohesive soil*": the effective friction component $\left(\tau_{\phi}\right)$, the "*effective cohesion*" component $\left(c_e\right)$ and the dilatancy component $\left(\tau_d\right)$. Thus,

$$\tau_{ff} = \tau_{\phi} + c_e + \tau_d \tag{16}$$

In a normally consolidated clay, which has a contractile behaviour, $\tau_d = 0$. The component is a function of the effective stress and is expressed by

$$\tau_{\phi} = \sigma'_{ff} \tan\phi'_e \tag{17}$$

Yet, according to Hvorslev (1960), "*cohesive soils*" (which, due to the confusion created by the term "*cohesive*", the author prefers to call plastic soils) are those which have a strength component c_e. Instead of commenting, it is better to quote how Hvorslev (1960) viewed the c_e component:

> "*Most cohesive soils possess an apparent structural viscosity and their deformations are of visco-elastic character. The corresponding strength component may be called the "viscous component", but factors other than viscosity seem to be involved, and the more inclusive term "rheological component" and the notation* c_v *are proposed. It will be assumed that* c_v *forms a part of the effective cohesion component,* c_e*, because the effective friction component,* τ_{ϕ}*, of a remolded clay does not seem to be affected by the increased rate of deformation after failure, provided the soil structure is not changed;see section 8. However, this assumption is in need of further experimental corroboration. The value of* c_v converges on zero with increasing time or decreasing rate of deformation, whereas c_e at the same time approaches an ultimate value, c_u, which may be called the "ultimate cohesion component." By definition, the following relation exists at any given test duration or rate of deformation $c_e = c_u + c_v$".

Hvorslev (1960) still adds the following passage:

> "*For the purpose of definition and experimental determination of the individual components (individual components of shear strength), the basic assumption is made that the cohesion and rheological components are constant when (1) the void ratio or water content of saturated clays is constant, (2) the rate of deformation or test duration is constant, and (3) there is no significant difference in the geometric structure of the clays during a given test series."* (Hvorslev, 1960, p. 183).

It is worth observing the reference that Hvorslev (1960) made to the strain rate influence. Nevertheless, the approach given to the subject does not explicitly translate the strain rate influence by means of a mathematical expression that quantifies the physical phenomenon. This issue has only become to be coherently approached by Leroueil et al. (1985), showing that, as concerns one-dimensional consolidation, there is a unique relationship among the axial (vertical) strain $\left(\varepsilon_a\right)$, the effective vertical stress $\left(\sigma'_v\right)$ and the axial (vertical) strain rate $\left(\dot{\varepsilon}_a\right)$. However, as far as the author's knowledge

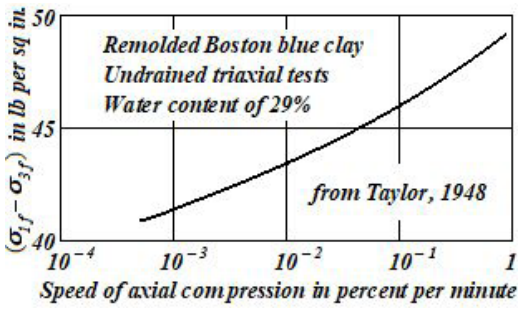

Figure 17. Effect of speed of shear on the compressive strength of clay (Taylor, 1948).

is concerned, Taylor (1948) was the first researcher not only to physically explain the "*effective cohesion*" as being of a viscous origin but also to physically quantify it by means of a mathematical expression.

According to Taylor (1948, pp. 377-378), all viscous materials and all plastic materials exhibit a resistance to shearing strain that varies with the speed at which the shearing strain occurs (see section 3.3). Taylor (1948) called such a kind of resistance in clays as "*plastic resistance*". Figure 17 shows the dependence of the deviator stress at failure $\left(\sigma_{1f} - \sigma_{3f}\right) = \left(\sigma_{af} - \sigma_{rf}\right)$ on the axial strain rate of CIUCL tests. The test results shown in Figure 17 were carried out on remoulded specimens of Boston Blue Clay with the same water content, but subjected to different axial strain rates $\left(\dot{\varepsilon}_a\right)$ (corresponding to different speeds of shear or different shear strain rates).

Also, according to Taylor (1942), experimental results indicated that "*plastic resistance*" under any speed of shear in a given clay with different void ratios is proportional to the effective stress. Assuming that "*plastic resistance*" depends on effective stress and shear strain rate, Taylor (1948) wrote the following equation for the shear strength τ_{ff} of a clay:

$$\tau_{ff} = \left(\sigma'_{ff} + \sigma'_i\right)\left[\tan\phi' + f\left(\partial\varepsilon_s / \partial t\right)\right] \tag{18}$$

where τ_{ff} and σ'_{ff} are, respectively, the shear stress and the effective normal stress on the failure plane at failure, σ'_i is the "*intrinsic pressure*", as defined in section 4.1, ϕ' is the angle of internal friction (to be discussed further again) and $\left(\partial\varepsilon_s / \partial t\right)$ is the shear strain rate on the failure plane. The following passage quoted from Taylor (1948) summarizes the conception of the above-mentioned mechanism. In order to avoid loss of fidelity, it is suitable to quote the referred passage:

> "*The effect of speed of shear on the strength is believed to be caused by the viscous or plastic characteristics of material in the adsorption zones in the vicinity of points of contact or near contact of clay particles. Thus this effect is a colloidal phenomenon, and it is of sufficient importance to justify a detailed discussion.*
> *The following hypothetical explanation of plastic resistance and of time relationships was first presented (*Taylor, 1942*) for one-dimensional compressions, but it may be extended*

to the action of clays in shear. If a drained clay sample is maintained under any given system of constant applied direct and shearing stresses that do not cause failure, it gradually approaches an ultimate shape and an ultimate void ratio at which there is static equilibrium. Ages may be required to reach this state of equilibrium, but when it is reached the applied stresses are equal to static internal resistances and they have values that are free of plastic resistance and all other time effects. During the approach to equilibrium, however, the applied stresses are made up in part of the stresses required to overcome the plastic resistance. The plastic resistance is usually considered to depend mainly on the speed of strain although possibly it depends also on such factors as changes in type or degree of adsorption. As the clay specimen approaches the static case, the strains continuously decrease in speed and the plastic resistance decreases in magnitude; however, the speed becomes almost imperceptibly small when the plastic resistance is still quite large and the strains and the void ratio still have a considerable change to undergo before they reach the static case. Secondary compression, as it occurs in consolidation tests, is a good illustration of this condition. From these concepts it appears that a clay that has reached static equilibrium in nature after the lapse of many centuries and is suddenly subjected to stress increases of relatively small magnitude may be expect immediately to exert a plastic resistance that is equal to the stress increase, and it is possible that the speed of distortion required for the exerting of this amount of plastic resistance may be too small to be noticeable. In such a case the plastic resistance cannot be distinguished from a bond, and the occurrence of bonds of this type is possible both when the shearing stresses are small and when they are relatively large." (Taylor, 1948, pp. 379-380).

From now on the expression "*plastic resistance*" used by Taylor (1948) will be called *viscous resistance*.

5. A possible additional equation for the principle of effective stress (PES)

5.1 The viscosity concept

As the approach of strain rate effects on plastic soils strength is concerned, it is usual to make use of the term viscosity without defining, however, what is understood by soil viscosity. In soil mechanics, the term is generically used without a clear definition (Schnaid et al., 2021). The viscosity concept was introduced by Newton via Newton's law of viscosity: *The tangential stress between neighbouring layers of a fluid in a laminar flow is proportional to the ratio dv / dy with which speed v varies in the transverse direction of flow y* (see Figure 18).

Newton's law of viscosity is written as:

$$\tau = \mu\left(dv/dy\right) \tag{19}$$

which can be written alternatively as:

$$\tau = \mu\frac{dv}{dy} = \mu\lim_{\delta t\to 0}\frac{\delta x}{\delta y.\delta t} = \mu\lim_{\delta t\to 0}\left(\frac{\delta x}{\delta y}\right)/\delta t = \mu\frac{d\gamma}{dt} = \mu\dot{\gamma} \tag{20}$$

The coefficient μ is called *coefficient of viscosity* or simply *viscosity* and $d\gamma/dt = \dot{\gamma}$ is called distortion rate. Every fluid which obeys Equations 19 or 20 is said to be considered a newtonian fluid.

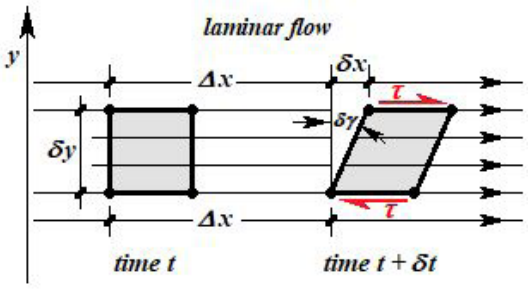

Figure 18. Newton's law of viscosity.

5.2 Shearing of clayey soils – a working hypothesis

The approach presented next is only based on mechanical interactions, which greatly simplify the interaction among clay particles. However, as argued by Bjerrum (1973), in spite of admittedly being an oversimplification, this approach gathers the essential characteristics of the behaviour of plastic soils as far as strain rate effects are concerned.

According to Terzaghi (1941), clay particles are involved by a viscous adsorbed water layer. In the particles surface vicinity, adsorbed water is in a solid state and strongly adhered to grains surface. As the distance from particles surface increases, the adsorbed water viscosity decreases until water becomes free water beyond a certain distance "*d*" (Figure 19). Distance *d* depends on the physico-chemical properties of the minerals of the clay particles and on other substances in the adsorption region.

Also, according to Terzaghi (1941), contacts between grains can occur through solid water (solid to solid contacts) or through viscous water (viscous contacts) and both types of contact transmit effective stresses.

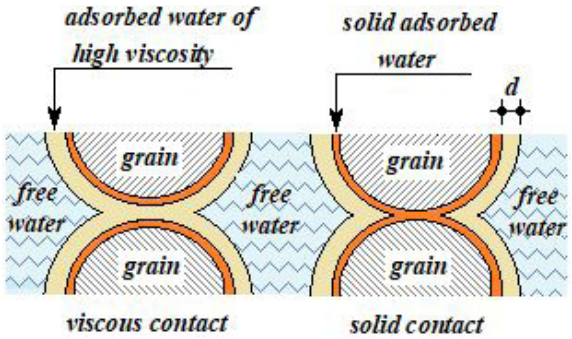

Figure 19. Illustration of adsorbed water and types of contact between clay particles (Terzaghi, 1941).

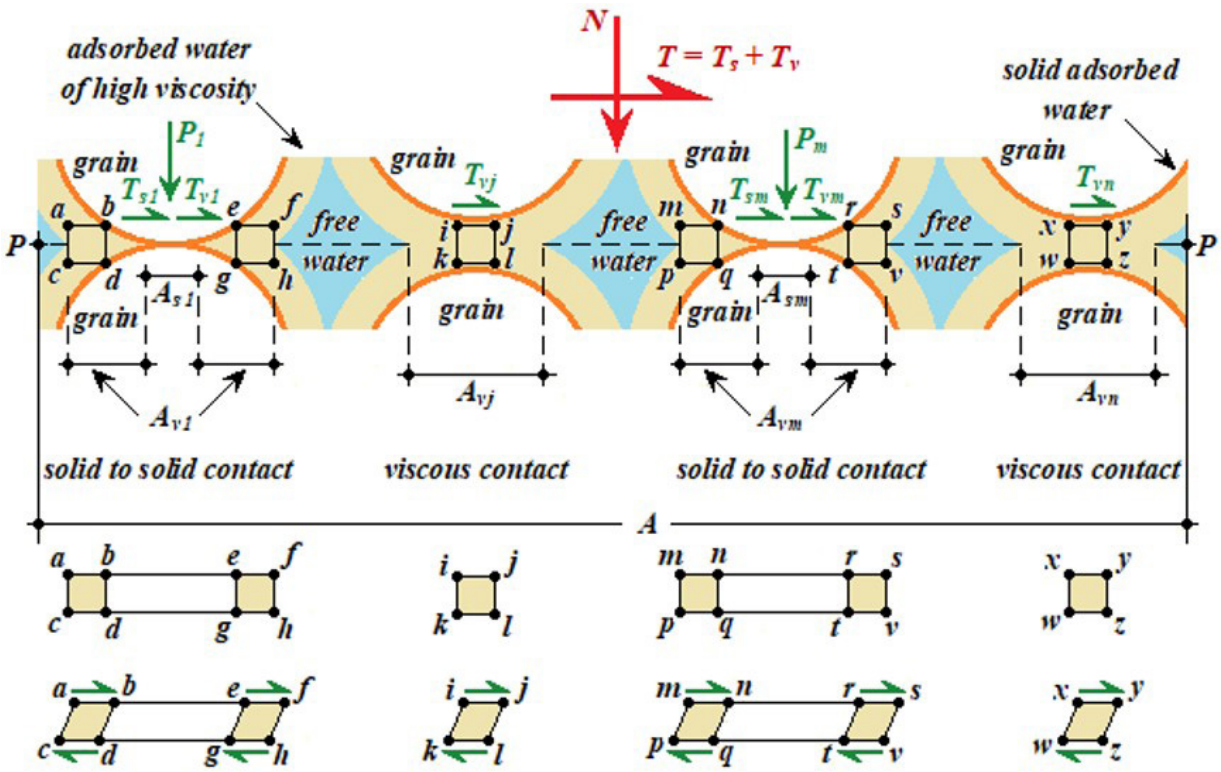

Figure 20. Forces acting on a plane ***P – P*** passing through a plastic soil mass.

Starting from the conception of Terzaghi & Frölich (1936) to explain clay shear strength and assuming some additional hypotheses, Martins (1992) obtained the results whose essence is presented as follows.

Considering an imaginary plane ***P – P*** passing through a plastic soil mass, it will pass by solid to solid and viscous contacts (Figure 20). Consider now a region of area A ($A = A \times 1u \cdot c$, where $1u \cdot c$ is a unitary length in the normal direction to the plane of Figure 20). Also consider that the normal force N and the tangential force T are acting on the area A.

Assuming that only solid contacts can transmit effective normal stresses, the balance of forces in the normal direction of the plane ***P – P*** leads to the PES equation, $\sigma = \sigma - u \cdot$ A more general hypothesis according to which viscous contacts can also transmit effective stresses is being developed but this approach will not be discussed herein.

The tangential force T acting on area A divided by is by definition the shear stress on the area A along plane ***P – P***. Force T can be expressed by the sum of tangential forces, which causes the relative displacement between the particles from the upper side and the lower side of the plane ***P – P*** (see Figure 20). According to the mechanism posed by Terzaghi & Frölich (1936), force T consists in summing up the friction resistance component T_s, which exists in solid contacts, and the viscous resistance component T_v, due to the distortion of the adsorbed water.

Suppose there are m solid to solid contacts within the area A in Figure 20. The friction force T_{si} acts at the solid to solid contact of order i as a local reaction to the applied force T. Therefore, the friction resistance component T_s mobilized as a partial reaction to force T can be written as:

$$T_s = \sum_{i=1}^{m} T_{si} = \sum_{i=1}^{m} \xi_i P_i \tan \phi_i' \tag{21}$$

where ϕ_i' is the friction angle of the solid to solid contact of order i and ξ_i is the degree or percentage of the friction strength mobilized at the solid to solid contact of order i. Thus, Equation 21 provides the mobilized friction resistance component T_s along the plane ***P – P***. It is possible to rewrite Equation 21 defining for each solid to solid contact of order i, within the area A, a coefficient ξ_i such that $\xi_i \tan \phi_i' = \xi_i^* \tan \phi_e'$, being ϕ_e' the Hvorslev's true angle of friction. Thus, Equation 21 can be rewritten as Equation 22:

$$\sum_{i=1}^{m} \xi_i P_i \tan \phi_i' = \sum_{i=1}^{m} \xi_i^* P_i \tan \phi_e' \tag{22}$$

Finally, denoting by $\bar{\xi}$ the average value of all ξ_i^* values taken over area A, one obtains:

$$T_s = \tan \phi_e' \sum_{i=1}^{m} \xi_i^* P_i = \bar{\xi} \tan \phi_e' \sum_{i=1}^{m} P_i \tag{23}$$

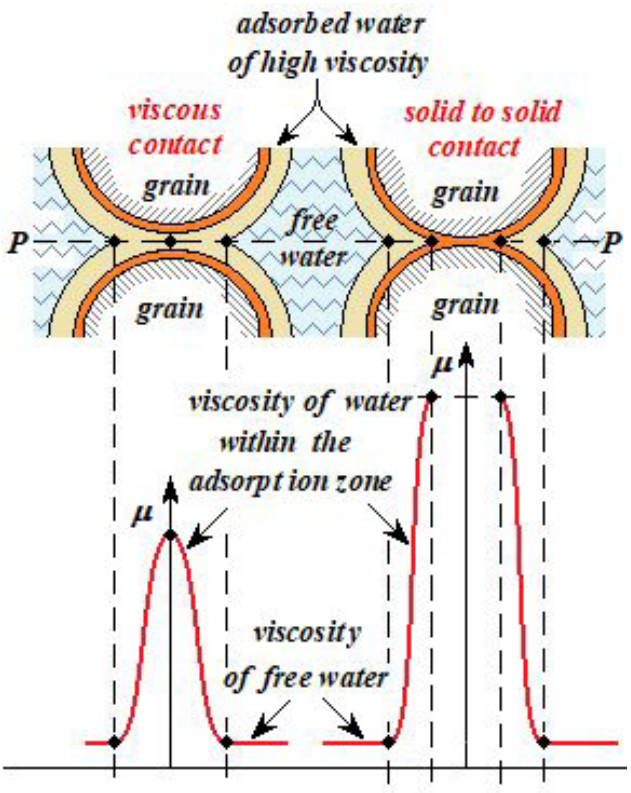

Figure 21. Hypothetical variation of the coefficient of viscosity μ of the adsorbed water along the plane ***P – P*** within the contact zones between clay particles.

Suppose now that the total number of contacts within area A is n. In all contacts, irrespective of their type, there will be viscous resistance. For instance, at the contact between the intermediate couple of grains in Figure 20, viscous resistance comes from the shear strain rate of the adsorbed water element ***ijkl***. Such viscous resistance is also present in the solid to solid contacts. This is illustrated in Figure 20 by the shearing strain of the ring shaped element whose transversal section is ***abcd*** – ***efgh***.

The viscous resistance existing in a viscous contact caused by the shear strain rate of an element of section ***ijkl*** or in a solid to solid contact by the shear strain rate of a ring shaped element whose section is ***abcd – efgh*** varies along the contact. This occurs because the viscosity coefficient μ of the adsorbed water at points within the contact zones along the plane ***P – P*** depends on the distances from these points to the particles surface (see Figure 21).

There is also an extremely important issue concerning the behaviour of viscous fluids, as highlighted by Rouse & Howe (1953). As presented in Figure 18, the concept of individual layers or fluid laminae flowing side by side is merely a question of convenience in order to model the phenomenon mathematically. Such a model can lead to the false idea that in a laminar flow fluid laminae can literally slide one over the others producing a kind of mechanical drag measured in terms of the viscous resistance τ, as expressed by Equation 19. In fact, in a submicroscopic scale, viscous resistance results from the interaction of fluid molecules whenever any portion of fluid, no matter how small it is, is subjected to shear strains. A fundamental feature of a viscous fluid is the fact that a slip along a surface between two neighbouring layers of the fluid (inside a fluid mass) or between a viscous fluid and a solid contour cannot occur because this would result in an infinite value for the ratio dv / dy in Equations 19 and 20. Thus, regardless the fluid nature, molecular interactions compel to the condition of identical velocities along both sides of any fluid surface, real or imaginary. For this reason, the velocity of a moving fluid at the surface of contact with a solid contour will be exactly the same as the velocity of the contour itself. If the contour is at rest, the fluid in contact with this contour will also be at rest, irrespective of how great its velocity may be a short distance away. This means that, during shear, relative displacements between soil grains occur without slippage along the surface of contact between viscous adsorbed water and solid grains contours. This also means that during relative displacements, for instance, along the plane ***P – P*** in Figure 20, soil grains are subjected to drag forces due to shear strain of their viscous adsorbed water layers. The resultant of these viscous forces, denoted by T_v, is the viscous component proposed by Terzaghi & Frölich (1936), which, added to the friction resistance component T_s, gives the internal reaction to the applied tangential force T.

As the viscous resistance is present in all n contacts within the area A, irrespective of the type of contacts, T_v can be written as:

$$T_v = \sum_{j=1}^{n} T_{vj} \tag{24}$$

being T_{vj} the local viscous resistance acting at the contact of order j. In its turn, T_{vj} can be written as**:**

$$T_{vj} = \frac{d\gamma_j}{dt} \int \mu dA_{vj} \tag{25}$$

Considering the viscosity of the free water as being negligible if compared to the viscosity of the adsorbed water, the integral in Equation 25 should be taken all over the viscous contact area A_{vj} of contact ***j*** (see Figures 20 and 21), along which μ varies. The term $d\gamma_j / dt$ is the distortion rate of the viscous adsorbed water of the contact of order ***j***, along the plane ***P – P***, in the direction of the tangential force T. Thus, the viscous component T_v acting all over the area A in the direction of T can be written as:

$$T_v = \sum_{j=1}^{n} \frac{d\gamma_j}{dt} \int \mu dA_{vj} \tag{26}$$

Taking $\overline{\mu}_j$ as the average value of μ over the area A_{vj}, $\int \mu dA_{vj}$ can be written as $\overline{\mu}_j A_{vj}$. Thus,

$$T_v = \sum_{j=1}^{n} \overline{\mu}_j A_{vj} \frac{d\gamma_j}{dt} \tag{27}$$

Denoting by $\overline{\overline{\mu}}$ the average value of all $\overline{\mu}_j$ values and taking into account that the distortion γ_{P-P} of a clay along the plane $\boldsymbol{P-P}$ in Figure 20 is the result of the gathered relative displacements of particles from both sides of plane $\boldsymbol{P-P}$, Equation 27 can be rewritten as:

$$T_v = \overline{\overline{\mu}} \frac{d\gamma_{P-P}}{dt} \sum\nolimits_{j=1}^{n} A_{vj} \tag{28}$$

Summing up the friction resistance component $\left(T_s\right)$ and the viscous resistance component $\left(T_v\right)$ and dividing by the area A, on which the sum $\left(T_s + T_v\right)$ acts, Equation 29 is obtained, as follows.

$$\frac{T}{A} = \frac{T_s + T_v}{A} = \frac{\overline{\xi}\, tan\,\phi'_e \sum\nolimits_{i=1}^{m} P_i}{A} + \frac{\overline{\overline{\mu}} \frac{d\gamma_{P-P}}{dt} \sum\nolimits_{j=1}^{n} A_{vj}}{A} \tag{29}$$

The left hand side of Equation 29 $\left(T / A\right)$ is by definition the shear stress τ over area A of the plane $\boldsymbol{P-P}$, as shown in Figure 20. The summation $\sum\nolimits_{i=1}^{m} P_i / A$ is, by definition, the effective normal stress σ' acting on the area A of the plane $\boldsymbol{P-P}$. The product $\overline{\xi}\, tan\,\phi'_e$ in the first part of the right hand side of Equation 29 is the mobilized degree $\left(\overline{\xi}\right)$ of the friction coefficient $tan\,\phi'_e$. Denoting $\overline{\xi}\, tan\,\phi'_e$ by $tan\,\phi'_{mob}$, the first part of the right hand side of Equation 29 can be written as:

$$\tau_\phi = \frac{T_s}{A} = \frac{\overline{\xi}\, tan\,\phi'_e \sum\nolimits_{i=1}^{m} P_i}{A} = \sigma'\, tan\,\phi'_{mob} \tag{30}$$

being T_s the mobilized friction resistance, which is a part of the internal reaction to the applied horizontal force T (see Figure 20). As T / A is the shear stress τ acting over the area A, the ratio T_s / A, denoted by τ_ϕ, is the part of the shear resistance due to friction mobilized on the area A along the plane $\boldsymbol{P-P}$.

In the second part of the right hand side of Equation 29, $\overline{\overline{\mu}}$ is a function of the distance between neighbouring particles and, therefore, of the void ratio $\left(e\right)$. However, $\overline{\overline{\mu}}$ is also a function of the relative position according to which clay particles are arranged along the plane $\boldsymbol{P-P}$, that is to say, a function of the structure. Nevertheless, the ratio $\sum\nolimits_{j=1}^{n} A_{vj} / A$ is an exclusive function of the void ratio. Thus, the product $\overline{\overline{\mu}}\left(\sum\nolimits_{j=1}^{n} A_{vj} / A\right)$ can be rewritten as a function $\eta(e)$, being $\eta(e)$ a function of the void ratio and the structure. Thereby, the second part of the right hand side of Equation 29, denoted by τ_η, can be rewritten as:

$$\tau_\eta = \eta\left(e\right)\left(d\gamma_{P-P} \Big/ dt\right) \tag{31}$$

being $\eta\left(e\right)$ here defined as the *viscosity of a plastic soil*. Thus, the expression for the shear stress τ_α of a plastic soil, at any instant, acting on plane $\boldsymbol{P-P}$ whose normal makes an angle α with the principal direction σ_1, being the soil at failure or not, can be written as:

$$\tau_\alpha = \tau_{\phi\alpha} + \tau_{\eta\alpha} = \sigma'_\alpha\, tan\,\phi'_{mob\alpha} + \eta\left(e\right)\left(d\gamma_\alpha \Big/ dt\right) \tag{32}$$

If the simplifying assumptions from which Equation 32 has been derived are accepted as valid, such equation will reveal that, at any moment, the shear stress τ_α on a plane whose normal makes an angle α with the direction of σ_1 will be internally resisted by the sum of a friction component $\tau_{\phi\alpha} = \sigma'_\alpha\, tan\,\phi'_{mob\alpha}$ and a viscous component $\tau_{\eta\alpha} = \eta\left(e\right)\left(d\gamma_\alpha / dt\right)$.

Equation 32 leads to the following immediate consequences:

1. It translates mathematically the mechanism conceived by Terzaghi & Frölich (1936) and by Taylor (1948), as presented in section 4.4, about clay behaviour in shear, where the shear resistance at any instant (and not only at failure) is given by the sum of a friction component $\left(\tau_{\phi\alpha}\right)$ and a viscous component $\left(\tau_{\eta\alpha}\right)$.
2. Part of the shear resistance existing in plastic soils is of a viscous origin. It is worth observing that the viscous component becomes zero when strain rate is zero, which does not correspond to the Coulomb's cohesion concept (Schofield, 1999), but corresponds to the viscous resistance concept introduced by Newton.
3. The viscous component $\left(\tau_{\eta\alpha}\right)$ would correspond to the "*true cohesion*" of Hvorslev (1960), an inappropriate name (in the author's opinion), since according to Hvorslev (1960) himself it would have a viscous feature (see section 4.4) and would be a function of three variables: the void ratio, the strain rate and the clay structure. These three variables are present in Equation 31.
4. Considering that shear stresses are internally resisted by a friction component and a viscous component, an additional equation which refers to shear stresses can be added to the PES. This suggests that Equation 18, presented by Taylor (1948), can be generalized, holding valid at any instant and not only at failure.
5. Equation 32 is also valid outside the soil mechanics domain since, if effective stress σ'_α is zero, friction strength will be zero and the resistance to shearing strain will only reside in viscosity, which is a feature of fluids.
6. Finally, Equation 32 explicitly shows the influence of strain rate on the shear strength [see for instance Taylor (1948), Bjerrum (1973), Berre & Bjerrum (1973), Lacerda & Houston (1973), Graham et al. (1983), Sheahan et al. (1996), Tatsuoka et al. (2002), and Aguiar (2014)] and on consolidation (Taylor, 1942; Graham et al., 1983; Leroueil et al., 1985; Andrade, 2014). As previously discussed, being the "*effective cohesion*" or "*true cohesion*", as defined by Terzaghi (1938) and Hvorslev (1937, 1960), of a viscous nature, it is expected that the greater the plasticity of a soil (given by its plasticity index I_p) the greater its viscosity

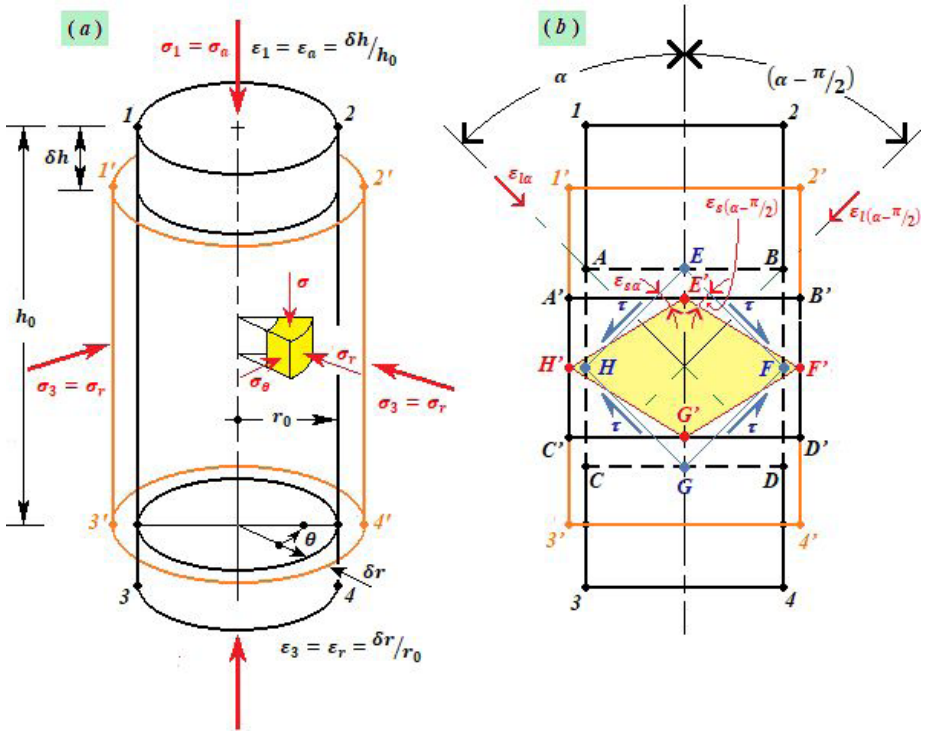

Figure 22. (a) State of stress in a $\overline{\text{CIUCL}}$ test during the undrained shear stage; (b) Corresponding state of strain.

$\eta(e)$. In the author's opinion, this might have been the main reason for Bjerrum (1973) having expressed the influence of strain rate on shear strength of plastic soils as a function of the plasticity index (I_p).

Last but not least, to avoid the confusion created by the inappropriate use of the term "*cohesion*", instead of using the words "*cohesive*" and "*non-cohesive*", it is suggested the use of the words "*plastic*" and "*non-plastic*" soils. By a plastic soil is to be meant a soil on which one can carry out plastic and liquid limit tests.

5.3 Mohr's circle of strain in a $\overline{\text{CIUCL}}$ test

The state of stress found in a $\overline{\text{CIUCL}}$ test is shown in Figure 22a. In this case, $\sigma_1 = \sigma_a$ and, due to the axisymmetry, $\sigma_3 = \sigma_\theta = \sigma_r$. Assuming the soil as isotropic, corresponding to the state of stress of Figure 22a, there is an axisymmetrical state of strain where $\varepsilon_1 = \varepsilon_a$ and $\varepsilon_3 = \varepsilon_2 = \varepsilon_r = \varepsilon_\theta$. In such a case, there will be no shearing strains on horizontal planes.

In a similar way to which has been done for stresses, it can be written:

$$\varepsilon_{l\alpha} = \frac{\varepsilon_1 + \varepsilon_3}{2} + \frac{\varepsilon_1 - \varepsilon_3}{2} cos\, 2\alpha \tag{33}$$

and

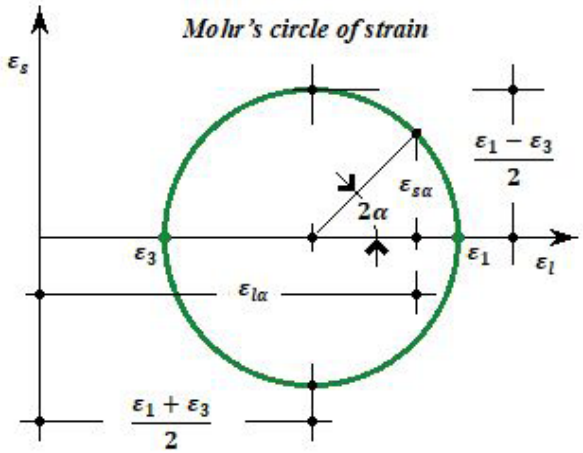

Figure 23. Mohr's circle of strain during the undrained shear stage of a $\overline{\text{CIUCL}}$ test.

$$\varepsilon_{s\alpha} = \frac{\varepsilon_1 - \varepsilon_3}{2} sin\, 2\alpha \tag{34}$$

where $\varepsilon_{l\alpha}$ is the normal linear strain (longitudinal strain) of an element of the vertical plane (like ***EFGH*** of Figure 22b) along the direction which makes an angle α with the direction of $\varepsilon_1 = \varepsilon_a$ (α being positive when taken in a counterclockwise sense) and $\varepsilon_{s\alpha}$ the shearing strain (see also Figure 22b).

Similarly to what has been done for stresses, Equations 33 and 34 can be represented on plane $\varepsilon_l \times \varepsilon_s$ (Figure 23) by a circle of radius $(\varepsilon_1 - \varepsilon_3)/2$ and center of coordinates $[(\varepsilon_1 + \varepsilon_3)/2, 0]$. It is the Mohr's circle of strain, shown in Figure 23.

In soil mechanics it is usual to take a normal linear strain as positive when the element suffers a reduction in length (shortening). On the contrary, an elongation is considered negative. In the case of the specimen shown in Figure 22, the axial strain $\varepsilon_a = \varepsilon_1 = -(\delta h / h_0)$ is positive (because δh is negative) and the radial strain $\varepsilon_r = \varepsilon_3 = -(\delta r / r_0)$ is negative (because δr is positive).

Being V_f and V_0, respectively, the final and the initial specimen volumes, the volumetric strain, denoted by ε_V, is by definition:

$$\varepsilon_V = \frac{(V_0 - V_f)}{V_0} \tag{35}$$

In soil mechanics it is usual to consider a compression (decrease of volume) as being positive. Thus, in the case of a triaxial test specimen (see Figure 22), ε_V, defined by Equation 35, is accurately given by:

$$\varepsilon_V = -\frac{\delta h}{h_0} - \frac{2\delta r}{r_0} - \frac{2\delta r \delta h}{r_0 h_0} - \frac{\delta r^2}{r_0^2} - \frac{\delta r^2 \delta h}{r_0^2 h_0} = \varepsilon_a + 2\varepsilon_r + \varepsilon_r\left[2\varepsilon_a + \varepsilon_r(1+\varepsilon_a)\right] \tag{36}$$

When ε_a and ε_r are small, Equation 36 can be simplified as $\varepsilon_V = \varepsilon_a + 2\varepsilon_r$. During the undrained shear of a saturated specimen in a $\overline{\text{CIUCL}}$ test, there is no volume change, so $\varepsilon_V = 0$. In this case $\varepsilon_r = -(\varepsilon_a / 2)$ and the specimen is distorted on planes which are not horizontal (see Figure 22b).

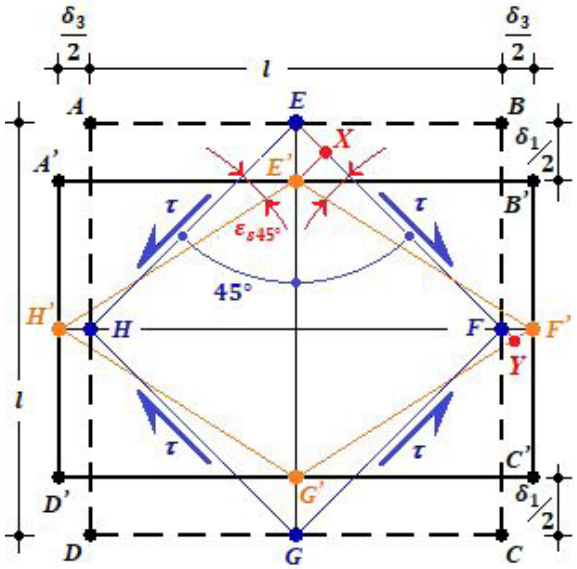

Figure 24. Normal linear strains and shear strains of elements ***ABCD*** and ***EFGH***.

Figure 22b shows the section ***1234*** made by a vertical plane that contains the axis of the specimen of Figure 22a. Consider now the square region ***ABCD*** on the section 1234 before deformation. Taking $\alpha = 45°$ in Figure 22b, the square ***ABCD*** of side l, shown in Figure 24, is deformed into the rectangle ***A'B'C'D'***. In a similar way, the square ***EFGH*** of side $l\sqrt{2}/2$ is deformed into the rhombus ***E'F'G'H'***.

According to Figure 24, $\varepsilon_1 = \varepsilon_a = \delta_1 / l$ and $\varepsilon_3 = \varepsilon_r = -\delta_3 / l = -\delta_1 / 2l$. Thus, $\varepsilon_{l45°}$ can be evaluated as shown in Figure 24.

$$\varepsilon_{l45°} = \frac{\overline{\boldsymbol{EE'}}\cos 45° - \overline{\boldsymbol{FF'}}\cos 45°}{\overline{\boldsymbol{EF}}} = \frac{\frac{\delta_1}{2}\frac{\sqrt{2}}{2} - \frac{\delta_3}{2}\frac{\sqrt{2}}{2}}{\frac{l\sqrt{2}}{2}} = \frac{\frac{\delta_1}{2} - \frac{\delta_3}{2}}{l} = \frac{\delta_1}{4l} = \frac{\varepsilon_1 + \varepsilon_3}{2} \tag{37}$$

It should be observed that δ_1 and δ_3 have opposite signs because δ_1 is a contraction and δ_3 an elongation. The expression for $\varepsilon_{l45°}$ given by Equation 37 can also be obtained via Equation 33, that is,

$$\varepsilon_{l45°} = \frac{\varepsilon_1 + \varepsilon_3}{2} + \frac{\varepsilon_1 - \varepsilon_3}{2}\cos 90° = \frac{\varepsilon_1 + \varepsilon_3}{2} = \frac{\frac{\delta_1}{l} - \frac{\delta_3}{l}}{2} = \frac{1}{2}\left(\frac{\delta_1}{l} - \frac{\delta_1}{2l}\right) = \frac{\delta_1}{4l} = \frac{\varepsilon_1}{4} \tag{38}$$

The value of $\varepsilon_{s45°}$ can be obtained, via Figure 24, taking the transversal component of the relative displacement between points ***E*** and ***F***, by unit length of the segment ***EF***, that is:

$$\varepsilon_{s45°} = \frac{\overline{\boldsymbol{EE'}}\sin 45° - \left(-\overline{\boldsymbol{FF'}}\sin 45°\right)}{\overline{\boldsymbol{EF}}} = \frac{\frac{\delta_1}{2}\frac{\sqrt{2}}{2} - \left(-\frac{\delta_3}{2}\frac{\sqrt{2}}{2}\right)}{\frac{l\sqrt{2}}{2}} = \frac{\frac{\delta_1}{2} + \frac{\delta_3}{2}}{l} = \frac{3}{4}\varepsilon_1 \tag{39}$$

The value of Equation 39 can also be obtained using $\alpha = 45°$ in Equation 34, that is:

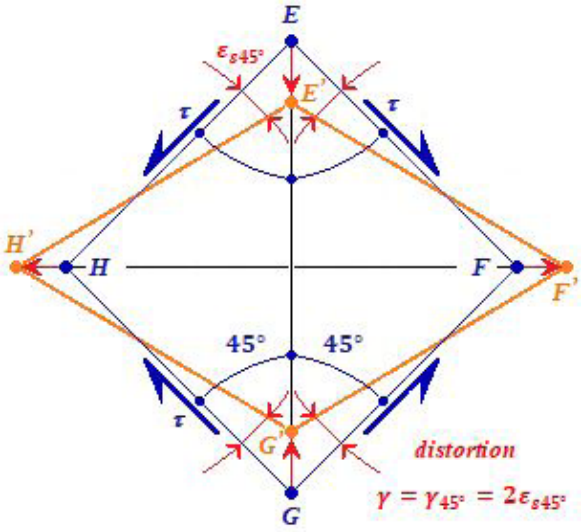

Figure 25. Definition of distortion $= \gamma_{45°} = 2\varepsilon_{s45°}$.

$$\varepsilon_{s45°} = \frac{\varepsilon_1 - \varepsilon_3}{2}\sin 90° = \frac{\frac{\delta_1}{l} - \left(-\frac{\delta_3}{l}\right)}{2} = \frac{\frac{\delta_1}{l} - \left(-\frac{\delta_1}{2l}\right)}{2} = \frac{3}{4}\frac{\delta_1}{l} = \frac{3}{4}\varepsilon_1 \quad (40)$$

Finally, the distortion, denoted by γ_α, is the angular change between two fibres of the vertical plane of Figure 22b, which were originally at right angles one to another and whose normal directions make the angles α and $\left(\alpha - \pi/2\right)$ with the direction of ε_1 (see Figure 22b). Thus, the distortion γ_α can be determined via Equation 34 as $\gamma_\alpha = \varepsilon_{s\alpha} - \varepsilon_{s\left(\alpha-\pi/2\right)}$, that is,

$$\gamma_\alpha = \frac{\left(\varepsilon_1 - \varepsilon_3\right)}{2}\sin 2\alpha - \frac{\left(\varepsilon_1 - \varepsilon_3\right)}{2}\sin 2\left(\alpha - \pi/2\right) = \left(\varepsilon_1 - \varepsilon_3\right)\sin 2\alpha = 2\varepsilon_{s\alpha} \quad (41)$$

The maximum distortion $\gamma_{45°}$, or simply the distortion γ, is the angular change between two fibres of the vertical plane of Figure 22b, which were originally at right angles one to another and whose normal directions make the angles +45° and –45° with the direction of ε_1 (see Figure 25). This distortion γ, during the undrained shear stage of a $\overline{\text{CIUCL}}$ test, can be obtained using $\alpha = 45°$ in Equation 41 to obtain:

$$\gamma_{45°} = \gamma = \varepsilon_1 - \varepsilon_3 = \frac{3}{2}\varepsilon_1 \quad (42)$$

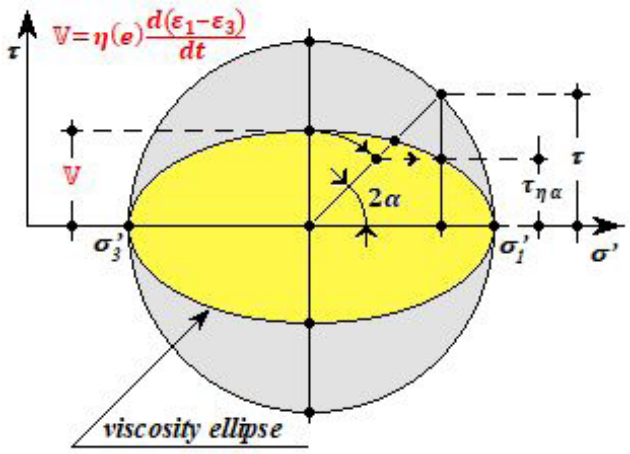

Figure 26. The viscosity ellipse or Taylor's ellipse.

5.4 The Mohr's circle, the viscosity ellipse and the friction ellipse

Considering Equation 31 and assuming $\eta(e)$ does not vary with direction (soil is assumed to be isotropic) and also recalling that distortion γ_α is twice the shear strain $\varepsilon_{s\alpha}$, the viscous component of the shear stress $\tau_{\eta\alpha}$ along a plane whose normal makes an angle α with the σ_1 or ε_1 direction can be written as:

$$\tau_{\eta\alpha} = \eta(e)\left(d\gamma_\alpha / dt\right) = \eta(e)\left(d2\varepsilon_{s\alpha} / dt\right) = 2\eta(e)\left(d\varepsilon_{s\alpha} / dt\right) \quad (43)$$

Recalling that $\varepsilon_{s\alpha} = \left[\left(\varepsilon_1 - \varepsilon_3\right)/2\right]sin\,2\alpha$, then

$$\tau_{\eta\alpha} = 2\eta(e)\left(d\varepsilon_{s\alpha} / dt\right) = \eta(e)\left[d\left(\varepsilon_1 - \varepsilon_3\right)/dt\right]sin\,2\alpha \quad (44)$$

At a given instant of a triaxial compression test, whether it is drained or undrained, provided that accelerations are negligible (so that equilibrium equations can be written), the *state of mobilized viscosity* is given by:

$$\sigma'_\alpha = \frac{\sigma'_1 + \sigma'_3}{2} + \frac{\sigma'_1 - \sigma'_3}{2}cos\,2\alpha \quad (45)$$

and

$$\tau_{\eta\alpha} = \eta(e)\frac{d\left(\varepsilon_1 - \varepsilon_3\right)}{dt}sin\,2\alpha \quad (46)$$

Equations 45 and 46 are the parametric equations of an ellipse whose centre has coordinates $\left[\left(\sigma'_1 + \sigma'_3\right)/2, 0\right]$ and whose major and minor axes are respectively $\left(\sigma'_1 - \sigma'_3\right)$ and $2\eta(e)d\left(\varepsilon_1 - \varepsilon_3\right)/dt$. This ellipse, as shown in Figure 26, will be called viscosity ellipse or Taylor's ellipse, in honour of Donald Wood Taylor, since, in fact, all these concepts are expressed in several of his writings, though not in detail.

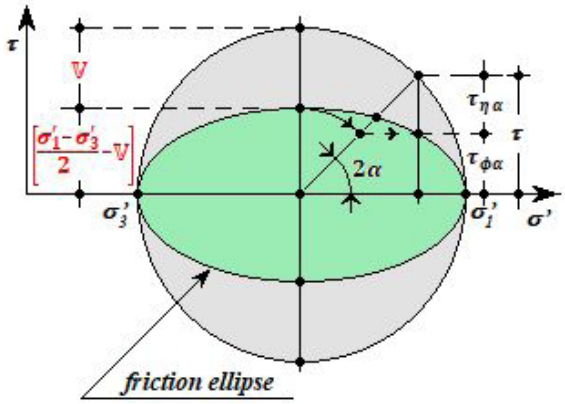

Figure 27. The friction ellipse or Coulomb's ellipse.

From now on, the maximum ordinate of the viscosity ellipse will be denoted by $\mathbb{V}$ and expressed by:

$$\mathbb{V} = \eta(e)\frac{d(\varepsilon_1 - \varepsilon_3)}{dt} = \eta(e)\dot{\gamma} \tag{47}$$

From the above exposed, the friction component of the shear stress $\tau_{\phi\alpha}$, acting on the same plane on which the viscous portion $\tau_{\eta\alpha}$ acts, is given by:

$$\tau_{\phi\alpha} = \tau_\alpha - \tau_{\eta\alpha} = \left[\frac{(\sigma'_1 - \sigma'_3)}{2} - \mathbb{V}\right] sin\,2\alpha \tag{48}$$

Based on Equations 45 and 48, the *state of mobilized friction* is defined. One can observe that Equations 45 and 48 are the equations of another ellipse whose centre has coordinates $\left[(\sigma'_1 + \sigma'_3)/2, 0\right]$ and whose major and minor axes are, respectively, $(\sigma'_1 - \sigma'_3)$ and $\left[(\sigma'_1 - \sigma'_3) - 2\mathbb{V}\right]$. This ellipse, as shown in Figure 27, will be called friction ellipse or Coulomb's ellipse.

It is noteworthy that the Mohr's circle of effective stresses is the result of summing up the viscosity and the friction ellipses. However, the ellipses cannot exist separately since equilibrium conditions are only fulfilled by the Mohr's circle of stress. Thus, the shear stress τ_α, which acts on a plane whose normal makes an angle α with the σ_1 direction, consists of two parts: a friction part $\tau_{\phi\alpha}$ and a viscous part $\tau_{\eta\alpha}$.

5.5 A failure criterion for soils taking into account the strain rate effect

The ideas herein exposed can be generalized for any stress and strain states. Nevertheless, as this text deals with fundamentals, only $\overline{\text{CIUCL}}$ triaxial tests on normally consolidated specimens will be discussed. In this type of test, $\sigma'_1 = \sigma'_a$, $\sigma'_3 = \sigma'_r$, $\varepsilon_1 = \varepsilon_a$ and $\varepsilon_3 = \varepsilon_r$ (see Figure 22a).

When carrying out a $\overline{\text{CIUCL}}$ triaxial test in a saturated soil, since the water compressibility is negligible, the volumetric strain ε_v is assumed to be zero during the shearing stage. Thus, $\varepsilon_v = \varepsilon_1 + 2\varepsilon_3 = 0$, then $\varepsilon_3 = -\varepsilon_1/2$ or $\varepsilon_r = -\varepsilon_a/2$. So, $\varepsilon_1 - \varepsilon_3 = 3/2(\varepsilon_1) = 3/2(\varepsilon_a)$, and the viscous component of the shear stress $\tau_{\eta\alpha}$ corresponds to:

$$\tau_{\eta\alpha} = \eta(e)\frac{d(\varepsilon_1 - \varepsilon_3)}{dt} sin\,2\alpha = \frac{3}{2}\eta(e)\frac{d\varepsilon_a}{dt} sin\,2\alpha \tag{49}$$

As in the shear stage of a conventional $\overline{\text{CIUCL}}$ test the axial strain rate $\dot{\varepsilon}_a = d\varepsilon_a/dt$ = constant, Equation 49 reveals that, when a fixed plane is considered, whatever it is, the viscous component $\tau_{\eta\alpha}$ of the shear stress on that plane will remain constant during all test (provided that during shear the soil structure remains approximately constant, so that $\eta(e)$ will keep approximately constant). Thus, according to Equation 49, as soon as the load frame motor is switched on with the strain rate corresponding to $\dot{\varepsilon}_a$, the viscous component will be mobilized immediately (with $\varepsilon_a = 0$), and remaining constant, for each fixed plane, up to the end of shear. Notwithstanding, although the viscous resistance will be fully mobilized immediately and remaining constant along the whole shear, the deviator stress will increase as the specimen strains up to failure. This means that during shear the frictional resistance will be mobilized as the test takes place, contrarily to the viscous resistance mobilization, which occurs instantaneously. The immediate consequences of such mechanism are listed as follows:

1. To mobilize the frictional resistance, it is necessary to strain the specimen and, as it begins to be strained, the deviator stress will begin to increase up to the specimen reaches failure. As during the shear stage of a $\overline{\text{CIUCL}}$ test there are no volume changes, only shear strains occur. Thus, the mobilization of the frictional component is intimately related to shear strains and, therefore, failure will occur when the frictional component is fully mobilized. The conclusion is that shear strains and failure are governed by the mobilization of the frictional component. In the very beginning of shear, there is immediate viscous resistance mobilization, whatever the plane may be. On a fixed plane, viscous resistance will be acting with a value that will be kept constant up to failure (provided that $\dot{\varepsilon}_a$ and soil structure remain the same). As shear strains take place, deviator stress will increase due to the mobilization of the frictional resistance component. When the frictional resistance component is entirely mobilized, failure occurs.
2. As regards specimens with the same void ratio and the same structure, the viscous resistance component at failure, i.e., the viscous part of the undrained shear strength, only depends on the strain rate. Thus, the shear strain rate only affects the shear

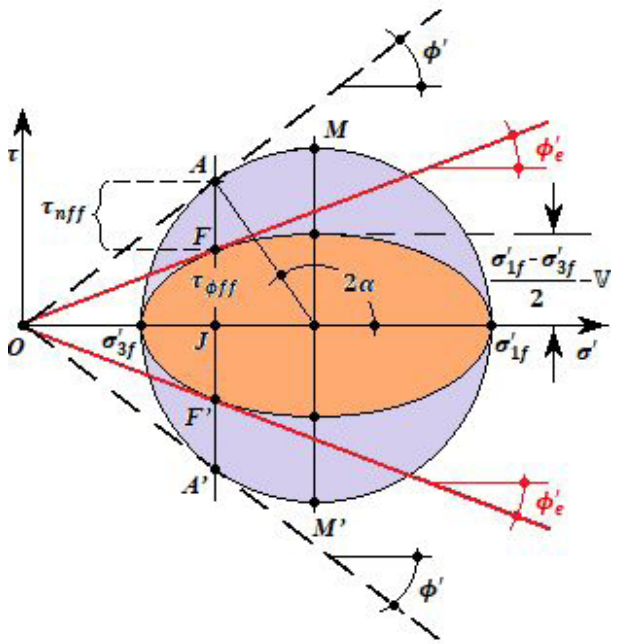

Figure 28. Failure criterion for a normally consolidated clay.

strength value but does not affect strains. This is illustrated by the test results shown in Figure 5 (see also Figure 6). As the field vane test is usually carried out with a higher speed of shear than those observed in real failures in the field, the results of Figures 5 and 6 also explain the need for Bjerrum (1973) having proposed the correction factor to be applied to undrained shear strength results obtained via field vane tests.

3. If failure is commanded by the mobilization of the frictional component of the shear strength and if the frictional part of the shear stress is given by the friction ellipse ordinates, then, if the failure criterion established by Hvorslev (1937) holds valid, failure must occur whenever the friction ellipse touches the strength envelope. Remembering that the approach in this article is limited to the normally consolidated specimens, the strength envelope to be considered is that one which passes through the origin and has slope $\tan\phi'_e$ (see Figure 28).

Denoting by τ_{ff} the shear stress on the failure plane at failure,

$$\tau_{ff} = \tau_{\phi ff} + \tau_{\eta ff} \tag{50}$$

where $\tau_{\phi ff}$ and $\tau_{\eta ff}$ are, respectively, the friction and viscosity parts of the shear stress on the failure plane at failure. As friction is what commands failure, failure occurs according to Mohr-Coulomb-Hvorslev's envelope, which is the straight line that passes through the origin and has slope $tan\,\phi'_e$ (see Figure 28). Thus, failure occurs in the maximum obliquity plane, taking into account only the frictional part of the shear stress, given by:

$$tan\,\phi'_{emob} = \left(\tau_{\phi\alpha} \Big/ \sigma'_{\alpha}\right)_{max} \tag{51}$$

Being ϕ'_e the limiting angle of maximum obliquity, $tan\,\phi'_e$ is the maximum value of $tan\,\phi'_{emob}$.

At each moment of a test, $tan\,\phi'_{emob}$ can be obtained by determining $\left(\tau_{\phi\alpha} / \sigma'_{\alpha}\right)_{max}$. This occurs when

$$\frac{\partial\left(\frac{\tau_{\phi\alpha}}{\sigma'_{\alpha}}\right)}{\partial\alpha} = 0 \tag{52}$$

$$\frac{\partial\left(\frac{\tau_{\phi\alpha}}{\sigma'_{\alpha}}\right)}{\partial\alpha} = \frac{\partial}{\partial\alpha}\left\{\frac{\left[\frac{\left(\sigma'_1-\sigma'_3\right)}{2}-\mathbb{V}\right]sin\,2\alpha}{\frac{\left(\sigma'_1+\sigma'_3\right)}{2}+\frac{\left(\sigma'_1-\sigma'_3\right)}{2}cos\,2\alpha}\right\} = \frac{\partial}{\partial\alpha}\left[\frac{\left(t'-\mathbb{V}\right)sin\,2\alpha}{s'+t'cos\,2\alpha}\right] = 0 \tag{53}$$

$$\frac{\partial\left(\frac{\tau_{\phi\alpha}}{\sigma'_{\alpha}}\right)}{\partial\alpha} = \frac{2\left(t'-\mathbb{V}\right)\cos 2\alpha\left(s'+t'\cos 2\alpha\right)}{\left(s'+t'\cos 2\alpha\right)^2} + \frac{2t'\left(t'-\mathbb{V}\right)\sin^2 2\alpha}{\left(s'+t'\cos 2\alpha\right)^2} = 0 \tag{54}$$

Solving Equation 54, one obtains:

$$cos\,2\alpha = -\frac{t'}{s'} = -\frac{\sigma'_1-\sigma'_3}{\sigma'_1+\sigma'_3} \tag{55}$$

Replacing the result of Equation 55 into Equation 51, one finally obtains:

$$tan\,\phi'_{emob} = \frac{\left(\frac{\sigma'_1-\sigma'_3}{2}-\mathbb{V}\right)}{\sqrt{\sigma'_1\sigma'_3}} = \frac{\left(t'-\mathbb{V}\right)}{\sqrt{s'^2-t'^2}} \tag{56}$$

where

$$s' = \frac{\sigma'_1+\sigma'_3}{2} = \frac{\sigma'_a+\sigma'_r}{2} \tag{57}$$

and

$$t' = \frac{\sigma'_1-\sigma'_3}{2} = \frac{\sigma'_a-\sigma'_r}{2} \tag{58}$$

6. $\overline{\text{CIUCL}}$ tests under the light of the concepts presented in the previous section

6.1 Introduction and summary of the main points of previous section

Although the concepts presented in section 5 can be extended to more general cases, the approach herein presented is restricted to normally consolidated saturated plastic soils subjected to $\overline{\text{CIUCL}}$ tests. Such approach describes and considers the effect of strain rate on clays behaviour based on a mechanical view, via viscosity. Considering the strain rate effect via viscosity greatly simplifies the phenomenon of interaction between clay particles. Nevertheless, this kind of approach captures the essence of the strain rate effects on plastic soils behaviour, making its understanding easier.

The assumptions used in this approach are the following:

1. Soil is seen as a set of grains, each one involved by a highly viscous adsorbed water. The closer the adsorbed water is to the grain surface, the higher its viscosity.
2. Contacts between grains are of two types: solid to solid and viscous (Figures 20 and 21).
3. In a plane passing through a "point" of a soil mass in equilibrium whose normal makes an angle α with the σ_1 direction the effective normal stress σ'_α is written as: $\sigma'_\alpha = \sigma_\alpha - u$, being σ_α the total normal stress and u the pore pressure.
4. Along the tangential direction of the same plane described in (3), the shear stress τ_α consists of two parts: a frictional part $\tau_{\phi\alpha}$ and a viscous part $\tau_{\eta\alpha}$, or rather $\tau_\alpha = \tau_{\phi\alpha} + \tau_{\eta\alpha}$.
5. The viscous part of the shear stress $\tau_{\eta\alpha}$, given by Equation 44, is a function of the void ratio, the soil structure and the distortion rate $\dot{\gamma}$. The friction part $\tau_{\phi\alpha}$, given by Equation 48, is a function of the effective stress σ'_α and the mobilized friction angle $\phi'_{mob\alpha}$ on the plane where σ'_α acts, i.e., $\tau_{\phi\alpha} = \sigma'_\alpha \tan\phi'_{mob\alpha}$ (see Equation 32). It should be reminded here that there is a difference between $\phi'_{mob\alpha}$ and ϕ'_{emob}. For any state of effective stress, $\tan\phi'_{mob\alpha}$ is, by definition, the ratio $\left(\tau_{\phi\alpha} / \sigma'_\alpha\right)$ in a plane given by α, whereas $\tan\phi'_{emob}$ is, for the same state of effective stress, given by $\left(\tau_{\phi\alpha} / \sigma'_\alpha\right)_{max}$ (see Equation 51). When failure is reached, $\phi'_{emob} = \phi'_e$.
6. The ordered pairs $\left(\sigma'_\alpha, \tau_{\eta\alpha}\right)$ define the *state of mobilized viscosity* of a soil, which is represented by the viscosity ellipse or Taylor's ellipse. On the other hand, the pairs $\left(\sigma'_\alpha, \tau_{\phi\alpha}\right)$ define the *state of mobilized friction*, represented by the friction ellipse or Coulomb's ellipse.
7. The two ellipses cannot exist separately since only the stresses given by the Mohr's circle can fulfill equilibrium conditions.
8. In a $\overline{\text{CIUCL}}$ test carried out with $\dot{\varepsilon}_a$ = constant and assuming that there is no significant change in soil structure, $\eta(e)$ = constant. Thus, the viscous part of the shear resistance $\tau_{\eta\alpha}$ is instantaneously mobilized at the beginning of the shear stage, remaining constant on that fixed plane given by α throughout the shear stage.
9. Since the deviator stress increases along the shear stage as ε_a increases, a conclusion to be drawn is that such deviator stress increase should be assigned to the mobilization of frictional resistance.
10. Failure occurs when frictional resistance is fully mobilized. Therefore, failure is ruled by the mobilization of the frictional resistance.
11. Failure occurs when $\tan\phi'_{emob} = \left(\tau_{\phi\alpha} / \sigma'_\alpha\right)_{max} = \tan\phi'_e$, which graphically corresponds to the friction ellipse tangency to the strength envelope, whose slope is $\tan\phi'_e$, being ϕ'_e the Hvorslev's *true angle of friction*.
12. Since there are no volume changes during the shear stage of a $\overline{\text{CIUCL}}$ test, there are only shear strains. Thus, frictional resistance mobilization is closely related to shear strains.
13. The frictional resistance mobilization at any instant of the shear stage of a $\overline{\text{CIUCL}}$ test can be quantified by $\tan\phi'_{emob} = \left(t' - \mathbb{V}\right) / \sqrt{s'^2 - t'^2}$.

6.2 Ideal $\overline{\text{CIUCL}}$ tests

During the shear stage of $\overline{\text{CIUCL}}$ tests it is usual to plot the deviator stress $\left(\sigma'_a - \sigma'_r\right)$ × axial strain $\left(\varepsilon_a\right)$ and developed pore pressure $\left(\Delta u\right)$ × $\left(\varepsilon_a\right)$. As in the shear

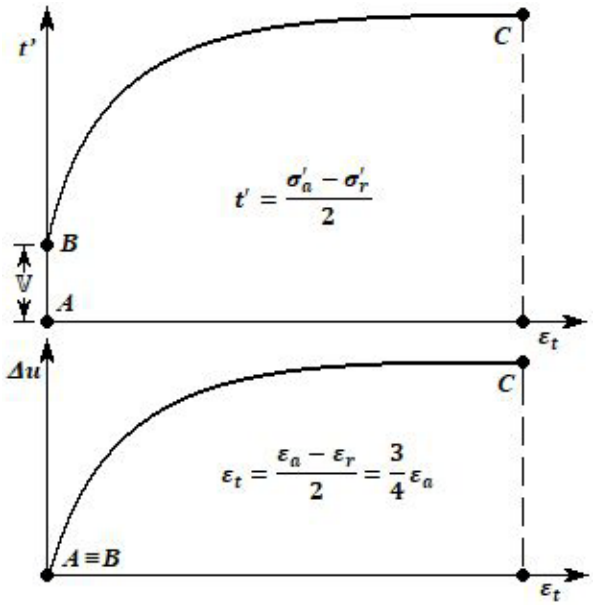

Figure 29. "Viscosity jump"- instantaneous mobilization of viscous resistance in $t' \times \varepsilon_t$ and $\Delta u \times \varepsilon_t$ plots (Martins, 1992).

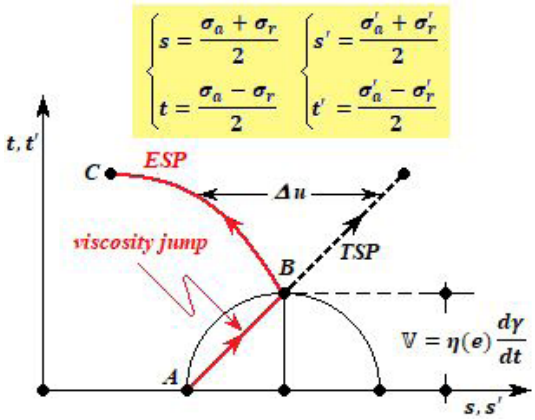

Figure 30. "Viscosity jump"- instantaneous mobilization of viscous resistance in $s' \times t'$ and $s \times t$ plots (Martins, 1992).

stage of a $\overline{\text{CIUCL}}$ test $\varepsilon_r = -\varepsilon_a / 2$, then the shear strain $\varepsilon_{s45^\circ} = (\varepsilon_a - \varepsilon_r)/2 = (3/4)\varepsilon_a$.

Denoting ε_{s45° by ε_t, the shear stress associated with ε_t is $\tau_{45^\circ} = \left(\sigma'_a - \sigma'_r\right)/2 = t'$. Thus, just as a matter of coherence, graphs $t' \times \varepsilon_t$ and $\Delta u \times \varepsilon_t$ will be plotted. As in $\overline{\text{CIUCL}}$ tests $\varepsilon_t = (3/4)\varepsilon_a$, the use of ε_t instead of ε_a for abscissa of $t' \times \varepsilon_t$ and $\Delta u \times \varepsilon_t$ plots does not alter their shapes.

Figure 29 presents curves $t' \times \varepsilon_t$ and $\Delta u \times \varepsilon_t$ expected for normally consolidated clays in a $\overline{\text{CIUCL}}$ test. This figure shows in the $t' \times \varepsilon_t$ plot an "initial jump" ***AB*** at $\varepsilon_t = 0$. Such "initial jump" or "viscosity jump" corresponds to the instantaneous mobilization of the viscous resistance given by $t' = \mathbb{V} = \eta(e)\dot{\gamma}$. Since the viscous part of the shear resistance is a function of the shear strain rate (and not of the shear strain), when the load frame motor is turned on, the viscous resistance will start to act immediately, when both shear strain $(\ _t)$ and excess pore-pressure (Δu) are still zero. Thereafter, if the shear stage continues running with the same strain rate $\dot{\varepsilon}_t = \dot{\gamma}/2$, this viscous resistance will remain constant for the rest of the test.

The "viscosity jump" appears in both $s' \times t'$ effective stress path (from now on called ESP) and $s \times t$ total stress path (from now on called TSP), as shown in Figure 30. From point ***B*** in Figures 29 and 30, friction resistance begins to be mobilized gradually, pore pressure begins to increase and the specimen begins to undergo shear strains until reaching point ***C***, where all the available friction resistance is mobilized. It is when failure takes place.

In Figure 30, along the "viscosity jump", which goes from ***A*** to ***B*** instantaneously, the ESP and TSP are coincident. This "viscosity jump" causes the ESPs of normally consolidated clays to move to the right afterwards changing their direction moving to the left, as shown in Figure 30. It is important to note that the frictional resistance mobilized at point ***B*** is zero and, therefore, at point ***B*** there is only mobilization of viscous resistance.

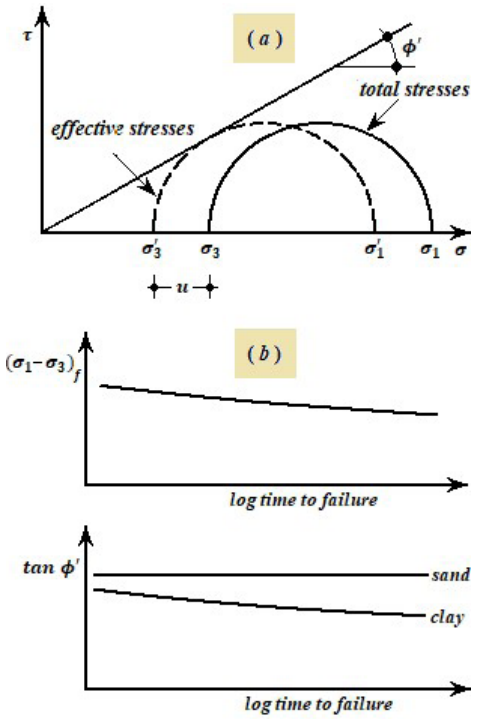

Figure 31. The effect of duration of test on undrained strength [adapted from Bishop & Henkel (1962)]: (a) Mohr circles at failure for a consolidated-undrained test on a normally consolidated clay; (b) Variation in measured strength with time to failure.

This shape of ESPs in $\overline{\text{CIUCL}}$ tests, as shown in Figure 30, seems to have been originally presented by Leroueil et al. cited by Jamiolkowski et al. (1991) and is reproduced in Figure 7. Such a feature suggests that both the critical state line (CSL) and the state boundary surface are not unique but dependent on the strain rate $\dot{\varepsilon}_t = d\varepsilon_t / dt$, or rather one CSL and one state boundary surface exist for each $\dot{\varepsilon}_t$ value. There are several experimental evidences supporting this idea. One of them is found in the following passage from Bishop & Henkel (1962), which refers to strain rate (although the phenomenon has been described as duration of test):

> *[IV] Duration of Test. The duration of test commonly used in the triaxial apparatus and the parameters by which the results are expressed are open to criticism on the grounds that they take no account of the phenomena of creep in soils [for example, Geuze, 1953].*
> *As the criticism is usually based on the results of undrained tests, it is necessary to separate the factors involved. The application of a shear stress to a saturated sample will result, under undrained conditions, in an excess pore pressure. Failure conditions in a consolidated-undrained test on a normally consolidated clay are represented in Figure 1a* (an adaptation is presented in Figure 31a of this article*) by an excess pore pressure u and an effective stress circle tangential to a failure envelope defined by the angle ϕ', c' being zero. If a sample consolidated under the same conditions is tested*

at a much lower rate of testing, it is found that the undrained strength $(\sigma_1 - \sigma_3)$ *is lower and that* ϕ' *has also decreased a little (*Figure 1b*)* (an adaptation is presented in Figure 31b of this article). *The drop in* ϕ' *is negligible for sands but may amount in some clays to about 5% decrease in tan* ϕ' *for each increase of ×10 in the duration of the test*. (Bishop & Henkel, 1962, pp. 30-31).

Taking into account that in a normally consolidated clay failure conditions ind icate that CSL is written as $q'_f = M\ p'_f$, being q'_f the deviator stress at failure $(q'_f = (\sigma'_a - \sigma'_r)_f)$ and p'_f the mean effective stress at failure $p'_f = [(\sigma'_a + 2\sigma'_r)/3]_f$, with $M = 6\,sin\phi'/(3 - sin\phi')$, it is clear that if $tan\phi'$ increases with $\dot{\varepsilon}_a$, M must also increase with $\dot{\varepsilon}_a$, or rather the CSL is dependent on the strain rate $\dot{\varepsilon}_a$. In this case, the CSL cannot be a clay property in the sense of being something intrinsic to the clay, a sense used by Burland (1990) for the word intrinsic. The same fact holds for Roscoe's surface, which would depend on strain rate. These two aspects are illustrated in Figure 7 (Leroueil et al. cited by Jamiolkowski et al., 1991). According to Figure 31, strain rate would not affect sands since they do not present the viscous effects because they do not have plasticity. Evidence that Bjerrum (1973) grasped the essence of the phenomenon mechanism as being of a viscous nature is the fact that he related its importance and magnitude to plasticity (evaluated by the plasticity index I_p).

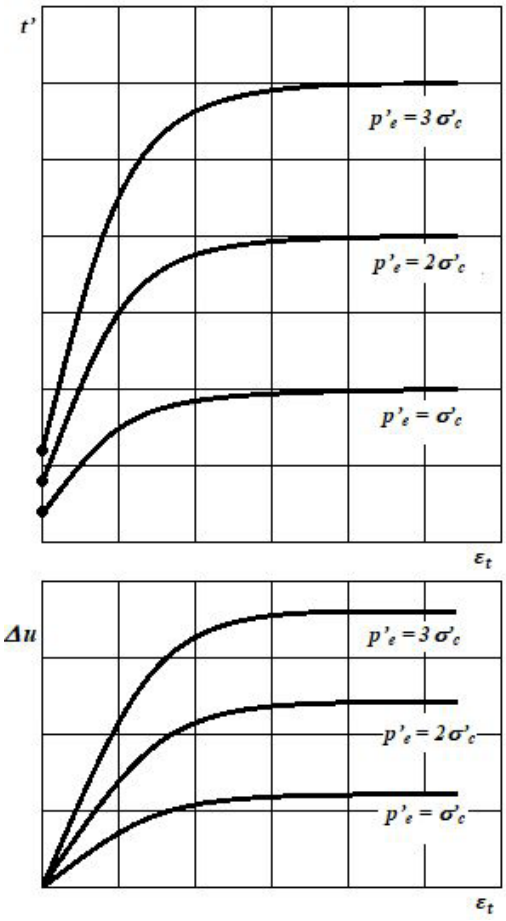

Figure 32. Curves $t' \times \varepsilon_t$ and $\Delta u \times \varepsilon_t$ for a set of ideal CIUCL tests on a normally consolidated clay.

6.3 A set of ideal CIUCL tests

The advantage of working with the mean effective stress $p' = (\sigma'_a + 2\sigma'_r)/3$ and the deviator stress $q' = (\sigma'_a - \sigma'_r)$ is their correspondence to the variables ε_v and γ. However, as there is a one-to-one correspondence between the ordered pairs (p', q') and (s', t'), it will make no difference whether one works with the pair (p', q') or with the pair (s', t') to draw stress paths. In this article, it has been preferred to work with the variables $s'$and t', as a matter of convenience.

Now, one will consider the results of three ideal CIUCL tests carried out on a normally consolidated clay, under isotropic effective stresses p'_e equal to $\sigma'_c, 2\sigma'_c$ and$3\sigma'_c$. The expected $t' \times \varepsilon_t$ and $\Delta u \times \varepsilon_t$ curves are shown in Figure 32: the curves are proportional to p'_e.

The effective stress paths on the $s' \times t'$ plane of these tests are presented in Figure 33 together with their curves $s' \times e$. The ESPs in the upper part of Figure 33 are homothetic with point ***O*** being the centre of homothety. Thus, the generated pore

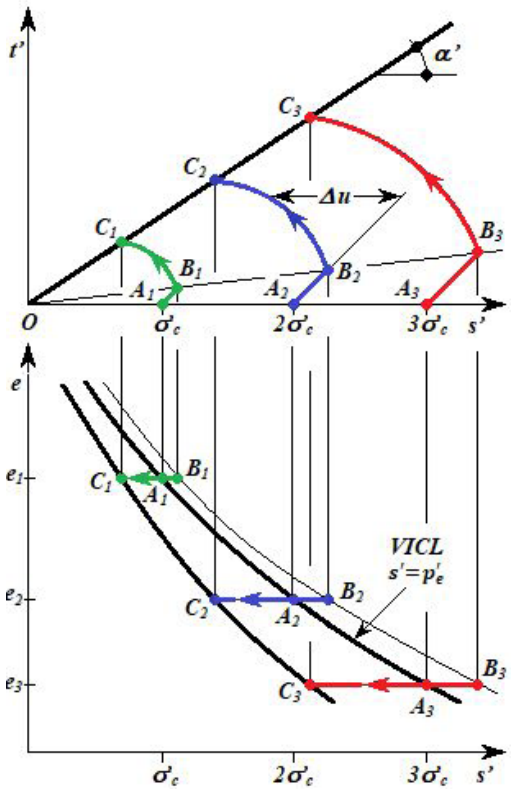

Figure 33. Paths on the $s' \times t'$ and $s' \times e$ planes followed by ideal CIUCL tests carried out on normally consolidated clay specimens under a given shear strain rate $\dot{\varepsilon}_t$ = constant.

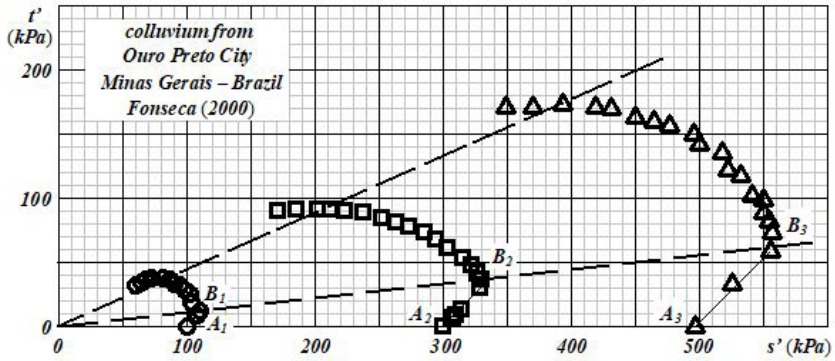

Figure 34. Effective stress paths in $\overline{\text{CIUCL}}$ tests and their respective "viscosity jumps" [adapted from Fonseca (2000)].

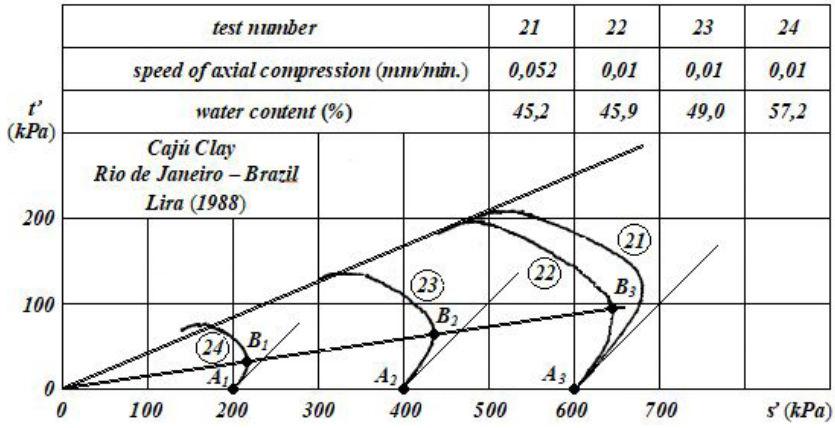

Figure 35. Effective stress paths in $\overline{\text{CIUCL}}$ tests and their respective "viscosity jumps" [adapted from Lira (1988)].

pressures (Δu) also form homothetic geometric figures. The paths followed on the plane $s' \times e$ (lower part of Figure 33) start on the virgin isotropic compression line (VICL), on the floor of the $s' \times t' \times e$ space, and develop on planes for which e = constant. Paths on plane $s' \times e$ start from points $\boldsymbol{A}_1$, $\boldsymbol{A}_2$ and $\boldsymbol{A}_3$ and instantaneously move to the right to points $\boldsymbol{B}_1$, $\boldsymbol{B}_2$ and $\boldsymbol{B}_3$, respectively, forming the viscosity jumps $\boldsymbol{A}_1\boldsymbol{B}_1$, $\boldsymbol{A}_2\boldsymbol{B}_2$ and $\boldsymbol{A}_3\boldsymbol{B}_3$. Along the segments $\boldsymbol{A}_1\boldsymbol{B}_1$, $\boldsymbol{A}_2\boldsymbol{B}_2$ and $\boldsymbol{A}_3\boldsymbol{B}_3$ there is neither shear strain nor pore pressure generation. From points $\boldsymbol{B}_1$, $\boldsymbol{B}_2$ and $\boldsymbol{B}_3$ on, shear strains begin to be developed, the frictional resistance begins to be mobilized and there is pore pressure generation. Specimens fail when points $\boldsymbol{C}_1$, $\boldsymbol{C}_2$ and $\boldsymbol{C}_3$ are reached, on the failure envelope. In the space $p' \times q' \times v$ (where v is the specific volume, $v = 1 + e$), points $\boldsymbol{C}_1$, $\boldsymbol{C}_2$ and $\boldsymbol{C}_3$ are on a critical state line corresponding to the same strain rate $\dot{\varepsilon}_t$ used in the three tests.

According to Equation 47, for a given clay and for a given point (e, p'_e) on the VICL, the "viscosity jump" $\mathbb{V}$ would be proportional to the distortion rate $\dot{\gamma}$. Nevertheless, experimental results have been shown that viscous resistance is not proportional to $\dot{\gamma}$. Thus, it is more correct to rewrite the viscous resistance parameter $\mathbb{V}$ as a non-linear function f of the distortion rate, or rather

$$\mathbb{V} = \eta(e) f(\dot{\gamma}) \tag{59}$$

being f an exclusive function of the distortion rate $(\dot{\gamma})$ and not of the angle α, which indicates the plane considered. Then, for e and $\dot{\gamma}$ as constants, $\mathbb{V} = \eta(e) f(\dot{\gamma})$ is also a constant. Thus, Equation 46 can be rewritten as:

$$\tau_{\eta\alpha} = \eta(e) f\left[\frac{d(\varepsilon_a - \varepsilon_r)}{dt}\right] sin\,2\alpha = \eta(e) f(\dot{\gamma}) sin\,2\alpha \tag{60}$$

Thus, in a test where $\dot{\gamma}$ = constant, $f(\dot{\gamma})$ = constant and, therefore, both the viscosity ellipse, whose half of minor axis corresponds to $\mathbb{V} = \eta(e) f(\dot{\gamma})$, and the friction ellipse remain valid. The only difference is that the viscous resistance does not follow Newton's law of viscosity, or rather viscous resistance in plastic soils is non-newtonian. Furthermore, Equations 52 to 56 remain valid since derivatives are taken respective to angle α with the aim of determining $tan\,\phi'_{emob}$. Thus, Equation 56 still holds valid.

Regardless of function type, the viscous resistance component $\mathbb{V}$ must have the physical dimension of stress. Experimental data suggest that for normally consolidated clays the "viscosity jump" $\mathbb{V}$ is proportional to the isotropic consolidation stress p'_e, a feature that had already been identified by Taylor (1948, pp. 377-378). Such a feature can be observed for two clays in Figures 34 and 35.

Based on these experimental evidences, it can be written as

$$\mathbb{V} = \eta(e) f(\dot{\gamma}) = C_\eta(\dot{\gamma}) p'_e \tag{61}$$

Thus, viscous resistance $\mathbb{V}$, geometrically identified by the "viscosity jump", can be written as a linear function of p'_e, whose coefficient C_η is a non – linear function of the distortion rate $\dot{\gamma}$ (and also of the soil structure).

The viscosity jumps $\boldsymbol{A_1B_1}$, $\boldsymbol{A_2B_2}$ and $\boldsymbol{A_3B_3}$ in Figures 33 to 35 do not always appear clearly. The author does not know how to explain precisely the reason for that. The author believes that some of the possible reasons are the filter paper and porous stones adjustments, the non-coaxiality between the piston and the specimen axes, the silicone grease when lubricated ends are used, etc. Even when the same equipment, the same soil, the same specimen preparation and the same test procedures are used, sometimes the viscosity jump clearly appears and other times it does not. Although this issue will not be discussed here, it is a practical aspect that deserves more investigation.

7. A model of behaviour for saturated normally consolidated clays taking into account strain rate in $\overline{\text{CIUCL}}$ tests

7.1 Normalization of $s' \times t'$, $t' \times \varepsilon_t$ and $\Delta u \times \varepsilon_t$ curves

This work is supported by experimental evidences and basic hypotheses.

The experimental evidences, which are also considered as hypotheses, are as follows:

1. Normally consolidated, saturated specimens of a given clay consolidated to different isotropic stresses p'_e in $\overline{\text{CIUCL}}$ tests and sheared with the same $\dot{\varepsilon}_t = \dot{\gamma}/2 = \text{constant}$ show geometrically similar curves $t' \times \varepsilon_t$ and $\Delta u \times \varepsilon_t$. They also show homothetic $p' \times q'$ and $s' \times t'$ effective stress paths with origin as the centre of homothety. This is to say: for a fixed strain rate $\dot{\varepsilon}_t$ the clay exhibit normalized behaviour respective to p'_e.
2. For a given strain rate $\dot{\varepsilon}_t$, the ordered triples (p'_f, q'_f, v_f) with subscripts *f* denoting failure define a smooth curve in the (p', q', v) space called the critical state line (CSL) associated with that given strain rate $\dot{\varepsilon}_t$. For each strain rate there is only one corresponding CSL.
3. The projection of a CSL associated with a fixed $\dot{\varepsilon}_t$ on the planes $p' \times q'$ and $s' \times t'$ is a straight line passing through the origin.

The basic hypotheses are the following:

4. Validity of PES equation: $\sigma' = \sigma - u$.
5. At any instant the shear stress τ_α acting on plane whose normal makes an angle α with the direction of σ_1 consists of two parts: a friction part $\tau_{\phi\alpha}$ and a viscous part $\tau_{\eta\alpha}$, or rather $\tau_\alpha = \tau_{\phi\alpha} + \tau_{\eta\alpha}$.
6. The viscous part $\tau_{\eta\alpha}$ is written as $\tau_{\eta\alpha} = \eta(e) f(\dot{\gamma}) sin\, 2\alpha$, being $\eta(e)$ defined as the soil viscosity, a function of void ratio and structure, and $f(\dot{\gamma})$ an exclusive function of distortion rate $\dot{\gamma}$. On the plane whose normal makes 45º with the direction of σ_1, $2\alpha = 90°$ and $\tau_{\eta 45°} = \eta(e) f(d(\varepsilon_1 - \varepsilon_3)/dt) = \eta(e) f(\dot{\gamma}) = \mathbb{V}$.
7. The friction part on a plane whose normal makes an angle α with the direction of σ_1 corresponds to $\tau_{\phi\alpha} = \tau - \tau_{\eta\alpha} = \left[(\sigma'_1 - \sigma'_3)/2 - \mathbb{V}\right] sin\, 2\alpha$.
8. The couples $(\sigma'_\alpha, \tau_{\eta\alpha})$ define the *state of mobilized viscosity* of a soil, which is represented by the viscosity ellipse. The couples $(\sigma'_\alpha, \tau_{\phi\alpha})$ define the *state of mobilized friction*, which is represented by the friction ellipse. The sum of these two ellipses corresponds to the Mohr's circle of effective stress and, therefore, they cannot exist separately since only the stresses given by the Mohr's circle meet equilibrium.
9. As a consequence of hypotheses (5) and (6), during the undrained shear stage of a $\overline{\text{CIUCL}}$ test carried out with $\dot{\varepsilon}_t = \text{constant}$, $\tau_{\eta\alpha}$ is instantaneously mobilized and remains constant up to the end of shear. During the undrained shear of a $\overline{\text{CIUCL}}$ test there is no volume change but only shear strains. Thus, the increase of the deviator stress along the undrained shear is due to the frictional resistance mobilization, which occurs due to the development of shear strains. Therefore, the failure process is ruled by the frictional resistance mobilization. For a given distortion γ, the frictional resistance is fully mobilized and failure occurs. This means that, in a normally consolidated clay, failure occurs when the friction ellipse touches the strength envelope, which is the straight line with slope $tan\,\phi'_e$, as illustrated in Figure 28. In other words, failure occurs when

$$tan\,\phi'_{emob} = \frac{\left(\frac{\sigma'_{1f} - \sigma'_{3f}}{2} - \mathbb{V}\right)}{\sqrt{\sigma'_{1f}\sigma'_{3f}}} = \frac{\left(t'_f - \mathbb{V}\right)}{\sqrt{s'^2_f - t'^2_f}} = tan\,\phi'_e \tag{62}$$

where subscript *f* indicates failure and ϕ'_e is the Hvorslev's "*true angle of internal friction*".

10. Finally, another hypothesis concerning viscous resistance $\mathbb{V}$, which comes from experimental evidences, is that $\mathbb{V}$ is proportional to isotropic consolidation stress p'_e. Thus, $\mathbb{V} = \eta(e) f(\dot{\gamma}) = C_\eta(\dot{\gamma})\, p'_e$ (see Equation 61 and Figures 34 and 35), being $C_\eta(\dot{\gamma})$ a non-linear function of distortion rate $\dot{\gamma}$ and of soil structure.

Although this article is limited to normally consolidated clays subjected to CIUCL tests, it is possible to extend the model presented herein to overconsolidated clays. Part of the ten items listed above can be viewed as an extension of Terzaghi's PES and make it possible to consider the influence of strain rate on a failure criterion which gathers concepts from Newton, Mohr, Coulomb, Terzaghi, Hvorslev, Taylor and Bjerrum. Such influence of strain rate occurs by means of Newton's viscosity concept, despite soils viscous resistance does not obey Newton's law of viscosity. In plastic soils the viscous resistance to shear comes from the distortion of viscous adsorbed water whenever two clay particles in contact are moving relative to each other (Terzaghi & Frölich, 1936; Terzaghi, 1941; Taylor, 1942; Taylor, 1948). Such viscous adsorbed water provides clayey soils with plasticity. It is for that reason that Bjerrum (1973) associates strain rate effects with plasticity index. Unfortunately, many times the viscous component of shear resistance is inadequately called "cohesion". As understood by Coulomb and explained by Schofield (1999, 2001), cohesion originates from cementation between grains, like in rocks and saprolites, providing materials with a tensile strength, which is a consequence of true cohesion, as discussed in section 4.1. Therefore, cohesion as defined by Coulomb has a different physical meaning from the "true cohesion" as defined by Hvorslev. Unfortunately, the expression "true cohesion" was used by Hvorslev (1937, 1960) and Terzaghi (1938) improperly, bringing the conceptual confusion raised up by Schofield (1999, 2001). In this article, the strain rate effect on the undrained shear strength is evaluated via viscous resistance originating from the action of adsorbed water on the behaviour of plastic soils.

Back to the geometric similarity in Figure 32 and to the homothety of the ESPs in Figure 33, the curves $t' \times \varepsilon_t$ and $\Delta u \times \varepsilon_t$ and ESPs $s' \times t'$ can be scaled by division by p'_e. Thereby, the normalized curves $(t'/p'_e) \times \varepsilon_t$ and $(\Delta u/p'_e) \times \varepsilon_t$ and the normalized ESPs $(s'/p'_e) \times (t'/p'_e)$ in Figure 36 are obtained, provided the strain rate $\dot{\boldsymbol{\varepsilon}}_{\boldsymbol{t}}$ is the same and kept constant for all tests.

The straight line with slope $tan\,\phi'$ passing through the origin, shown in Figures 15 and 28, is the strength envelope for a normally consolidated clay on the $\tau \times \sigma'$ plane. According to the approach herein developed, such an envelope includes two strength components: the frictional component and the viscous component. Moreover, as stated in experimental

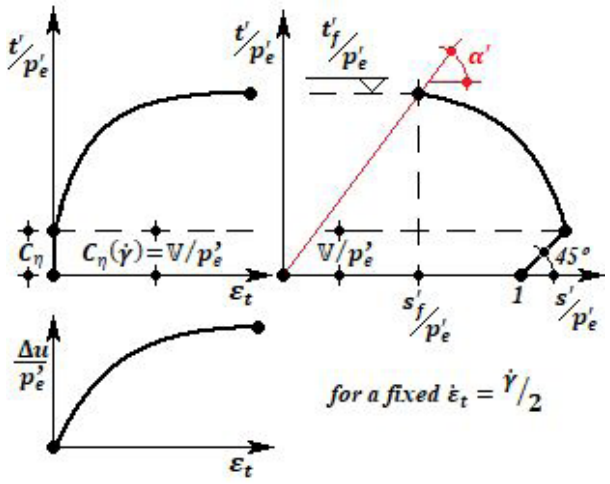

Figure 36. Normalized curves $(t'/p'_e) \times \varepsilon_t$ and $(\Delta u/p'_e) \times \varepsilon_t$ and normalized ESPs $(s'/p'_e) \times (t'/p'_e)$ for a fixed strain rate $\dot{\varepsilon}_t$.

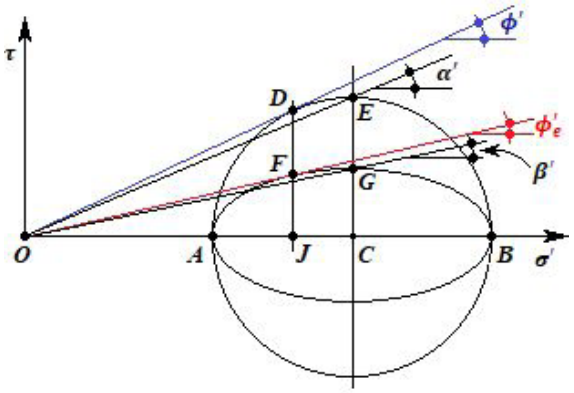

Figure 37. Definition of angles α', β', ϕ' and ϕ'_e.

evidence (1) of this section, for a fixed strain rate $\dot{\varepsilon}_t$, all ESPs on the $s' \times t'$ plane are homothetic with the origin as the centre of homothety. However, according to hypothesis (9), failure is not determined when the Mohr's circle of effective stresses touches the envelope with slope $tan\,\phi'$, but when the friction ellipse touches the straight line whose slope is $tan\,\phi'_e$, being ϕ'_e the Hvorslev's true angle of internal friction, which is a property of the soil. Thus, the question to be answered is: how can one explain and conciliate the envelope with slope $tan\,\phi'$, which gives the real strength of the soil, and the envelope whose slope is $tan\,\phi'_e$, by which failure is ruled? To answer this question, one must take into account the experimental evidences and basic hypotheses listed in the beginning of this section as well as the following discussion based on Figure 37.

From Figure 37 it immediately follows that points ***D*** and ***F*** lie on the same vertical straight line since ellipse ***AFGB*** can be obtained from a rotation of Mohr's circle

ADEB around the σ' axis of an angle $\theta = arc\ \cos\left(\boldsymbol{CG / CE}\right)$. Moreover, since normalization respective to p'_e holds valid, Figure 37 could be drawn using for abscissas and ordinates the normalized parameters s' / p'_e and t' / p'_e, respectively. Accordingly, one can go back to Figure 36 and write:

$$t'_f / p'_e = \left(s'_f / p'_e\right) tan\,\alpha' \tag{63}$$

Owing to the homothety of tests results carried out with $\dot{\gamma} = \text{constant}$, one comes to the conclusion that, for a given normally consolidated clay, when $\dot{\gamma}$ is fixed, the s'_f / p'_e and t'_f / p'_e values will automatically be determined, or rather $\left(s'_f / p'_e\right) = f_1\left(\dot{\gamma}\right)$ and $\left(t'_f / p'_e\right) = f_2\left(\dot{\gamma}\right)$, being f_1 and f_2 exclusive functions of $\dot{\gamma}$. Now recalling the hypothesis which assumes that shear stress consists of a frictional component and a viscous component, one can write that at failure

$$t'_f = s'_f\, tan\,\beta' + \mathbb{V} \tag{64}$$

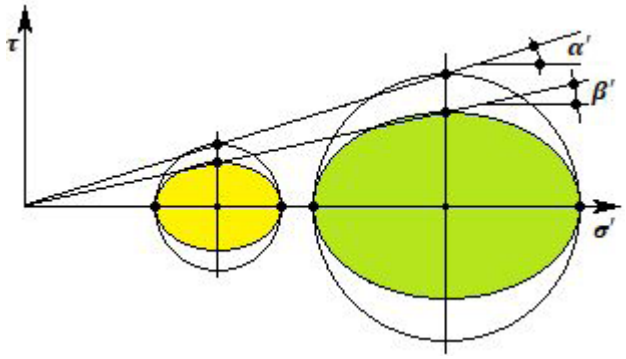

Figure 38. Homothetic (same eccentricity) friction ellipses at failure.

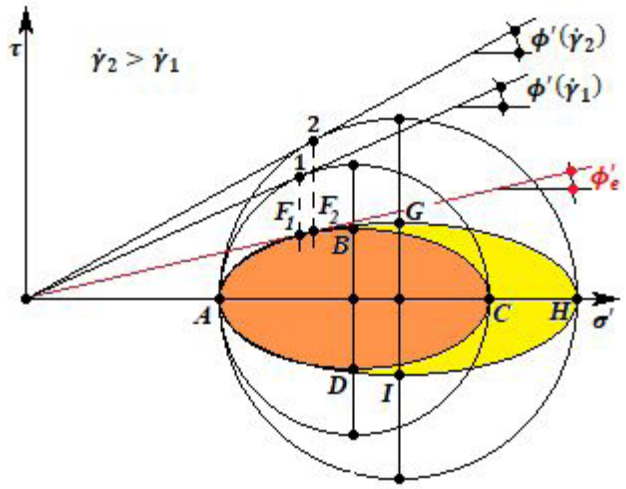

Figure 39. Friction ellipses at failure with different eccentricities, both tangent to the same failure envelope of slope $tan\,\phi'_e$, resulting from CIUCL tests with different distortion rates $\dot{\gamma}$.

Dividing both sides of Equation 64 by p'_e, Equation 65 is obtained as follows:

$$t'_f / p'_e = \left(s'_f / p'_e\right) tan\,\beta' + \mathbb{V} / p'_e \tag{65}$$

However, as $\left(s'_f / p'_e\right) = f_1\left(\dot{\gamma}\right)$, $\left(t'_f / p'_e\right) = f_2\left(\dot{\gamma}\right)$ and, according to Equation 61, $\mathbb{V} / p'_e = C_\eta\left(\dot{\gamma}\right)$, Equation 65 can be rewritten as

$$f_2\left(\dot{\gamma}\right) = f_1\left(\dot{\gamma}\right) tan\,\beta' + C_\eta\left(\dot{\gamma}\right) \tag{66}$$

or

$$tan\,\beta' = \frac{f_2\left(\dot{\gamma}\right) - C_\eta\left(\dot{\gamma}\right)}{f_1\left(\dot{\gamma}\right)} \tag{67}$$

Equation 67 leads to the conclusion that, assuming shear resistance consists of a frictional component and a viscous component, whenever a given normally consolidated clay, sheared with $\dot{\gamma} = \text{constant}$ in a CIUCL test, presents homothetic ESPs, friction ellipses at failure will be homothetic, or rather they will have the same eccentricity, as shown in Figure 38.

When two or more specimens of the same clay are normally consolidated to the same isotropic stress in CIUCL tests, but sheared with different distortion rates, for instance, $\dot{\gamma}_2 > \dot{\gamma}_1$, the friction angle $\phi'\left(\dot{\gamma}_2\right)$ will be greater than the friction angle $\phi'\left(\dot{\gamma}_1\right)$ (see Figure 39). In this case, the friction ellipse at failure ***AGHI*** will present a greater eccentricity than that of the friction ellipse at failure ***ABCD***. The Mohr's circle of effective stresses at failure corresponding to the test carried out with $\dot{\gamma}_2$ will be larger than that obtained from the test carried out with $\dot{\gamma}_1$. However, both friction ellipses at failure will be tangent to the friction envelope at points $\boldsymbol{F_1}$ and $\boldsymbol{F_2}$. This friction envelope, which is unique for a given normally consolidated clay, is the straight line passing through the origin with slope $tan\,\phi'_e$. Thus, any CIUCL test carried out on the same normally consolidated clay, irrespective of the distortion rate $\dot{\gamma}$ and irrespective of p'_e, will present at failure a friction ellipse which will be tangent to the straight line envelope whose slope is $tan\,\phi'_e$.

7.2 Strain rate effects – additional experimental evidences

In order to quantify the strain rate in the shear stage of a CIUCL test, the variable $\dot{\varepsilon}_t$ will be used from now on. Recalling that as $\varepsilon_t = \left(\varepsilon_a - \varepsilon_r\right)/2$ or $\varepsilon_t = \left(\gamma / 2\right)$ and that during the shear stage of a CIUCL test there is no volume change, one concludes that $\varepsilon_t = \left(3/4\right)\varepsilon_a$, which entails that $\dot{\varepsilon}_t = \left(3/4\right)\dot{\varepsilon}_a$.

Lacerda (1976) carried out a set of CIUCL tests on San Francisco Bay Mud samples, applying different strain rates in the undrained shear phase, during which stress

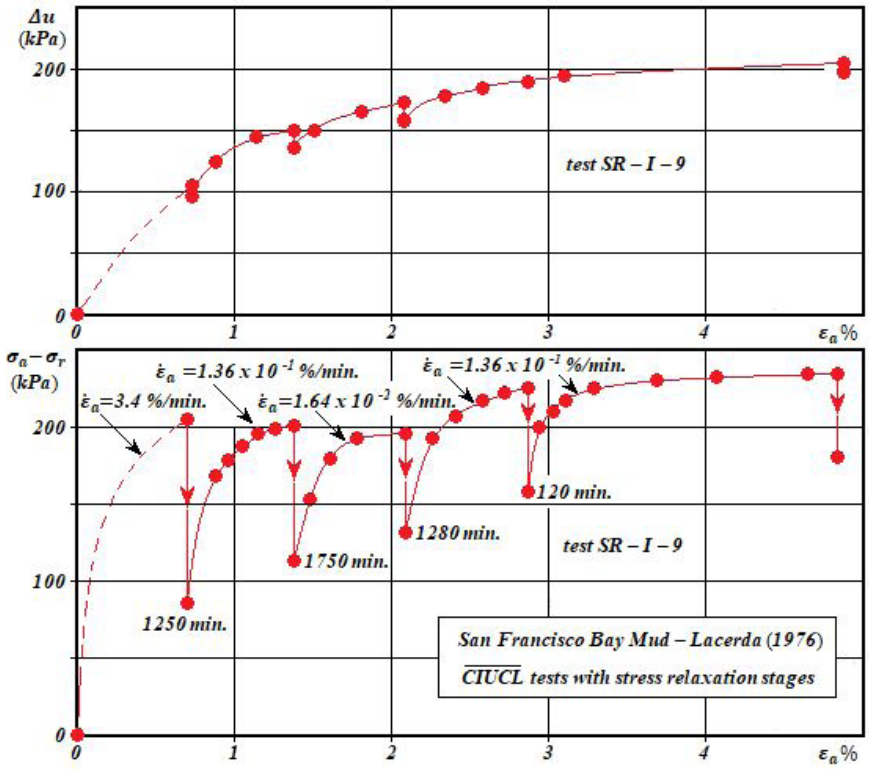

Figure 40. $\overline{\text{CIUCL}}$ test with different strain rates and stress relaxation stages.

relaxation stages were accomplished (see Figure 40). Such stress relaxation stages consist in turning off the load frame motor during the undrained shear phase, for a given time interval, monitoring deviator stress and pore pressure over time.

With the load frame motor turned off, $\dot{\varepsilon}_t$ becomes zero and, therefore, during a stress relaxation stage carried out in the undrained shear phase of a $\overline{\text{CIUCL}}$ test, both volume and shear strains changes are zero. This kind of test, usually called stress relaxation test, would more properly be called $\overline{\text{CIUCL}}$ test with stress relaxation stages. Lacerda (1976) investigated strain rate effects by turning on the load frame motor after the end of the stress relaxation stages at different speeds. A typical result of such a test is shown in Figure 40.

The main features observed by Lacerda (1976), common to all $\overline{\text{CIUCL}}$ tests with stress relaxation stages carried out with different $\dot{\varepsilon}_t$ values on normally consolidated specimens from San Francisco Bay Mud, were the following:

a) The size of $\Delta u \times \varepsilon_t$ curves is proportional to the isotropic stress p'_e to which the specimen was consolidated.

b) For a given isotropic consolidation stress p'_e, the curve $\Delta u \times \varepsilon_t$ is unique, regardless of the shear strain rate $\dot{\varepsilon}_t$.

c) Tests with greater $\dot{\boldsymbol{\varepsilon}}_{\boldsymbol{t}}$ values present higher $(\sigma_a - \sigma_r)$ values for the same ε_t.

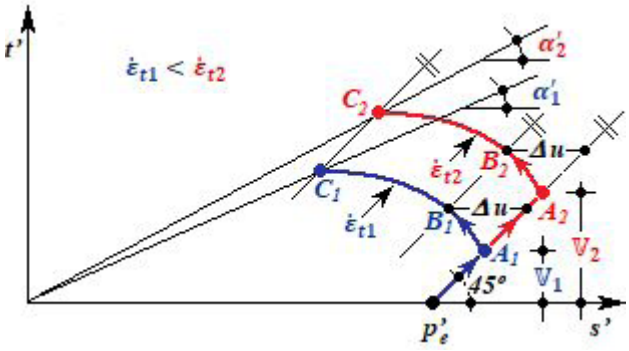

Figure 41. Effective stress paths for $\overline{\text{CIUCL}}$ tests starting out from the same p'_e but corresponding to different strain rates $\dot{\varepsilon}_{t1}$ and $\dot{\varepsilon}_{t2}$ with $\dot{\varepsilon}_{t1} < \dot{\varepsilon}_{t2}$.

d) The pore pressure decrease observed during stress relaxation stages are very small if compared to the deviator stress decrease.

Features b) and d) allow to assume, as an additional hypothesis, that pore pressure does not depend on the shear strain rate $\dot{\varepsilon}_t$, being only dependent on the shear strain ε_t and on the isotropic effective stress p'_e to which the specimen was consolidated. The assumption that pore pressure does

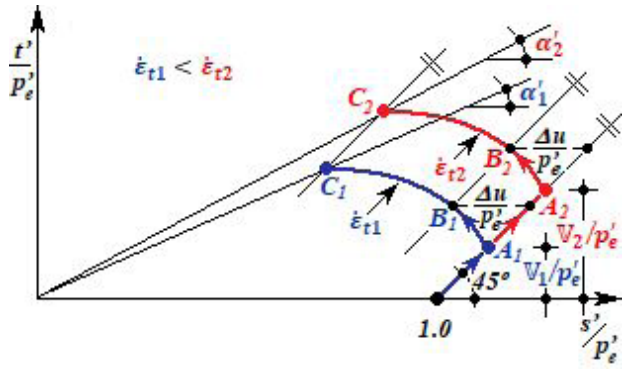

Figure 42. Normalized effective stress paths $\left(s'/p'_e\right)\times\left(t'/p'_e\right)$ for $\overline{\text{CIUCL}}$ tests corresponding to different strain rates $\dot{\varepsilon}_{t1}$ and $\dot{\varepsilon}_{t2}$ with $\dot{\varepsilon}_{t1}<\dot{\varepsilon}_{t2}$.

not depend on $\dot{\varepsilon}_t$ means that pore pressure will remain constant even during a stress relaxation stage, when $\dot{\varepsilon}_t=0$. This additional assumption, based on such experimental evidences, allows Figure 41 to be drawn.

Figure 41 shows that tests starting from the same isotropic effective stress p'_e, but carried out with different $\dot{\varepsilon}_t$ values, will present, after the viscosity jumps, ESPs which change their directions to the left, until they attain envelopes with different α' values. Nevertheless, as previously explained, all the states of fully mobilized friction are represented by their respective friction ellipses at failure, which are tangent to the same friction strength envelope whose slope is $tan\,\phi'_e$ (see Figure 39).

Taking into account that $tan\,\phi'_{emob}=\left(t'-\mathbb{V}\right)/\sqrt{s'^2-t'^2}$, it can be concluded that, at points $\boldsymbol{A}_1$ and $\boldsymbol{A}_2$ in Figure 41, $tan\,\phi'_{emob}=0$. In a similar way, at points $\boldsymbol{C}_1$ and $\boldsymbol{C}_2$, which represent failure, $tan\,\phi'_{emob}=tan\,\phi'_e$. Besides, experimental evidences indicate that, during $\overline{\text{CIUCL}}$ tests on two normally consolidated specimens of the same clay starting from the same p'_e, the following features are observed:

a) Pore pressure Δu does not depend on the shear strain rate $\dot{\varepsilon}_t$.
b) Pore pressure Δu does depend on the strain ε_t.

Thus, it is expected that points like $\boldsymbol{B}_1$ and $\boldsymbol{B}_2$ in Figure 41 have the same values of ε_t, Δu and $tan\,\phi'_{emob}$, irrespective of the shear strain rate $\dot{\varepsilon}_t$. This working hypothesis, whose validity must be checked experimentally, may be presented in the *complementary principle 1*, as stated below:

Complementary principle 1: All $\overline{\text{CIUCL}}$ tests carried out on a given normally consolidated clay compressed to the same isotropic effective stress p'_e will present, for any fixed shear strain ε_t, the same pore pressure Δu and the same ϕ'_{emob}, provided the points taken from the several ESPs (each ESP corresponding to a different $\dot{\varepsilon}_t$) lie on the same 45° sloped straight line. In other words: points of intersection between a 45° sloped straight line and ESPs corresponding to different shear strain rates $\dot{\varepsilon}_t$ have the same ε_t, Δu and ϕ'_{emob} (see points $\boldsymbol{B}_1$ and $\boldsymbol{B}_2$ in Figure 41).

It should be added that, in $\overline{\text{CIUCL}}$ tests carried out with the same $\dot{\varepsilon}_t$, the curves $t'\times\varepsilon_t$ and $\Delta u\times\varepsilon_t$ and ESPs can be normalized with respect to p'_e. This means that, for $\overline{\text{CIUCL}}$ tests carried out with the same $\dot{\varepsilon}_t$, the curves $t'/p'_e\times\varepsilon_t$, $\Delta u/p'_e\times\varepsilon_t$ and the normalized ESPs in the plane $\left(s'/p'_e\right)\times\left(t'/p'_e\right)$ will also be unique. However, if the pore pressure during $\overline{\text{CIUCL}}$ tests is not affected by the shear strain rate $\dot{\varepsilon}_t$, the curves $\Delta u/p'_e\times\varepsilon_t$ will be unique, irrespective of the $\dot{\varepsilon}_t$ value. Thus, Figure 41 can be redrawn in the $\left(s'/p'_e\right)\times\left(t'/p'_e\right)$ plane and pore pressure can also be normalized with respect to p'_e, as shown in Figure 42.

7.3 Strain rate effects – basic curves

In order to generalize the concepts presented in section 7.2, two $\overline{\text{CIUCL}}$ tests carried out on a normally consolidated clay will now be considered, both starting from the same isotropic effective stress p'_e. In one of these tests $\dot{\varepsilon}_t\neq 0$ whereas in the other $\dot{\varepsilon}_t=0$. It is obvious that a real $\overline{\text{CIUCL}}$ test cannot be carried out with $\dot{\varepsilon}_t=0$. However, assuming valid the *complementary principle 1*, the curves $t'\times\varepsilon_t$ and $\Delta u\times\varepsilon_t$ and the ESP on the $s'\times t'$ plane, all corresponding to $\dot{\varepsilon}_t=0$, can be obtained from the curves $t'\times\varepsilon_t$ and $\Delta u\times\varepsilon_t$ and the ESP on the $s'\times t'$ plane achieved from a test carried out with $\dot{\varepsilon}_t\neq 0$. That is what will be explained next.

The name *basic curves* (denoted by the subscript b in the parameters s' and t' as s'_b and t'_b) will be given to all curves corresponding to $\dot{\varepsilon}_t=0$. Such basic curves can be drawn from the tests carried out with $\dot{\varepsilon}_t\neq 0$ subtracting the viscous resistance effects.

The main advantage of plotting basic curves is that they are free from viscous effects and, therefore, they are not dependent on the shear strain rate $\dot{\varepsilon}_t$. Thus, such basic curves only give the effects of the frictional resistance.

Figure 43 shows the curves $t'\times\varepsilon_t$ and $\Delta u\times\varepsilon_t$ and the ESP on the $s'\times t'$ plane for a given p'_e and a given $\dot{\varepsilon}_t\neq 0$. The basic curves $t'_b\times\varepsilon_t$ and $\Delta u\times\varepsilon_t$ and the ESP $t'_b\times s'_b$ for the same p'_e and $\dot{\varepsilon}_t=0$ are also shown in Figure 43. The effective stress path for which $\dot{\varepsilon}_t=0$ will be called *basic effective stress path* and denoted by bESP.

In Figure 43 the curve $t'\times\varepsilon_t$ and the ESP of the test carried out with $\dot{\varepsilon}_t\neq 0$ show the initial jump ***AB*** corresponding to the instantaneous mobilization of the viscous resistance. From point ***B*** on, the test carried out with $\dot{\varepsilon}_t\neq 0$ begins to develop shear strains ε_t and pore pressures Δu, with friction mobilization, following the curves ***BYN***, until failure is reached at point ***N***. The basic curves, corresponding to $\dot{\varepsilon}_t=0$, do not show the initial jump since for $\dot{\varepsilon}_t=0$ the

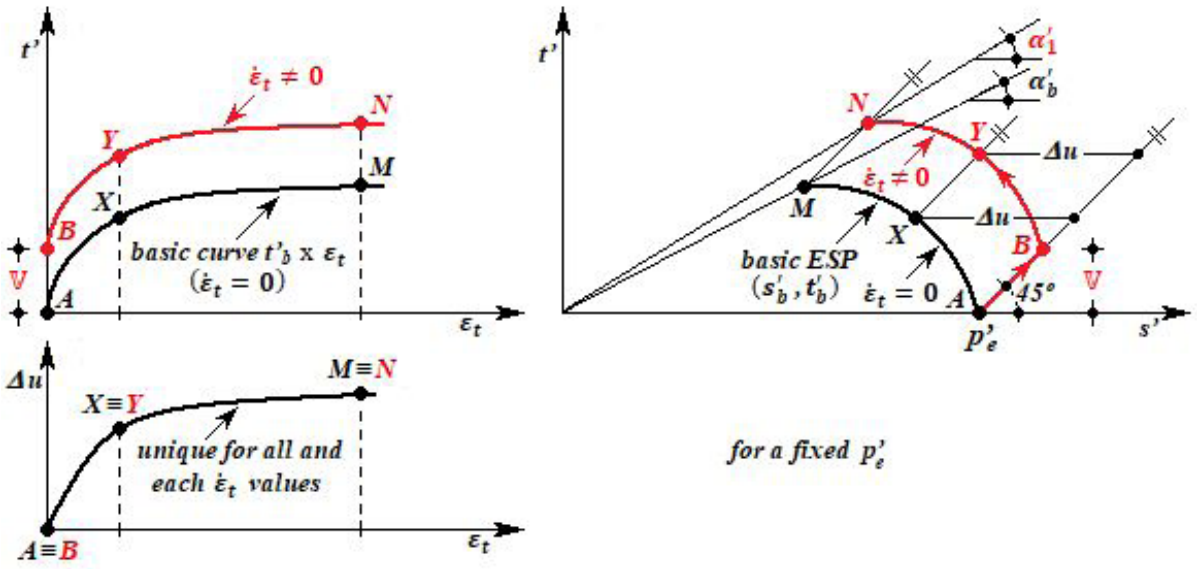

Figure 43. $\overline{\text{CIUCL}}$ tests carried out with a fixed p'_e and $\dot{\varepsilon}_t \neq 0$ and $\dot{\varepsilon}_t = 0$ (basic curves).

viscous resistance vanishes. Thus, when $\dot{\varepsilon}_t = 0$, there is only friction mobilization, which occurs as soil is deformed in shear along the curves ***AXM***.

Another feature which is worth noting in Figure 43 is that for a given p'_e the curve $\Delta u \times \varepsilon_t$ is unique since pore pressure is assumed to be not dependent on $\dot{\varepsilon}_t$. Recalling that this is an assumption based on experimental evidences, as shown in Figure 40.

The relationship between the coordinates of point ***Y*** which lies on the ESP associated with a fixed $\dot{\varepsilon}_t \neq 0$ and the coordinates of point ***X*** which lies on the bESP (associated with $\dot{\varepsilon}_t = 0$), both points lying on the same 45º sloped straight line, can now be derived considering Figure 44.

In Figure 44 the ESP defined by points ***BYN*** corresponds to the shear stage of a $\overline{\text{CIUCL}}$ test carried out with a fixed $\dot{\varepsilon}_t \neq 0$. The coordinates of points ***B***, ***Y*** and ***N*** are $\left(s'(\boldsymbol{B}), t'(\boldsymbol{B})\right)$, $\left(s'(\boldsymbol{Y}), t'(\boldsymbol{Y})\right)$ and $\left(s'(\boldsymbol{N}), t'(\boldsymbol{N})\right)$ respectively. On the other hand, the bESP, corresponding to a $\overline{\text{CIUCL}}$ test carried out with $\dot{\varepsilon}_t = 0$, is the curve defined by points ***A***, ***X*** and ***M***, whose coordinates are, respectively, $\left(s'_b(\boldsymbol{A}), t'_b(\boldsymbol{A})\right)$, $\left(s'_b(\boldsymbol{X}), t'_b(\boldsymbol{X})\right)$ and $\left(s'_b(\boldsymbol{M}), t'_b(\boldsymbol{M})\right)$. According to the *complementary principle 1*, points ***Y*** and ***X*** which lie on the same 45º sloped straight line have the same values of $tan\phi'_{emob}$, that is:

$$tan\phi'_{emob}(\boldsymbol{Y}) = \frac{t'(\boldsymbol{Y}) - \mathbb{V}}{\sqrt{\left(s'(\boldsymbol{Y})\right)^2 - \left(t'(\boldsymbol{Y})\right)^2}} =$$

$$tan\phi'_{emob}(\boldsymbol{X}) = \frac{t'_b(\boldsymbol{X})}{\sqrt{\left(s'_b(\boldsymbol{X})\right)^2 - \left(t'_b(\boldsymbol{X})\right)^2}} \qquad (68)$$

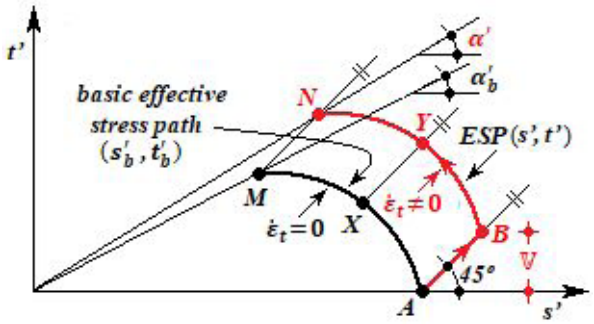

Figure 44. Relationship between coordinates of a point ***Y*** on the ESP for a fixed $\dot{\varepsilon}_t \neq 0$ and coordinates of a corresponding point ***X*** on the bESP (associated with $\dot{\varepsilon}_t = 0$).

Besides,

$$\frac{t'(\boldsymbol{Y}) - t'_b(\boldsymbol{X})}{s'(\boldsymbol{Y}) - s'_b(\boldsymbol{X})} = 1 \qquad (69)$$

Particularly, for points ***A*** and ***B***,

$$tan\phi'_{emob}(\boldsymbol{B}) = tan\phi'_{emob}(\boldsymbol{A}) = 0 \qquad (70)$$

and for points ***N*** and ***M***, corresponding to failure,

$$tan\phi'_{emob}(\boldsymbol{N}) = tan\phi'_{emob}(\boldsymbol{M}) = tan\phi'_e \qquad (71)$$

From the coordinates of points ***Y*** that define the ESP of a real $\overline{\text{CIUCL}}$ test carried out with a fixed $\dot{\varepsilon}_t \neq 0$, the coordinates of points ***X*** that define the bESP can be determined (see Figures 44 and 45).

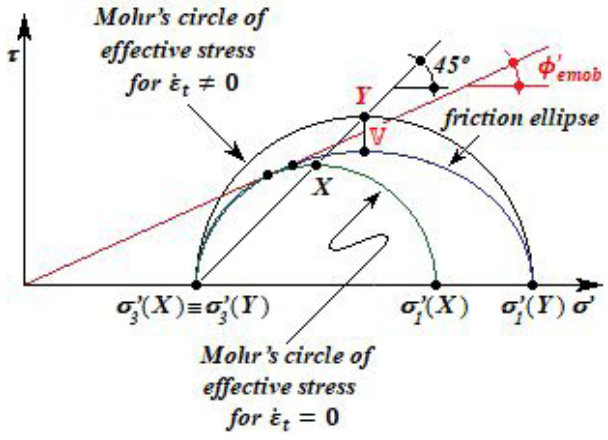

Figure 45. A point ***Y*** on the ESP of a $\overline{\text{CIUCL}}$ test carried out with $\dot{\varepsilon}_t \neq 0$ and its corresponding point ***X*** on the bESP (associated with $\dot{\varepsilon}_t = 0$).

Solving Equations 68 and 69 for t'_b and s'_b, Equations 72 to 75 are obtained:

$$t'_b = tan^2\phi'_{emob}\left(1+csc\,\phi'_{emob}\right)\left(s'-t'\right) \tag{72}$$

or

$$t'_b = \frac{\left(t'-\mathbb{V}\right)^2}{\left(s'+t'\right)}\left[1+\frac{\sqrt{s'^2+\mathbb{V}^2-2\mathbb{V}t'}}{\left(t'-\mathbb{V}\right)}\right] \tag{73}$$

and

$$s'_b = sec^2\phi'_{emob}\left(1+sin\,\phi'_{emob}\right)\left(s'-t'\right) \tag{74}$$

or

$$s'_b = \left(s'-t'\right)+\frac{\left(t'-\mathbb{V}\right)^2}{\left(s'+t'\right)}\left[1+\frac{\sqrt{s'^2+\mathbb{V}^2-2\mathbb{V}t'}}{\left(t'-\mathbb{V}\right)}\right] \tag{75}$$

Conversely, from the coordinates $\left(s'_b, t'_b\right)$ of points ***X*** of a bESP, one can determine the coordinates $\left(s', t'\right)$ of the corresponding points ***Y*** of an ESP of a $\overline{\text{CIUCL}}$ test whose viscous resistance $\mathbb{V}$ is known. This can be done by solving Equations 68 and 69 for s' and t', which gives:

$$s' = \mathbb{V}+\frac{s'^2_b}{\left(s'_b+t'_b\right)}+\frac{t'_b}{\left(s'_b+t'_b\right)}\sqrt{s'^2_b+2\mathbb{V}\left(s'_b+t'_b\right)} \tag{76}$$

and

$$t' = \mathbb{V}+\frac{t'^2_b}{\left(s'_b+t'_b\right)}+\frac{t'_b}{\left(s'_b+t'_b\right)}\sqrt{s'^2_b+2\mathbb{V}\left(s'_b+t'_b\right)} \tag{77}$$

In order to check Equations 76 and 77, one can compute s' and t' for point ***B*** in Figure 44, replacing s'_b and t'_b by $s'_b\left(\boldsymbol{A}\right)$ and $t'_b\left(\boldsymbol{A}\right)$, respectively, in Equations 76 and 77. Since, for point ***A***, $s'_b\left(\boldsymbol{A}\right) = p'_e$ and $t'_b\left(\boldsymbol{A}\right) = 0$, one obtains, for point ***B***, $s'\left(\boldsymbol{B}\right) = \mathbb{V} + p'_e$ and $t'\left(\boldsymbol{B}\right) = \mathbb{V}$. It can also be observed that, when $\mathbb{V} = 0$, $s' = s'_b$ and $t' = t'_b$.

The discussion above leads to the conclusion that, from the results of a $\overline{\text{CIUCL}}$ test carried out on a specimen of a given plastic soil isotropically consolidated to p'_e and sheared with a strain rate $\dot{\varepsilon}_t$ there is a viscous resistance featured by the parameter $\mathbb{V} = C_\eta\left(\dot{\varepsilon}_t\right)p'_e$. With a $\mathbb{V}$ value obtained from a $\overline{\text{CIUCL}}$ test carried out with a given $\dot{\varepsilon}_t \neq 0$ and starting from an isotropic effective stress p'_e, it is possible to draw the corresponding basic curve $t'_b \times \varepsilon_t$ and the bESP (see Figure 43). Thereafter, knowing the function $C_\eta\left(\dot{\varepsilon}_t\right)$ (not discussed in this article), one can predict the curve $t' \times \varepsilon_t$ and the ESP for a $\overline{\text{CIUCL}}$ test starting out from the same p'_e but carried out with any $\dot{\varepsilon}_t$.

7.4 General normalization and basic curves

Consider the ESPs of the four $\overline{\text{CIUCL}}$ tests shown in Figure 46. The test carried out with the strain rate $\dot{\varepsilon}_{t1}$ starts from point ***A*** under the isotropic effective stress p'_{e1} and fails at point ***D*** following the ESP ***ABCD***. Another test carried out with the same strain rate $\dot{\boldsymbol{\varepsilon}}_{\boldsymbol{t1}}$ starts from point ***E*** under the isotropic effective stress p'_{e2} and fails at point ***H*** following the ESP ***EFGH***. A third test carried out with a strain rate $\dot{\varepsilon}_{t2} > \dot{\varepsilon}_{t1}$ also starts from point ***E*** and fails at point ***K*** following the ESP ***EIJK***. Finally, an imaginary fourth test starting from point ***A*** is "carried out" with $\dot{\varepsilon}_t = 0$ and after following the ESP ***AXM*** it fails at point ***M***.

According to the *complementary principle 1*, all points on ESPs starting out from the same p'_e, irrespective of the strain rate $\dot{\varepsilon}_t$ imposed, will show the same shear strain ε_t, the same excess pore pressure Δu and the same ϕ'_{emob} provided they are all on the same 45º sloped straight line. This is the case of points ***X*** and ***C*** and ***G*** and ***J*** in Figure 46. Take, for instance, points ***G*** and ***J*** that are on the same 45º sloped straight line and on the ESPs starting from p'_{e2} (point ***E***) with strain rates $\dot{\varepsilon}_{t1}$ and $\dot{\varepsilon}_{t2}$, respectively. According to the *complementary principle 1*, $\varepsilon_t\left(\boldsymbol{G}\right) = \varepsilon_t\left(\boldsymbol{J}\right)$, $\Delta u\left(\boldsymbol{G}\right) = \Delta u\left(\boldsymbol{J}\right) = \Delta u_2$ and $tan\,\phi'_{emob}\left(\boldsymbol{G}\right) = tan\,\phi'_{emob}\left(\boldsymbol{J}\right)$. Similarly, $\varepsilon_t\left(\boldsymbol{X}\right) = \varepsilon_t\left(\boldsymbol{C}\right)$, $\Delta u\left(\boldsymbol{X}\right) = \Delta u\left(\boldsymbol{C}\right) = \Delta u_1$ and $tan\,\phi'_{emob}\left(\boldsymbol{X}\right) = tan\,\phi'_{emob}\left(\boldsymbol{C}\right)$.

Consider now the ESPs ***ABCD*** and ***EFGH*** in Figure 46, both associated with the same strain rate $\dot{\varepsilon}_{t1}$ but starting from different isotropic effective stresses p'_{e1} and p'_{e2}, respectively. As both ESPs are associated with the same strain rate $\dot{\varepsilon}_{t1}$, they are homothetic by hypothesis. Thus, the following equations hold valid for points ***C*** and ***G***:

$$\frac{s'\left(\boldsymbol{C}\right)}{p'_{e1}} = \frac{s'\left(\boldsymbol{G}\right)}{p'_{e2}} \tag{78}$$

and

$$\frac{t'\left(\boldsymbol{C}\right)}{p'_{e1}} = \frac{t'\left(\boldsymbol{G}\right)}{p'_{e2}} \tag{79}$$

The value of $tan\,\phi'_{emob}\left(\boldsymbol{G}\right)$ is given by

$$tan\,\phi'_{emob}\left(\boldsymbol{G}\right) = \frac{t'\left(\boldsymbol{G}\right)-\mathbb{V}_{12}}{\sqrt{\left(s'\left(\boldsymbol{G}\right)\right)^2-\left(t'\left(\boldsymbol{G}\right)\right)^2}} \tag{80}$$

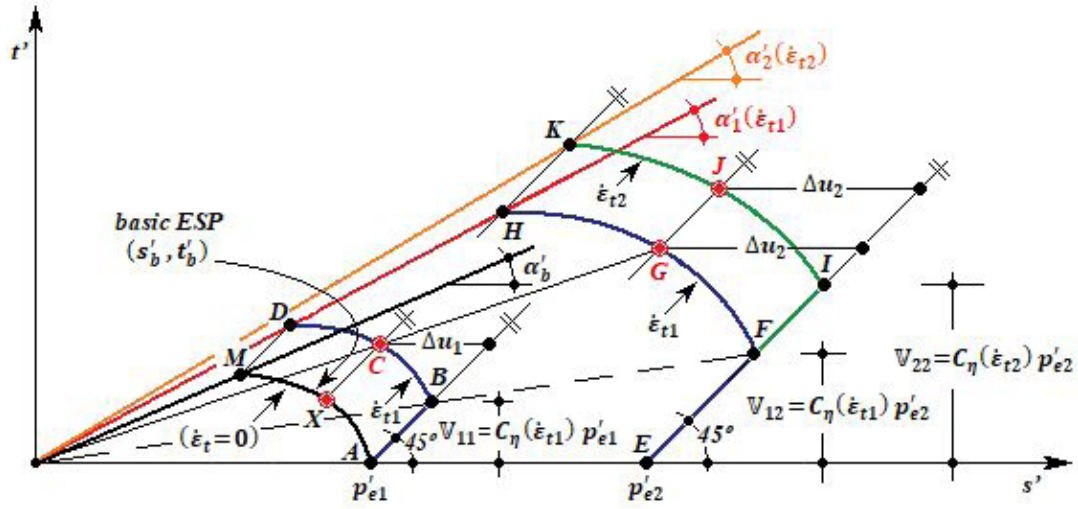

Figure 46. General normalization taking into account different values of p'_e and $\dot{\varepsilon}_t$.

Dividing both numerator and denominator of Equation 80 by p'_{e2}, one obtains:

$$tan\,\phi'_{emob}(\boldsymbol{G}) = \frac{\dfrac{t'(\boldsymbol{G})}{p'_{e2}} - \dfrac{\mathbb{V}_{12}}{p'_{e2}}}{\sqrt{\left(\dfrac{s'(\boldsymbol{G})}{p'_{e2}}\right)^2 - \left(\dfrac{t'(\boldsymbol{G})}{p'_{e2}}\right)^2}} \tag{81}$$

Replacing the values of $s'(\boldsymbol{G})/p'_{e2}$ and $t'(\boldsymbol{G})/p'_{e2}$ in Equation 81 by their respective values given by Equations 78 and 79 and recalling that $(\mathbb{V}_{12}/p'_{e2}) = (\mathbb{V}_{11}/p'_{e1}) = C_\eta(\dot{\varepsilon}_{t1})$, the following equation can be written:

$$tan\,\phi'_{emob}(\boldsymbol{G}) = \frac{\dfrac{t'(\boldsymbol{C})}{p'_{e1}} - \dfrac{\mathbb{V}_{11}}{p'_{e1}}}{\sqrt{\left(\dfrac{s'(\boldsymbol{C})}{p'_{e1}}\right)^2 - \left(\dfrac{t'(\boldsymbol{C})}{p'_{e1}}\right)^2}} \tag{82}$$

Multiplying numerator and denominator of the right hand side of Equation 82 by p'_{e1}, Equation 83 is obtained as shown below:

$$tan\,\phi'_{emob}(\boldsymbol{G}) = \frac{t'(\boldsymbol{C}) - \mathbb{V}_{11}}{\sqrt{\left(s'(\boldsymbol{C})\right)^2 - \left(t'(\boldsymbol{C})\right)^2}} \tag{83}$$

The right hand side of Equation 83 is the expression for $tan\phi'_{emob}(\boldsymbol{C})$. This leads to the conclusion that $tan\,\phi'_{emob}(\boldsymbol{G}) = tan\,\phi'_{emob}(\boldsymbol{J}) = tan\,\phi'_{emob}(\boldsymbol{C}) = tan\,\phi'_{emob}(\boldsymbol{X})$.

On the other hand, considering points ***C*** and ***G*** in Figure 46, both belonging to ESPs corresponding to the same strain rate $\dot{\varepsilon}_{t1}$, the following expression can be written:

$$\frac{\Delta u_1}{p'_{e1}} = \frac{\Delta u_2}{p'_{e2}} \tag{84}$$

Since for the same strain rate $\dot{\varepsilon}_{t1}$ the curve $\Delta u / p'_e \times \varepsilon_t$ is assumed to be unique, points ***C*** and ***G*** are assumed to have the same ε_t. On the other hand, it should be noted in Figure 46 that the ratio $(\Delta u_2 / p'_{e2})$ also holds for point ***J***, which belongs to an ESP whose strain rate is $\dot{\varepsilon}_{t2}$. It is worth recalling that points ***G*** and ***J*** belong to different ESPs departing from the same p'_{e2} but corresponding to the strain rates $\dot{\varepsilon}_{t1}$ and $\dot{\varepsilon}_{t2}$, respectively. However, for a fixed p'_e the pore pressure Δu does not depend on the strain rate $\dot{\varepsilon}_t$ (see hypothesis based on experimental evidences shown in section 7.2 – Figure 40). This leads to the conclusion that points ***X***, ***C***, ***G*** and ***J*** have the same values of ε_t, $(\Delta u / p'_e)$ and $tan\,\phi'_{emob}$. This conclusion, which comes from the *complementary principle 1* and the above reasoning, allows to redraw Figure 46 using the normalized parameters s'/p'_e and t'/p'_e for coordinate axes, as shown in Figure 47. Figure 47 shows that, although points ***X***, ***C***, ***G*** and ***J*** belong to distinct normalized ESPs associated with different strain rates $\dot{\varepsilon}_t$, they lie on the same 45º sloped straight line.

The discussion presented above leads to the generalization of the *complementary principle 1*, which can be stated as follows:

Generalized complementary principle 1: During undrained shear of CIUCL tests carried out on normally consolidated clay specimens, points on the plane $(s'/p'_e)\times(t'/p'_e)$ ***corresponding to the intersections of a given 45º sloped straight line and the several ESPs, each one associated with a different*** $\dot{\varepsilon}_t$ ***value, will show, whatever the shear strain rate*** $\dot{\varepsilon}_t$ ***is, the same values of*** ε_t, $(\Delta u / p'_e)$, ***and*** $tan\,\phi'_{emob}$ (see Figure 47 – section 7.4).

The *generalized complementary principle 1* leads to three corollaries, namely:

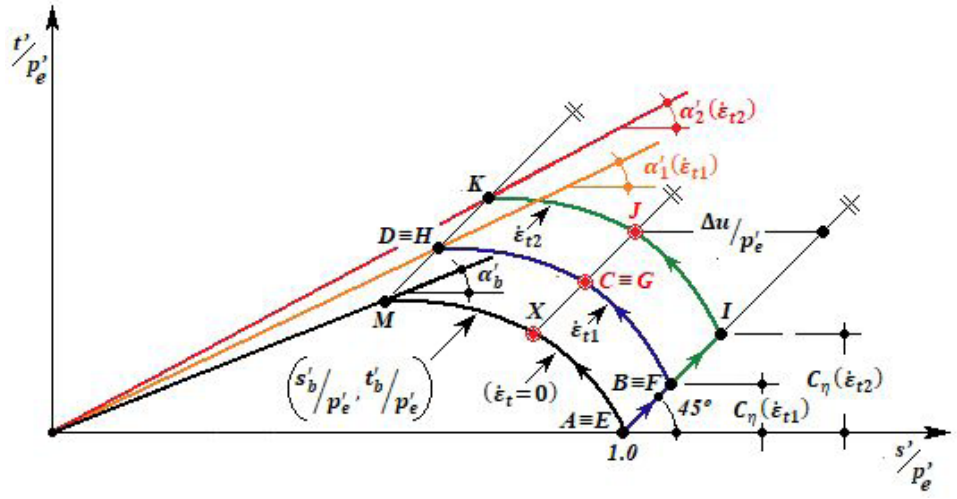

Figure 47. Normalized effective stress paths $s' / p'_e \times t' / p'_e$ for different strain rates $(\dot{\varepsilon}_t)$.

Corollary 1: ***$\overline{CIUCL}$ tests carried out on a normally consolidated clay showing homothetic ESPs for any fixed $\dot{\varepsilon}_t$ and a unique curve $\Delta u / p'_e \times \varepsilon_t$, irrespective of $\dot{\varepsilon}_t$, will show a unique basic curve $t'_b / p'_e \times \varepsilon_t$, whatever $\dot{\varepsilon}_t$ is.***

Corollary 1 can be demonstrated as follows:

According to the *generalized complementary principle 1* (see Figure 47), $\varepsilon_t(\boldsymbol{X}) = \varepsilon_t(\boldsymbol{C}) = \varepsilon_t(\boldsymbol{G}) = \varepsilon_t(\boldsymbol{J})$ and $tan\,\phi'_{emob}(\boldsymbol{G}) = tan\,\phi'_{emob}(\boldsymbol{J}) = tan\,\phi'_{emob}(\boldsymbol{C}) = tan\,\phi'_{emob}(\boldsymbol{X})$. Thus, Equation 83 can be rewritten as

$$tan\,\phi'_{emob}(\boldsymbol{X}) = tan\,\phi'_{emob}(\boldsymbol{C}) = tan\,\phi'_{emob}(\boldsymbol{G}) = tan\,\phi'_{emob}(\boldsymbol{J}) = \frac{t'_b(\boldsymbol{X})}{\sqrt{s'^2_b(\boldsymbol{X}) - t'^2_b(\boldsymbol{X})}} \tag{85}$$

Taking into account Figure 46, Equation 72 can be applied to points ***X*** and ***C***, which are on the same 45º sloped straight line, obtaining Equation 86:

$$t'_b(\boldsymbol{X}) = tan^2\phi'_{emob}(\boldsymbol{C})\left[1 + csc\,\phi'_{emob}(\boldsymbol{C})\right]\left[s'(\boldsymbol{C}) - t'(\boldsymbol{C})\right] \tag{86}$$

Dividing both sides of Equation 86 by p'_{e1}, Equation 87 is obtained:

$$\frac{t'_b(\boldsymbol{X})}{p'_{e1}} = tan^2\phi'_{emob}(\boldsymbol{C})\left[1 + csc\,\phi'_{emob}(\boldsymbol{C})\right]\left[\frac{s'(\boldsymbol{C})}{p'_{e1}} - \frac{t'(\boldsymbol{C})}{p'_{e1}}\right] \tag{87}$$

Besides the fact that $tan\,\phi'_{emob}(\boldsymbol{C}) = tan\,\phi'_{emob}(\boldsymbol{G})$, ***C*** and ***G*** are points from tests carried out with the same $\dot{\varepsilon}_t = \dot{\varepsilon}_{t1}$ (see Figure 46) but consolidated to isotropic stresses p'_{e1} and p'_{e2}, respectively. This leads to Equation 88:

$$\frac{s'(\boldsymbol{C})}{p'_{e1}} - \frac{t'(\boldsymbol{C})}{p'_{e1}} = \frac{s'(\boldsymbol{G})}{p'_{e2}} - \frac{t'(\boldsymbol{G})}{p'_{e2}} \tag{88}$$

Replacing $\phi'_{emob}(\boldsymbol{C})$ by $\phi'_{emob}(\boldsymbol{G})$ and $\left[s'(\boldsymbol{C}) / p'_{e1} - t'(\boldsymbol{C}) / p'_{e1}\right]$ by its equivalent value $\left[s'(\boldsymbol{G}) / p'_{e2} - t'(\boldsymbol{G}) / p'_{e2}\right]$ in Equation 87, Equation 89 is obtained as follows:

$$\frac{t'_b(\boldsymbol{X})}{p'_{e1}} = tan^2\phi'_{emob}(\boldsymbol{G})\left[1 + csc\,\phi'_{emob}(\boldsymbol{G})\right]\left[\frac{s'(\boldsymbol{G})}{p'_{e2}} - \frac{t'(\boldsymbol{G})}{p'_{e2}}\right] \tag{89}$$

As points ***G*** and ***J*** lie on the same 45º sloped straight line (see Figure 46) and on ESPs starting out from the same $p'_e = p'_{e2}$, one can write:

$$\frac{s'(\boldsymbol{G})}{p'_{e2}} - \frac{t'(\boldsymbol{G})}{p'_{e2}} = \frac{s'(\boldsymbol{J})}{p'_{e2}} - \frac{t'(\boldsymbol{J})}{p'_{e2}} \tag{90}$$

As $\phi'_{emob}(\boldsymbol{G}) = \phi'_{emob}(\boldsymbol{J})$, replacing $\phi'_{emob}(\boldsymbol{G})$ by $\phi'_{emob}(\boldsymbol{J})$ and $\left[s'(\boldsymbol{G}) / p'_{e2} - t'(\boldsymbol{G}) / p'_{e2}\right]$ by its equivalent value $\left[s'(\boldsymbol{J}) / p'_{e2} - t'(\boldsymbol{J}) / p'_{e2}\right]$ in Equation 89, Equation 91 is obtained:

$$\frac{t'_b(\boldsymbol{X})}{p'_{e1}} = tan^2\phi'_{emob}(\boldsymbol{J})\left[1 + csc\,\phi'_{emob}(\boldsymbol{J})\right]\left[\frac{s'(\boldsymbol{J})}{p'_{e2}} - \frac{t'(\boldsymbol{J})}{p'_{e2}}\right] \tag{91}$$

As points ***X***, **C**, ***G*** and ***J*** lie on the same 45º sloped straight line in the $(s' / p'_e) \times (t' / p'_e)$ plane, it can be observed from Figure 47 that $\left[s'_b(\boldsymbol{X}) / p'_{e1} - t'_b(\boldsymbol{X}) / p'_{e1}\right] = \left[s'(\boldsymbol{C}) / p'_{e1} - t'(\boldsymbol{C}) / p'_{e1}\right] = \left[s'(\boldsymbol{G}) / p'_{e2} - t'(\boldsymbol{G}) / p'_{e2}\right] = \left[s'(\boldsymbol{J}) / p'_{e2} - t'(\boldsymbol{J}) / p'_{e2}\right]$. Since point ***X*** is a generic point of the normalized basic effective stress path (from now on called bESPn), for which $\dot{\varepsilon}_t = 0$, Equation 91 holds valid for each and every point on the bESPn and can be written according to the generic form of Equation 92:

$$\frac{t'_b}{p'_e} = tan^2\phi'_{emob}\left(1 + csc\,\phi'_{emob}\right)\left[\frac{s'}{p'_e} - \frac{t'}{p'_e}\right] \tag{92}$$

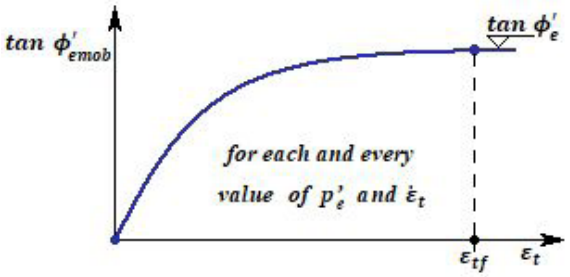

Figure 48. Uniqueness of $tan\,\phi'_{emob} \times \varepsilon_t$ relationship for each and every value of p'_e and $\dot{\varepsilon}_t$.

Finally, it is worth reminding that points ***X***, ***C***, ***G*** and ***J*** have the same shear strain ε_t, which implies a one-to-one correspondence between t'_b / p'_e and ε_t, leading to the conclusion that the basic curve $t'_b / p'_e \times \varepsilon_t$ is unique, as it was to be demonstrated.

Corollary 2: ***$\overline{CIUCL}$ tests carried out on a normally consolidated clay showing homothetic ESPs for any fixed $\dot{\varepsilon}_t$ and a unique curve $\Delta u / p'_e \times \varepsilon_t$, irrespective of $\dot{\varepsilon}_t$, will show a unique normalized basic effective stress path (bESPn) $\left(s'_b / p'_e, t'_b / p'_e\right)$, whatever $\dot{\varepsilon}_t$ is.***

Corollary 2 results from the following reasoning:

Starting from Equation 74, which gives the expression for s'_b, and following a similar line of reasoning adopted in the proof of *corollary 1*, it can be shown that a unique curve $s'_b / p'_e \times \varepsilon_t$ exists. Taking the t'_b / p'_e values of the unique $t'_b / p'_e \times \varepsilon_t$ curve, as shown in *corollary 1*, and associating them to the s'_b / p'_e values corresponding to the same ε_t values of the likewise unique $s'_b / p'_e \times \varepsilon_t$ curve, it will also be obtained a unique curve formed by the ordered pairs $(s'_b / p'_e, t'_b / p'_e)$, which is, by definition, the normalized basic effective stress path (bESPn).

Corollary 3: ***$\overline{CIUCL}$ tests carried out on a normally consolidated clay showing homothetic ESPs for any fixed $\dot{\varepsilon}_t$ and a unique curve $\Delta u / p'_e \times \varepsilon_t$, irrespective of $\dot{\varepsilon}_t$, will show a unique curve $tan\,\phi'_{emob} \times \varepsilon_t$, whatever $\dot{\varepsilon}_t$ is.***

Corollary 3 can be demonstrated following the reasoning presented below:

Considering corollaries 1 and 2, both curves $t'_b / p'_e \times \varepsilon_t$ and $s'_b / p'_e \times \varepsilon_t$ are unique. This means that one and only one value of shear strain ε_t is associated with each and every ordered pair $\left(s'_b / p'_e, t'_b / p'_e\right)$. However, $tan\,\phi'_{emob}$ can be written in terms of s'_b and t'_b as $tan\phi'_{emob} = t'_b / \sqrt{\left(s'_b\right)^2 - \left(t'_b\right)^2}$. Dividing both numerator and denominator of the right hand side of such expression by p'_e, Equation 93 is obtained:

$$tan\,\phi'_{emob} = \frac{t'_b / p'_e}{\sqrt{\left(s'_b / p'_e\right)^2 - \left(t'_b / p'_e\right)^2}} \tag{93}$$

As t'_b / p'_e and s'_b / p'_e are both exclusive functions of ε_t, thus $tan\,\phi_{emob}$ will also be a sole function of ε_t, which proves corollary 3, as illustrated in Figure 48.

Thus, it can be concluded that curves $t'_b / p'_e \times \varepsilon_t$, $tan\,\phi'_{emob} \times \varepsilon_t$ and the normalized basic effective stress path (bESPn), given by the ordered pairs $\left(s'_b / p'_e, t'_b / p'_e\right)$, are properties of a given normally consolidated plastic soil.

8. Real $\overline{CIUCL}$ tests

8.1 Introduction

A model of behaviour for saturated normally consolidated clays subjected to $\overline{CIUCL}$ tests taking into account strain rate $\left(\dot{\varepsilon}_t\right)$ was developed in section 7. Based on the developed model, the main results expected for an ideal plastic soil subjected to $\overline{CIUCL}$ tests were also presented.

At first, this work was intended to present a testing program consisting of $\overline{CIUCL}$, undrained creep and stress relaxation tests carried out on samples from a very soft clay deposit close to the city of Rio de Janeiro, called Sarapuí II [see Danziger et al. (2019)]. The main aim would be to check whether the results from such testing program could be predicted by the model presented in section 7. However, the arrival of the pandemic in the beginning of 2020 made such testing program unfeasible. For this reason, the tests herein analyzed are those carried out by Lacerda (1976) on San Francisco Bay Mud samples.

Although the Lacerda's (1976) testing program was not planned to study the behavioural aspects presented in section 7, it is suitable since it is consisted of $\overline{CIUCL}$, undrained creep and stress relaxation tests, which can be analyzed under the light of the proposed model. Furthermore, San Francisco Bay Mud is a worldwide known and comprehensively studied soil. The main disadvantage of using Lacerda's (1976) tests is that they were carried out when computer-aided data acquisition systems were not available for soil testing. This disadvantage makes it harder to experimentally identify special aspects already discussed such as the "viscosity jump". Nevertheless, the Lacerda's (1976) testing program is useful to check whether its experimental results are in agreement with the main propositions made by the presented model.

8.2 Summary of the model hypotheses and steps to be followed to check their validity

To check the validity of the model, it is necessary to verify if its 11 hypotheses are fulfilled. Among these hypotheses, listed below, the first four come from experimental evidences. The next six are working hypotheses of theoretical nature and the last one is hybrid since it comes from experimental evidences as well as from theoretical considerations.

These hypotheses are the following:

1. Normally consolidated, saturated specimens of a given clay compressed to different isotropic stresses p'_e in CIUCL tests and sheared with the same shear strain rate $\dot{\varepsilon}_t$ show similar curves $t' \times \varepsilon_t$ and $\Delta u \times \varepsilon_t$ and homothetic $p' \times q'$ or $s' \times t'$ effective stress paths with the origin as the centre of homothety. This means that for a fixed strain rate $\dot{\varepsilon}_t$ the clay exhibits normalized behaviour in relation to p'_e.
2. For a given strain rate $\dot{\varepsilon}_t$, the ordered triples $\left(p'_f, q'_f, v_f\right)$, with subscripts *f* denoting failure, define a smooth curve in the (p', q', v) space called critical state line (CSL) associated with this given shear strain rate $\dot{\varepsilon}_t$. For each shear strain rate $\dot{\varepsilon}_t$, there is only one corresponding CSL.
3. For a fixed $\dot{\varepsilon}_t$, the projection of the CSL on the plane $p' \times q'$ or $s' \times t'$ is a straight line passing through the origin.
4. When CIUCL tests are carried out with the same isotropic effective stress p'_e and different shear strain rates $\dot{\varepsilon}_t$, the deviator stresses are higher the higher the shear strain rate. However, pore pressure values are not affected by shear strain rate. This means that for each $\dot{\varepsilon}_t$ there is just one curve $t' / p'_e \times \varepsilon_t$, but the curve $\Delta u / p'_e \times \varepsilon_t$ is unique regardless of the $\dot{\varepsilon}_t$ value.
5. Validity of Terzaghi's PES equation: $\sigma' = \sigma - u$.
6. The shear stress τ_α acting on a plane whose normal makes an angle α with σ_1 direction consists of two parts: a friction part $\tau_{\phi\alpha}$ and a viscous part $\tau_{\eta\alpha}$, i.e., $\tau_\alpha = \tau_{\phi\alpha} + \tau_{\eta\alpha}$.
7. The viscous part of the shear stress $\tau_{\eta\alpha}$ is written as $\tau_{\eta\alpha} = \eta(e) f(\dot{\gamma}) sin 2\alpha$, being $\eta(e)$ defined as *soil viscosity*, a function of void ratio and of soil structure, and $f(\dot{\gamma})$ an exclusive function of distortion rate $\dot{\gamma}$. On planes whose normal makes 45º with σ_1 direction, $2\alpha = 90°$ and $\tau_{\eta 45°} = \eta(e) f\left(d\left(\varepsilon_1 - \varepsilon_3\right)/dt\right) = \eta(e) f(\dot{\gamma}) = \mathbb{V}$.
8. The friction part of the shear stress acting on a plane whose normal makes an angle α with σ_1 direction corresponds to $\tau_{\phi\alpha} = \tau_\alpha - \tau_{\eta\alpha} = \left[\left(\sigma'_1 - \sigma'_3\right)/2 - \mathbb{V}\right] sin 2\alpha$.
9. The ordered pairs $\left(\sigma'_\alpha, \tau_{\eta\alpha}\right)$ define the *state of mobilized viscosity* of a soil, which is represented by the viscosity ellipse. The ordered pairs $\left(\sigma'_\alpha, \tau_{\phi\alpha}\right)$ define the *state of mobilized friction*, which is represented by the friction ellipse. The sum of these two elipses corresponds to the Mohr's circle of effective stress Thus, the two ellipses cannot exist separately since only the stresses given by the Mohr's circle satisfy equilibrium.
10. As a consequence of hypotheses (6) and (7), during the undrained shear phase of a CIUCL test carried out with ε_t = constant , $\tau_{\eta\alpha}$ is instantaneously mobilized and remains constant up to the end of shear. During the undrained shear phase of a CIUCL test there is no volume change but only shear strains. Thus, the deviator stress increase during the undrained shear is due to friction mobilization, which occurs as shear strains increase. Therefore, failure process is ruled by friction mobilization. For a given distortion γ, friction is fully mobilized and failure occurs. This means that, in a normally consolidated clay, failure will occur when the friction ellipse touches the strength envelope, which is the straight line passing through the origin with slope $tan\phi'_e$, as illustrated in Figure 28. In other words, failure will occur when Equation 62 is met.
11. Finally, the last hypothesis assumes the viscous resistance $\mathbb{V} = \eta(e) f(\dot{\gamma}) = C_\eta(\dot{\gamma}) p'_e$. This means that, even though $C_\eta(\dot{\gamma})$ is a non-linear function of distortion rate and of soil structure, for any $\dot{\gamma}$ = constant $\mathbb{V}$ is proportional to p'_e. This hypothesis is a hybrid one because, although it comes from hypotheses (6) and (7), which are of theoretical nature, it also appears as experimental evidence via the "viscosity jumps", as shown in Figures 34 and 35. As $\mathbb{V}$ is proportional to p'_e, this hypothesis is also in agreement with hypothesis (1), which assumes a normalized behaviour in relation to p'_e.

Instead of using distortion γ and distortion rate $\dot{\gamma}$ as they appear in hypotheses (7), (10) and (11), the shear strain ε_t and the shear strain rate $\dot{\varepsilon}_t$ will respectively be used from now on.

The validity of hypotheses (1) to (4) can be directly checked by observing whether or not the plots mentioned in each of them are fulfilled. Hypotheses (6) to (10), of theoretical nature, are concerned with the effects of the viscous adsorbed water on the behaviour of plastic soils. Hypothesis (11), a hybrid one, concerns the "viscosity jump". The "viscosity jump" is a theoretical aspect of the instantaneous mobilization of the viscous resistance. On the other hand, experimental evidences show that the "viscosity jump" is proportional to the effective isotropic stress p'_e, as shown in Figures 34 and 35. The hybrid nature of hypothesis (11) resides in these two aspects.

The eleven hypotheses together with the discussions presented in section 7 lead to the *generalized complementary principle 1*, from which *corollaries 1*, *2* and *3* are consequences. Thus, in order to check whether or not the model holds valid for a given soil, it is enough to check if hypotheses (1) to (4) and (11) as well as the *generalized complementary principle 1* are fulfilled. If so, the other hypotheses will automatically be fulfilled since they are embedded in the *generalized complementary principle 1*. The same will happen to *corollaries 1*, *2* and *3* because they are consequences of the *generalized complementary principle 1*. This will be the

Table 1. Characterization tests results of San Francisco Bay Mud samples (Lacerda, 1976).

Natural water content w (%)	Liquid limit w_L (%)	Plastic limit w_P (%)	Plasticity index I_P (%)	Specific gravity G	Clay fraction % < 2μm	Activity
88 to 93	88 to 90	35 to 44	45 to 55	2.75	60	0.83

Table 2. Lacerda's tests (Lacerda, 1976) analyzed in this article.

Test	Description	Specific volume after isotropic consolidation v	Isotropic compression stress $p_e^{'}$ (kPa)	Shear strain rate $\dot{\varepsilon}_t$ $(\%/\text{min.})$
FP-13	$\overline{\text{CIUCL}}$	3.00	118	0.09
FP-23	$\overline{\text{CIUCL}}$	2.81	158	0.09
FP-32	$\overline{\text{CIUCL}}$	2.98	98.0	0.09
FP-42	$\overline{\text{CIUCL}}$	2.92	137	0.09
SR-I-5	stress relax.	3.11	78.4	1.15
SR-I-8	stress relax.	not informed	78.4	5.5×10^{-4}
SR-I-9	stress relax.	not informed	314	0.10
CR-I-1	undrained creep	3.15	78.4	variable
CR-I-2	undrained creep	3.02	78.4	variable
CR-71-1	undrained creep	2.78	196	variable
CR-I-ST-2	undr. step creep	2.60	314	variable

task to be accomplished in the next sections so as to check if Lacerda's (1976) $\overline{\text{CIUCL}}$ test results follow the predictions of the presented model.

8.3 Testing program carried out on San Francisco Bay Mud by Lacerda (1976)

The soil samples tested by Lacerda (1976) were taken with thin-walled 125 mm-diameter and 300 to 450 mm-long fixed piston samplers. The samples were taken at Hamilton Air Force Base, Marin County, between the 5.20 m and 7.60 m depth.

According to Lacerda's (1976) description, San Francisco Bay Mud "*is a normally consolidated, saturated clay, composed of illite, and chlorite with some montmorillonite, vermiculite and kaolinite. Very thin silty lenses are found along horizontal planes and small broken shells are occasionally present, but the soil as a whole is fairly intact and easily trimmable*" (Lacerda, 1976, p. 262). Characterization tests results are summarized in Table 1.

From the tests carried out by Lacerda (1976) only those which allow the comparison and interpretation of their results under the light of the concepts presented in section 7 were selected. Such tests are identified in the first two columns of Table 2. In the other columns of Table 2, the specific volume (v) after isotropic consolidation, the isotropic effective stress to which the specimen was consolidated $\left(p_e^{'}\right)$ and the shear strain rate $\left(\dot{\varepsilon}_t\right)$ during undrained shear are presented.

The terminology undrained creep test is herein used to denote a test where the specimen is initially consolidated to an isotropic effective stress $p_e^{'}$ followed by an undrained stage during which a constant deviator stress $\left(\sigma_1 - \sigma_3\right) = \left(\sigma_a - \sigma_r\right)$ is applied, being $\sigma_3 = \sigma_r = p_e^{'} + u_c$ and u_c the back pressure. During the undrained creep stage, shear strains ε_t $\left(\varepsilon_t = 3/4\,\varepsilon_a\right)$ and pore pressures Δu are measured over time and strain rates $\dot{\varepsilon}_t$ $\left(\dot{\varepsilon}_t = 3/4\dot{\varepsilon}_a\right)$ are also computed over time.

The undrained step creep test is similar to the undrained creep test, except for the fact that during the undrained creep stage the deviator stress $\left(\sigma_a - \sigma_r\right)$ is applied in steps, each step lasting for a given time period. At the beginning of a new step, the deviator stress is raised by increasing σ_a, whereas σ_r is kept constant throughout the whole test. During each step, shear strains ε_t and pore pressures Δu are measured over time and strain rates $\dot{\varepsilon}_t$ are computed. Thus, the undrained step creep test can be compared to the conventional $\overline{\text{CIUCL}}$ tests, made with $\dot{\varepsilon}_t$ = constant, provided the points to be compared from both test types have the same $\dot{\varepsilon}_t$ values. An undrained creep test where a single deviator stress value is applied during the whole undrained creep stage can also be compared to a $\overline{\text{CIUCL}}$ test. However, in this case, the comparison is restricted to only the two points having the

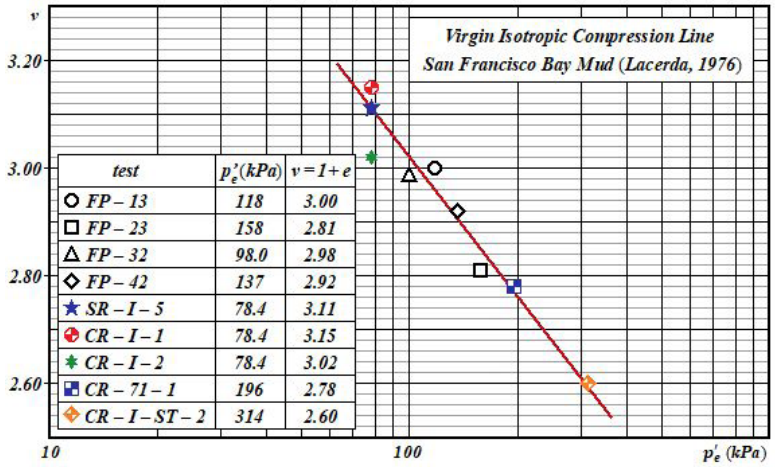

Figure 49. Virgin isotropic compression line – VICL – San Francisco Bay Mud (Lacerda, 1976).

same $\dot{\varepsilon}_t$ values. These questions will become clearer during the presentation of undrained creep tests data in section 8.4.

The name stress relaxation test is herein used to denote a $\overline{\text{CIUCL}}$ test where the undrained shear phase is carried out in consecutive stages of ε_t intervals, along which $\dot{\varepsilon}_t$ = constant. At the end of each interval the load frame motor is switched off, thus making $\dot{\ } = 0$ and starting a stress relaxation phase. Since the drainage is closed and the soil is saturated, during the stress relaxation phase there is neither volume changes nor shear strain changes. Keeping $\sigma_3 = \sigma_r = \left(p'_e + u_c\right)$ constant, deviator stress $\left(\sigma_a - \sigma_r\right)$ and pore pressure Δu are measured over time. After observing stress relaxation over a certain time period, the load frame motor is switched on again with the same or a different strain rate $\dot{\varepsilon}_t$ used during the ε_t interval which preceded the current stress relaxation phase. This is the case shown in Figure 40, where different shear strain rates $\dot{\varepsilon}_t$ were used between consecutive stress relaxations phases.

From now on, the Lacerda's (1976) tests results are compared to the predictions of the model presented in section 7.

The data concerning the isotropic compression of San Francisco Bay Mud normally consolidated specimens (presented in Table 2) are plotted in Figure 49. The virgin isotropic compression line (VICL) is presented in Figure 49, showing the relationship between specific volume v and isotropic effective stress p'_e obtained by Lacerda (1976) for San Francisco Bay Mud.

Although presented in Figure 49, test CR–I–2 will not be taken into account in the analysis that follows since it presents a specific volume which is considerably distant from the $v \times p'_e$ line. This suggests that such specimen is slightly overconsolidated, with an overconsolidation ratio of 1.3. The undrained shear phases of SR–I–5 test will not also be analysed herein since the shear strain rate $\dot{\varepsilon}_t = 1.15\,\%/\,\text{min.}$, applied up to $\varepsilon_a \cong 2.5$ %, is considered too high. Such strain rate has probably not allowed an adequate equalization degree of pore pressure measured at the base of the specimen.

8.4 Checking the model using San Francisco Bay Mud tests results

The eleven hypotheses listed in section 8.2 and the discussions of section 7 have led to the *generalized complementary principle 1*, from which *corollaries 1*, *2* and *3* emerge. Thus, to check whether or not the model holds valid for a given plastic soil, it is enough to verify if the hypotheses (1) to (4) and (11) and the *generalized complementary principle 1* are fulfilled. If so, the remaining hypotheses will automatically be fulfilled since they are embedded in the *generalized complementary principle 1*. Besides, once the validity of the *generalized complementary principle 1* is shown, *corollaries 1*, *2* and *3* will also be automatically fulfilled.

In a few words, to check whether or not San Francisco Bay Mud normally consolidated specimens fulfill the model presented in section 7, the tasks listed and explained at the end of section 8.2 must be carried out. These tasks are:

(i) Validity check of hypotheses (1) to (4), which come from experimental evidences.

(ii) Validity check of hypothesis (11) (from a hybrid nature – experimental + theoretical).

(iii) Validity check of the generalized *complementary principle 1*.

(iv) Validity check of *corollaries 1*, *2* and *3*.

Following the sequential tasks listed above, the first thing to do is to check the validity of hypothesis (1), that is: to verify if normally consolidated, saturated specimens of San Francisco Bay Mud subjected to $\overline{\text{CIUCL}}$ tests carried out with $\dot{\varepsilon}_t$ = constant really present similar $t' \times \varepsilon_t$ and $\Delta u \times \varepsilon_t$ curves and homothetic $s' \times t'$ ESPs with centre of homothety at the origin. If this hypothesis is fulfilled, the normalized

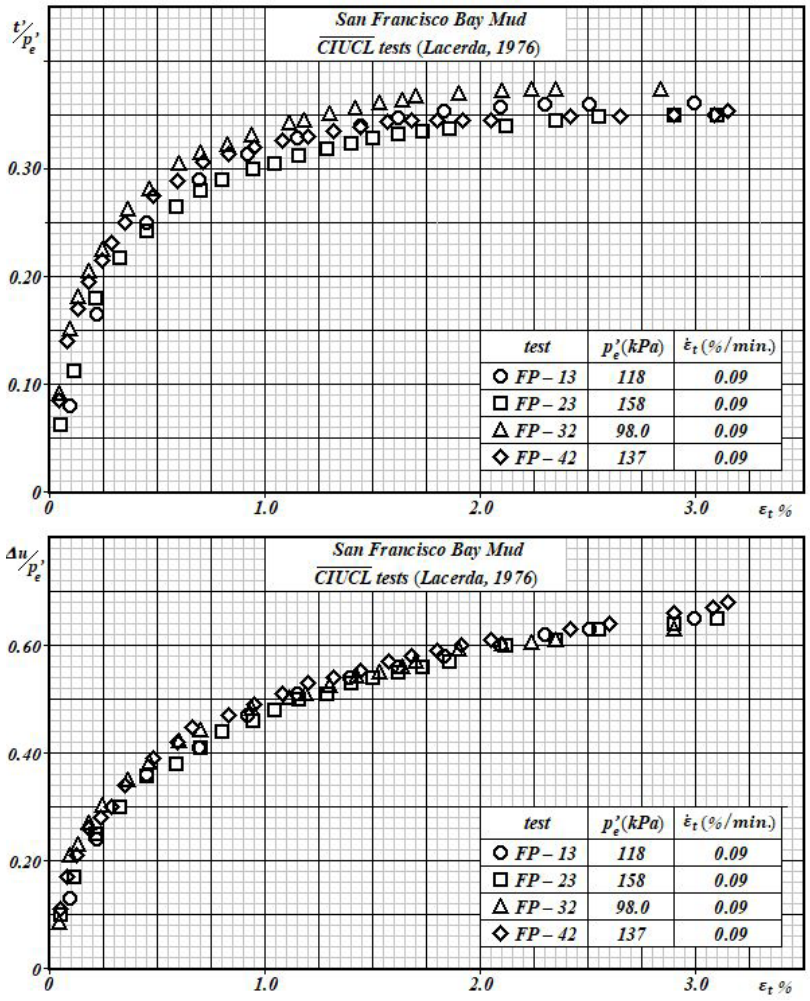

Figure 50. Curves $t' / p'_e \times \varepsilon_t$ and $\Delta u / p'_e \times \varepsilon_t$ for $\overline{\text{CIUCL}}$ tests on San Francisco Bay Mud carried out with $\dot{\varepsilon}_t = 0.09\% / \text{min.}$ [data from Lacerda (1976)].

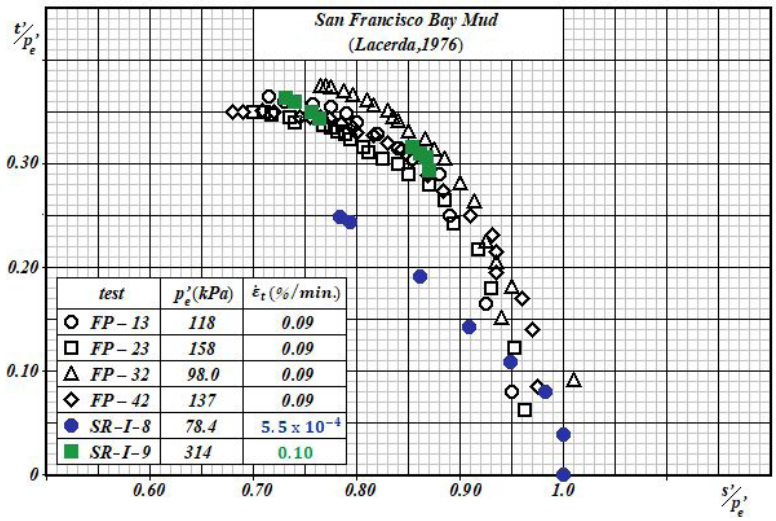

Figure 51. Normalized ESPs $\left(s' / p'_e\right) \times \left(t' / p'_e\right)$ for tests with a fixed strain rate $\dot{\varepsilon}_t$.

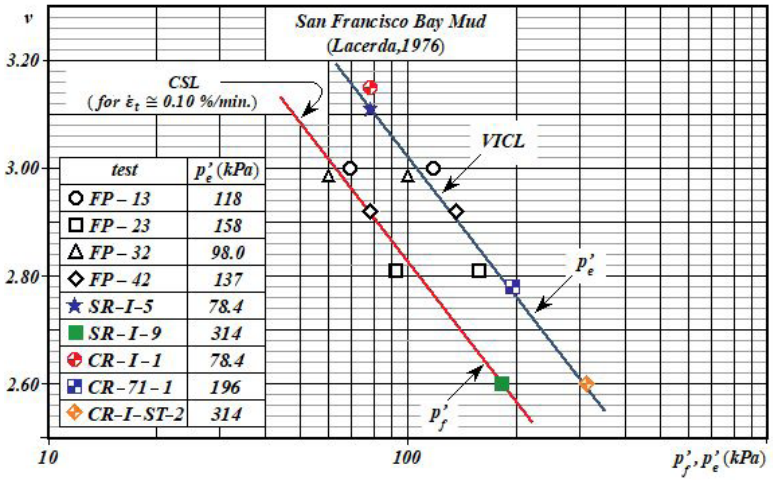

Figure 52. Virgin isotropic compression line (VICL) and critical state line (CSL) for San Francisco Bay Mud corresponding to a strain rate $\dot{\varepsilon}_t \cong 0.10\,\%/\,\text{min}$..

curves $t'/p'_e \times \varepsilon_t$ and $\Delta u/p'_e \times \varepsilon_t$ and the normalized ESP $s'/p'_e \times t'/p'_e$ will be unique for a fixed $\dot{\varepsilon}_t$.

This is the case indeed. Normalized curves $t'/p'_e \times \varepsilon_t$ and $\Delta u/p'_e \times \varepsilon_t$ from $\overline{\text{CIUCL}}$ tests carried out with $\dot{\varepsilon}_t = 0.09\,\%/\,\text{min}$.are shown in Figure 50. The set of curves $t'/p'_e \times \varepsilon_t$ can be fairly represented by a unique curve. The same occurs for the curves $\Delta u/p'_e \times \varepsilon_t$.

The normalized ESPs $s'/p'_e \times t'/p'_e$ of the tests plotted in Figure 50 are plotted in Figure 51, showing that ESPs corresponding to tests carried out with $\dot{\varepsilon}_t = 0.09\,\%/\,\text{min}$. can also be represented by a unique ESP. This means that ESPs corresponding to tests carried out with $\dot{\varepsilon}_t = 0.09\,\%/\,\text{min}$. are homothetic with the origin as the centre of homothety. Some points from test SR–I–9 where the shear strain rate is $\dot{\varepsilon}_t = 0.10\,\%/\,\text{min}$ are also plotted in Figure 51. $\dot{\varepsilon}_t = 0.10\,\%/\,\text{min}$. is almost the same strain rate of $\dot{\varepsilon}_t = 0.09\,\%/\,\text{min}$. used in tests FP–13, FP–23, FP–32 and FP–42. Although the results shown in Figures 50 and 51 are restricted to $\dot{\varepsilon}_t \cong 0.10\,\%/\,\text{min}$., they show that hypothesis (1) is fulfilled.

Figure 51 also shows the part of the ESP for SR–I–8 test up to the first stress relaxation stage where the shear strain rate applied was $\dot{\varepsilon}_t = 5.5\times10^{-4}\,\%/\,\text{min}$.. This illustrates that the lower the shear strain rate $\dot{\varepsilon}_t$, the lower the t'/p'_e values of the normalized ESP, which is in agreement with the model presented in section 7.

Hypothesis (2) states that for $\overline{\text{CIUCL}}$ tests carried out with a fixed shear strain rate $\dot{\varepsilon}_t$ the ordered triples $\left(p'_f, q'_f, v_f\right)$ at failure define a smooth curve in the $p' \times q' \times v$ space called critical state line (CSL) associated with that fixed shear strain rate $\dot{\varepsilon}_t$. This means: for a given shear strain rate $\dot{\varepsilon}_t$ there is only one corresponding CSL. This result is illustrated in Figures 52 and 53 for the $\overline{\text{CIUCL}}$ tests carried out with $\dot{\varepsilon}_t \cong 0.10\,\%/\,\text{min}$..

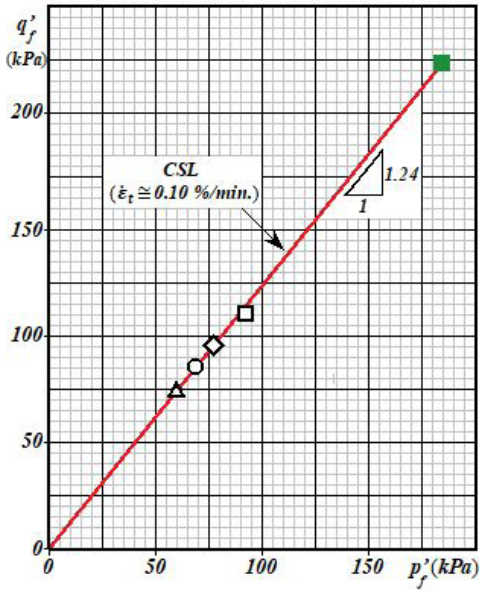

Figure 53. Critical state line for San Francisco Bay Mud corresponding to a strain rate $\dot{\varepsilon}_t \cong 0.10\,\%/\,\text{min}$. [data from Lacerda (1976)].

Figure 53 shows that the projection of the CSL onto the plane $p' \times q'$ (or $s' \times t'$) for the fixed $\dot{\varepsilon}_t \cong 0.10\,\%/\,\text{min}$. is a straight line passing through the origin. Thus, Figure 53 illustrates that hypothesis (3) is also fulfilled by San Francisco Bay Mud.

Based on the results from $\overline{\text{CIUCL}}$ tests carried out with $\dot{\varepsilon}_t \cong 0.10\,\%/\,\text{min}$, it is possible to obtain ϕ' for normally consolidated San Francisco Bay Mud corresponding to $\dot{\varepsilon}_t \cong 0.10\,\%/\,\text{min}$.. This can be done since M and ϕ' are related to each other by

$$M = 6\sin\phi'/\left(3-\sin\phi'\right) \tag{94}$$

where $M = q'_f / p'_f$ is the slope of the CSL corresponding to a given $\dot{\varepsilon}_t$ on the plane $p' \times q'$. From Figure 53, one obtains $M = 1.24$, which corresponds to $\phi' \cong 31°$ and to the ordered pair $\left(s'_f / p'_e, t'_f / p'_e\right) = (0,70; 0,36)$, assumed as the point representing failure in Figure 51.

Although there is a lack of data to obtain M and ϕ' corresponding to $\dot{\varepsilon}_t$ values different from $\cong 0.10\%$ / min., the available data corresponding to $\dot{\varepsilon}_t = 5.5 \times 10^{-4}\%$ / min. and $\cong 0.7\%$ / min., suggest that for each shear strain rate there is only one CSL (see also Figure 31 and the discussion associated with it).

Hypothesis (4) must be checked next. This hypothesis assumes that, in CIUCL tests, the higher the shear strain rate applied, the higher the values t' / p'_e in $t' / p'_e \times \varepsilon_t$ curves. On the other hand, hypothesis 4 also assumes that curves $\Delta u / p'_e \times \varepsilon_t$ do not depend on $\dot{\varepsilon}_t$.

Figure 54 shows $t' / p'_e \times \varepsilon_t$ and $\Delta u / p'_e \times \varepsilon_t$ curves corresponding to the undrained shear phases of stress relaxation tests SR–I–8 and SR–I–9. Strain rate effects are mainly observed on $t' / p'_e \times \varepsilon_t$ curves but hardly noted on $\Delta u / p'_e \times \varepsilon_t$, where, regardless the strain rate, experimental results fall within a narrow zone. In Figure 54 it should be noted that $\dot{\varepsilon}_t$ assumes four different orders of magnitude. One can argue that, with $\dot{\varepsilon}_t = 3.4\%$ / min., the strain rate criterion which should have been used aiming pore pressure equalization along the specimen was not probably fulfilled during the first undrained shear phase of test SR–I–9. Thus, Δu values measured during the first undrained shear phase of test SR–I–9 are probably underestimated. After this observation, it can be concluded from Figure 54 that curves $\Delta u / p'_e \times \varepsilon_t$ can be represented by a unique curve, which means that $\Delta u / p'_e \times \varepsilon_t$ curves can be considered to be independent of the strain rate $\dot{\varepsilon}_t$.

The assumption made in hypothesis (4) considering that strain rate effects are remarkable on $t' / p'_e \times \varepsilon_t$ curves but are practically absent in $\Delta u / p'_e \times \varepsilon_t$ curves is even clearer in Figure 55 obtained by overlapping Figures 50 and 54.

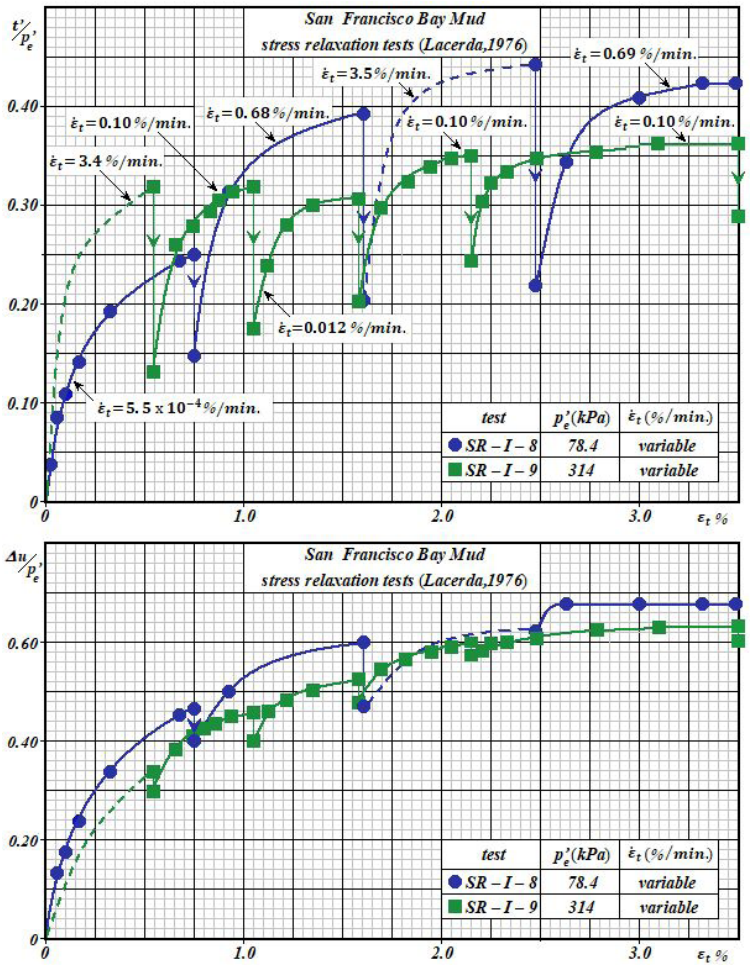

Figure 54. Curves $t' / p'_e \times \varepsilon_t$ and $\Delta u / p'_e \times \varepsilon_t$ for undrained shear phases of stress relaxation tests on San Francisco Bay Mud carried out with different values of $\dot{\varepsilon}_t$.

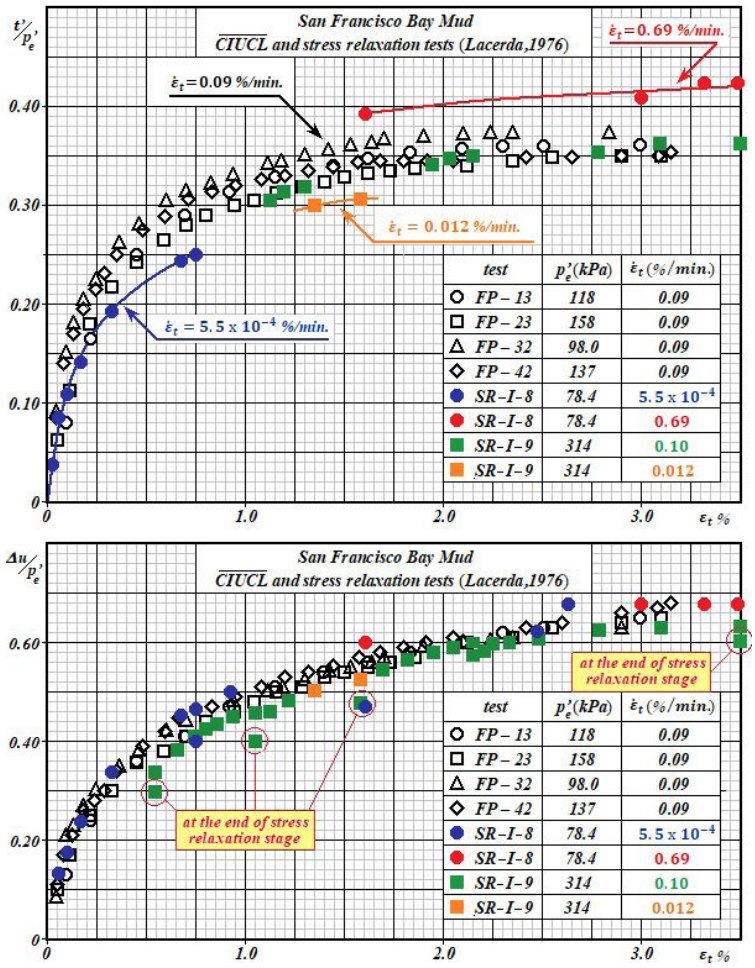

Figure 55. $t' / p'_e \times \varepsilon_t$ and $\Delta u / p'_e \times \varepsilon_t$ for $\overline{\text{CIUCL}}$ and stress relaxation tests on San Francisco Bay Mud for several different $\dot{\varepsilon}_t$ values [data from Lacerda (1976)].

After checking the validity of hypotheses (1) to (4), one can now check hypothesis (11), which, being from a hybrid nature, is made up of two parts: one that comes from experimental evidences and the other that comes from theoretical considerations.

According to hypothesis (11), $\mathbb{V} = \eta(e) f(\dot{\gamma}) = C_\eta(\dot{\gamma}) p'_e$ or, recalling that $\dot{\gamma} = 2\dot{\varepsilon}_t$, $\mathbb{V} = C_\eta(\dot{\varepsilon}_t) p'_e$. This means that for a given shear strain rate $\dot{\varepsilon}_t$ the "viscosity jump" is proportional to p'_e, as shown in Figures 34 and 35. Thus, the normalized ESPs $(s' / p'_e) \times (t' / p'_e)$ corresponding to the same $\dot{\varepsilon}_t$ should be represented by a unique ESP beginning with a "viscosity jump" along a 45º sloped straight line, which suddenly changes its direction moving up and to the left, showing an elbow shaped curve like those presented in Figure 47.

Although the normalized ESPs for $\dot{\varepsilon}_t \cong 0.10\% / \text{min.}$ in Figure 51 can be considered as a unique curve, the absence of the "viscosity jump" is noteworthy. Such absence can be possibly assigned to the fact that an automatic data acquisition system was not used, which greatly harms the measurement of *s'*, *t'* and *Δu* corresponding to the beginning of the tests. Another possible explanation for the absence of the "viscosity jump" is the occurrence of bedding errors, which will be not discussed here. One of the signs that some "disturbance" has affected the beginning of $\overline{\text{CIUCL}}$ test data is the fact that points belonging to ESPs associated with $\dot{\varepsilon}_t = 0.09\% / \text{min.}$ fall below points belonging to the ESP associated with $\dot{\varepsilon}_t = 5.5 \times 10^{-4} \% / \text{min.}$, as shown in Figure 51. Thus, one cannot evaluate $C_\eta(\dot{\varepsilon}_t)$ values and, consequently, ϕ'_e value via Figure 51.

In order to obtain $C_\eta(\dot{\varepsilon}_t)$ and ϕ'_e, it will be necessary to make use of the undrained creep tests data. As previously explained, undrained creep tests are carried out by keeping the deviator stress constant, measuring ε_t and Δu over time and evaluating $\dot{\varepsilon}_t$. This way of evaluating $\dot{\varepsilon}_t$ makes its values more reliable, particularly in the early phase of the test when bedding errors are of greater magnitude. Accordingly, the normalized ESPs for the undrained creep tests are shown in Figure 56.

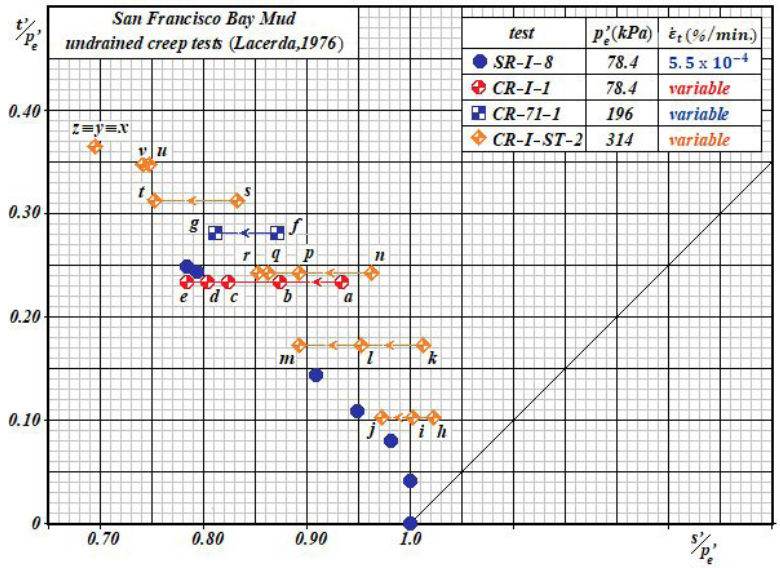

Figure 56. Normalized effective stress paths (ESPs) for undrained creep tests on normally consolidated specimens of San Francisco Bay Mud.

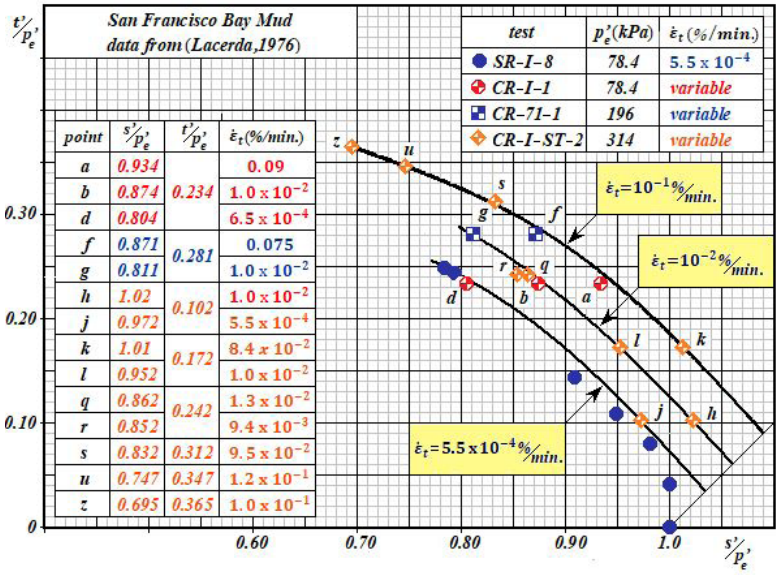

Figure 57. Normalized ESPs for 3 different $\dot{\varepsilon}_t$ values determined from undrained creep tests.

As a reference, the normalized ESP of test SR–I–8 carried out with $\dot{\varepsilon}_t = 5.5\times10^{-4}$ %/min. is also shown in Figure 56. Values of ε_t, $\dot{\varepsilon}_t$, t'/p'_e, s'/p'_e and $\Delta u/p'_e$, corresponding to the points shown in Figure 56, are presented in Table 3.

Based on values from Table 3 and on ESPs shown in Figures 51 and 56, ESPs for some selected shear strain rates $\dot{\varepsilon}_t$ can be sketched. ESPs sketches corresponding to $\dot{\varepsilon}_t = 10^{-1}$%/min., $\dot{\varepsilon}_t = 10^{-2}$%/min. and $\dot{\varepsilon}_t = 5.5\times10^{-4}$%/min. are shown in Figure 57.

In Figure 57, each ESP corresponding to a fixed $\dot{\varepsilon}_t$ intersects the normalized total stress path at a point whose ordinate gives the C_η value for that fixed $\dot{\varepsilon}_t$. Thus, from Figure 57 one can estimate the values of C_η for 5.5×10^{-4}%/min., 10^{-2}%/min. and 10^{-1}%/min. as being equal to 0.035, 0.06 and 0.09, respectively. With these C_η values, $\tan\phi'_e$ can be evaluated via Equation 62. Alternatively, $\tan\phi'_e$ can be evaluated using Equation 95, which is Equation 62 written in a normalized way, that is:

$$tan\,\phi'_e = \frac{\left(t'_f - \mathbb{V}\right)}{\sqrt{s'^2_f - t'^2_f}} = \frac{\left(t'_f / p'_e - \mathbb{V} / p'_e\right)}{\sqrt{\left(s'_f / p'_e\right)^2 - \left(t'_f / p'_e\right)^2}} = \frac{\left(t'_f / p'_e - C_\eta\left(\dot{\varepsilon}_t\right)\right)}{\sqrt{\left(s'_f / p'_e\right)^2 - \left(t'_f / p'_e\right)^2}} \quad (95)$$

Taking $C_\eta\left(10^{-1}\%/\text{min.}\right) = 0.09$ and the ordered pair $\left(s'_f / p'_e, t'_f / p'_e\right) = (0.70, 0.36)$ corresponding to stress states at failure in $\overline{\text{CIUCL}}$ tests on normally consolidated specimens of San Francisco Bay Mud carried out with $\dot{\varepsilon}_t = 0.1\%/\text{min.}$ and $0.09\%/\text{min.}$, one obtains:

$$tan\,\phi'_e = \frac{\left(t'_f / p'_e - C_\eta\left(\dot{\varepsilon}_t\right)\right)}{\sqrt{\left(s'_f / p'_e\right)^2 - \left(t'_f / p'_e\right)^2}} = \frac{0.36 - 0.09}{\sqrt{0.70^2 - 0.36^2}} = 0.45 \rightarrow \phi'_e \cong 24° \quad (96)$$

This means that, in the normally consolidated domain, the part of the undrained shear strength of San Francisco Bay Mud which can be assigned to friction can be evaluated using $\phi'_e \cong 24°$, being ϕ'_e the true angle of internal friction, as defined by Hvorslev. This also means that, embedded into the shear strength values of normally consolidated specimens of San Francisco Bay Mud calculated with $\phi' \cong 31°$, there is a part which must be assigned to the viscous resistance.

Back to Figure 51, it is observed that, as already discussed, the ESPs for $\overline{\text{CIUCL}}$ tests FP–13, FP–23, FP–32 and FP–42 seem to be affected by bedding errors, mainly occurring up to the point of coordinates $\left(s' / p'_e, t' / p'_e\right) \cong (0.92, 0.25)$. The shear strain $\varepsilon_t \cong 0.40\ \%$ is associated with $t' / p'_e = 0.25$ (see Figure 55). Thus, by neglecting the ESPs points concerning FP–13, FP–23, FP–32 and FP–42 tests for which $\varepsilon_t \leq 0.40\ \%$ and overlapping Figures 51 and 57, Figure 58 is obtained.

Figure 58 shows that, making the appropriate "corrections" of the initial parts of the ESPs in Figure 51 and taking into account the undrained creep tests, hypothesis (11) is also fulfilled.

The results of all tests ($\overline{\text{CIUCL}}$, stress relaxation and undrained creep) are presented in Figure 59 to show that normally consolidated San Francisco Bay Mud follows hypotheses (1) to (4) and (11), regardless of the test type.

Going ahead with the task of checking whether or not the model is appropriate to predict the behaviour of normally consolidated San Francisco Bay Mud, now it is necessary to check the validity of the *generalized complementary principle 1*, whose statement is repeated below.

Generalized complementary principle 1: During undrained shear of $\overline{\text{CIUCL}}$ tests carried out on normally consolidated clay specimens, points on the plane $\left(s' / p'_e\right) \times \left(t' / p'_e\right)$ corresponding to the intersections of any given 45º sloped straight line and the several ESPs, each one associated with a different $\dot{\varepsilon}_t$ value, will show the same values of ε_t, $\left(\Delta u / p'_e\right)$, and $tan\,\phi'_{emob}$, whatever the shear strain rate $\dot{\varepsilon}_t$ may be.

The *generalized complementary principle 1* is illustrated in Figure 47, where points ***X***, ***C***, ***G*** and ***J*** all have the same values of ε_t, $\left(\Delta u / p'_e\right)$ and $\tan\phi'_{emob}$.

The *generalized complementary principle 1* was stated by induction according to the following reasoning: In Figure 47, points ***A***, ***E***, ***B***, ***F*** and ***I*** lie on the same 45º sloped straight line and all of them have $\varepsilon_t = 0, \left(\Delta u / p'_e\right) = 0$ and $\tan\phi'_{emob} = 0$,

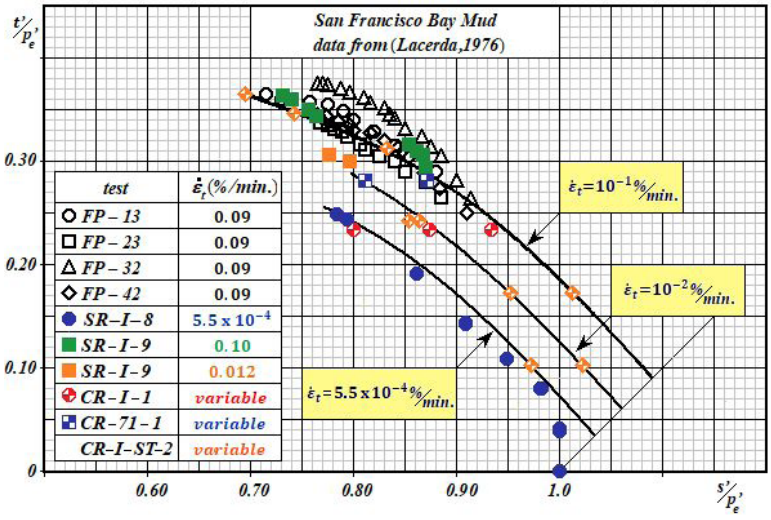

Figure 58. Normalized effective stress paths $\left(s' / p'_e\right) \times \left(t' / p'_e\right)$ for all tests with different strain rates $\left(\dot{\varepsilon}_t\right)$.

Table 4. Validation checking of the generalized ***complementary principle 1*** for San Francisco Bay Mud [data from Lacerda (1976)].

Test	$\varepsilon_t\,(\%)$	$\dot{\varepsilon}_t\,(\%/\text{min.})$	$t'\quad p_e$	s'/p'_e	$\Delta u/p'_e$	C_η	$tan\phi'_{emob}$
FP–23	0.13	~1.0×10^{-1}	0.123	0.953	0.17	0.09	0.035
FP–32	0.13	~1.0×10^{-1}	0.18	0.95	0.23	0.09	0.096
FP–42	0.13	~1.0×10^{-1}	0.17	0.960	0.21	0.09	0.075
CR–I–ST–2	0.14	8.4×10^{-2}	0.172	1.01	0.16	0.09	0.082
FP–32	0.29	~1.0×10^{-1}	0.241	0.920	0.32	0.09	0.170
FP–42	0.29	~1.0×10^{-1}	0.231	0.931	0.30	0.09	0.156
CR–I–1	0.29	0.09	0.234	0.934	0.300	0.09	0.159
FP–23	0.35	~1.0×10^{-1}	0.217	0.917	0.30	0.09	0.143
FP–32	0.36	~1.0×10^{-1}	0.264	0.914	0.35	0.09	0.199
FP–42	0.35	~1.0×10^{-1}	0.25	0.91	0.34	0.09	0.183
SR–I–8	0.33	5.5×10^{-4}	0.193	0.866	0.33	0.035	0.187
FP–23	0.45	~1.0×10^{-1}	0.25	0.89	0.36	0.09	0.187
FP–32	0.46	~1.0×10^{-1}	0.28	0.90	0.38	0.09	0.222
CR–I–1	0.45	1.0×10^{-2}	0.234	0.874	0.36	0.06	0.207
CR–I–ST–2	0.55	1.0×10^{-2}	0.242	0.852	0.39	0.06	0.223
FP–23	0.58	~1.0×10^{-1}	0.265	0.885	0.38	0.09	0.207
CR–71–1	0.60	0.075	0.281	0.871	0.41	~0.09	0.232
SR–I–8	0.68	5.5 × 10-4	0.244	0.794	0.45	0.04	0.270
FP–13	0.69	~1.0×10^{-1}	0.29	0.88	0.41	0.09	0.241
FP–23	0.70	~1.0×10^{-1}	0.28	0.87	0.41	0.09	0.231
FP–32	0.70	~1.0×10^{-1}	0.315	0.875	0.44	0.09	0.276
FP–42	0.71	~1.0×10^{-1}	0.304	0.854	0.45	0.09	0.268
CR–I–1	0.75	6.5×10^{-4}	0.234	0.804	0.43	0.04	0.252
SR–I–8	0.75	5.5×10^{-4}	0.247	0.784	0.46	0.035	0.285
FP–23	0.75	~1.0×10^{-1}	0.285	0.86	0.43	0.09	0.240
FP–42	0.75	~1.0×10^{-1}	0.304	0.851	0.46	0.09	0.269
FP–13	1.0	~1.0×10^{-1}	0.319	0.833	0.48	0.09	0.298
FP–23	1.0	~1.0×10^{-1}	0.325	0.833	0.47	0.09	0.306
FP–32	1.0	~1.0×10^{-1}	0.334	0.846	0.49	0.09	0.314
FP–42	1.0	~1.0×10^{-1}	0.322	0.825	0.50	0.09	0.305
SR–I–9	1.0	1.0×10^{-1}	0.317	0.863	0.45	0.09	0.283
CR–71–1	0.97	~1.0×10^{-2}	0.281	0.811	0.47	0.06	0.290
CR–I–ST–2	1.00	~1.0×10^{-1}	0.312	0.832	0.48	0.09	0.288
FP–13	1.15	~1.0×10^{-1}	0.328	0.82	0.51	0.09	0.317
FP–23	1.16	~1.0×10^{-1}	0.312	0.812	0.50	0.09	0.296
FP–32	1.18	~1.0×10^{-1}	0.345	0.835	0.51	0.09	0.335
FP–42	1.20	~1.0×10^{-1}	0.33	0.800	0.53	0.09	0.329
FP–13	1.38	~1.0×10^{-1}	0.34	0.80	0.54	0.09	0.345
FP–23	1.40	~1.0×10^{-1}	0.324	0.794	0.53	0.09	0.323
FP–32	1.42	~1.0×10^{-1}	0.356	0.816	0.54	0.09	0.362
FP–42	1.44	~1.0×10^{-1}	0.339	0.784	0.56	0.09	0.352
FP–13	1.62	~1.0×10^{-1}	0.347	0.79	0.56	0.09	0.362
FP–23	1.62	~1.0×10^{-1}	0.332	0.782	0.55	0.09	0.342
FP–32	1.64	~1.0×10^{-1}	0.364	0.809	0.56	0.09	0.379
FP–13	1.83	~1.0×10^{-1}	0.354	0.774	0.58	0.09	0.384
FP–23	1.86	~1.0×10^{-1}	0.336	0.766	0.57	0.09	0.357
FP–42	1.80	~1.0×10^{-1}	0.345	0.755	0.59	0.09	0.380
FP–42	2.05	~1.0×10^{-1}	0.345	0.735	0.61	0.09	0.393
FP–13	2.08	~1.0×10^{-1}	0.357	0.757	0.60	0.09	0.400
FP–23	2.12	~1.0×10^{-1}	0.34	0.74	0.60	0.09	0.380
FP–32	2.10	~1.0×10^{-1}	0.372	0.772	0.60	0.09	0.417
CR–I–ST–2	2.21	~1.0×10^{-1}	0.347	0.742	0.61	0.09	0.392
FP–32	2.24	~1.0×10^{-1}	0.375	0.770	0.61	0.09	0.424
FP–13	2.30	~1.0×10^{-1}	0.36	0.74	0.62	0.09	0.418
FP–23	2.35	~1.0×10^{-1}	0.345	0.735	0.61	0.09	0.393
FP–32	2.35	~1.0×10^{-1}	0.375	0.765	0.61	0.09	0.427
FP–42	2.42	~1.0×10^{-1}	0.349	0.719	0.63	0.09	0.412
FP–13	2.51	~1.0×10^{-1}	0.36	0.73	0.63	0.09	0.425
FP–23	2.55	~1.0×10^{-1}	0.347	0.717	0.63	0.09	0.410
FP–32	2.84	~1.0×10^{-1}	0.375	0.750	0.63	0.09	0.439
FP–23	2.90	~1.0×10^{-1}	0.35	0.710	0.64	0.09	0.421
FP–13	2.98	~1.0×10^{-1}	0.365	0.715	0.65	0.09	0.447

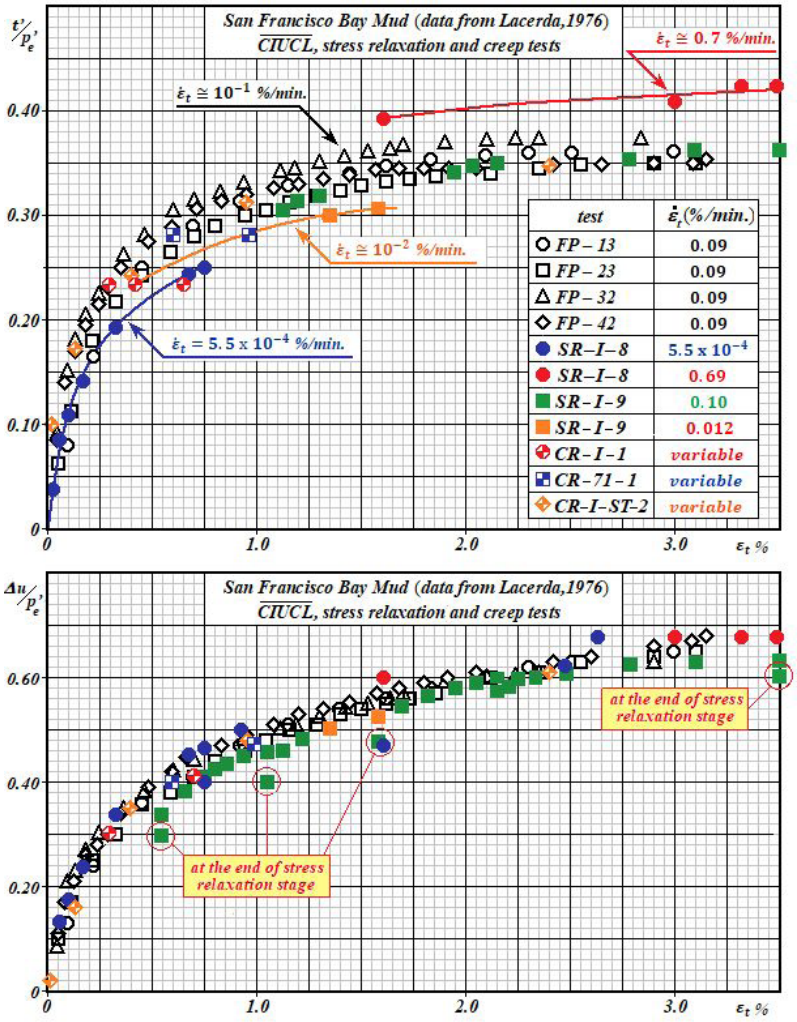

Figure 59. $\left(t' / p'_e\right) \times \varepsilon_t$ and $\left(\Delta u / p'_e\right) \times \varepsilon_t$ curves for $\overline{\text{CIUCL}}$, stress relaxation and undrained creep tests for different strain rates $\dot{\varepsilon}_t$.

regardless of the test strain rate $\dot{\varepsilon}_t$. Similarly, points ***M***, ***D***, ***H*** and ***K*** also lie on another 45º sloped straight line and all of them are at failure. Such points are assumed to have the same ε_t and $\left(\Delta u / p'_e\right)$ values and, for being at failure, $\tan\phi'_{emob} = \tan\phi'_e$. Thus, it has been assumed by induction that points ***X***, ***C***, ***G*** and ***J***, which lie on a generic 45º sloped straight line, also have the same ε_t, $\left(\Delta u / p'_e\right)$ and $\tan\phi'_{emob}$ values.

The validity of the *generalized complementary principle 1* for normally consolidated San Francisco Bay Mud can be checked by observing a summary of the Lacerda's (1976) tests results shown in Table 4, where $tan\,\phi'_{emob}$ values were computed by applying the equation $tan\,\phi'_{emob} = \left[t' / p'_e - C_\eta\left(\dot{\varepsilon}_t\right)\right] / \sqrt{\left(s' / p'_e\right)^2 - \left(t' / p'_e\right)^2}$, obtained from Equation 56 normalized in relation to p'_e. According to the *generalized complementary principle 1*, for each ε_t value there will be only one $\left(\Delta u / p'_e\right)$ value and only one $tan\,\phi'_{emob}$ value, regardless of the shear strain rate $\dot{\varepsilon}_t$. This is what is shown in Table 4, as well as in Figures 59 and 62. Although there is some scattering, considering that soil specimens were trimmed from natural undisturbed samples, it can be concluded that the experimental data are in fair agreement with the *generalized complementary principle 1*.

As already highlighted, by showing that the *generalized complementary principle 1* holds valid, *corollaries 1*, *2* and *3* will be automatically satisfied, as it will be shown next.

Corollary 1, whose statement is repeated below, will be firstly shown to be valid.

Corollary 1: $\overline{\text{CIUCL}}$ tests carried out on a normally consolidated clay showing homothetic ESPs for any fixed $\dot{\varepsilon}_t$ and a unique curve $\Delta u / p'_e \times \varepsilon_t$, regardless of $\dot{\varepsilon}_t$, will show a unique basic curve $t'_b / p'_e \times \varepsilon_t$, whatever $\dot{\varepsilon}_t$ is.

In order to show that *corollary 1* holds valid, it is necessary to plot the basic curves $t'_b / p'_e \times \varepsilon_t$. This can be done by dividing

both sides of Equation 73 by p'_e to obtain an expression for t'_b / p'_e, which is given by Equation 97 shown below:

$$t'_b / p'_e = \frac{\left(t' / p'_e - \mathbb{V} / p'_e\right)^2}{\left(s' / p'_e + t' / p'_e\right)}\left[1 + \frac{\sqrt{\left(s' / p'_e\right)^2 + \left(\mathbb{V} / p'_e\right)^2 - 2\mathbb{V}t' / p'^2_e}}{\left(t' / p'_e - \mathbb{V} / p'_e\right)}\right] \quad (97)$$

As $\mathbb{V} / p'_e = C_\eta\left(\dot{\varepsilon}_t\right)$, thus Equation 97 can be rewritten as:

$$t'_b / p'_e = \frac{\left(t' / p'_e - C_\eta\left(\dot{\varepsilon}_t\right)\right)^2}{\left(s' / p'_e + t' / p'_e\right)}\left\{1 + \frac{\sqrt{\left(s' / p'_e\right)^2 + \left[C_\eta\left(\dot{\varepsilon}_t\right)\right]^2 - 2\left(t' / p'_e\right)C_\eta\left(\dot{\varepsilon}_t\right)}}{\left(t' / p'_e - C_\eta\left(\dot{\varepsilon}_t\right)\right)}\right\} \quad (98)$$

Alternatively, t'_b / p'_e values can be more simply computed by applying Equation 72, dividing its both sides by p'_e to obtain an expression for t'_b / p'_e, given by Equation 99:

$$t'_b / p'_e = tan^2\phi'_{emob}\left(1 + csc\,\phi'_{emob}\right)\left(s' / p'_e - t' / p'_e\right) \quad (99)$$

Based on Lacerda's (1976) tests results, t'_b / p'_e values can be computed via Equation 98 and the normalized basic curve $t'_b / p'_e \times \dot{\varepsilon}_t$ can be plotted, as presented in Figure 60, which clearly shows the validity of *corollary 1.*

It will be shown next that normally consolidated specimens of San Francisco Bay Mud also fulfill *corollary 2*, whose statement is repeated below:

Corollary 2: ***$\overline{CIUCL}$ tests carried out on a normally consolidated clay showing homothetic ESPs for any fixed $\dot{\varepsilon}_t$ and a unique curve $\Delta u / p'_e \times \varepsilon_t$, regardless of $\dot{\varepsilon}_t$, will show a unique normalized basic effective stress path $\left(s'_b / p'_e, t'_b / p'_e\right)$, whatever $\dot{\varepsilon}_t$ is.***

In order to plot the normalized basic effective stress path for normally consolidated San Francisco Bay Mud, the ordered pairs $(s'_b / p'_e, t'_b / p'_e)$ might be obtained. (t'_b / p'_e) can be obtained by Equation 98 or 99. An expression for (s'_b / p'_e) can be obtained by dividing both sides of Equation 75 by p'_e to obtain Equation 100 shown below:

$$\frac{s'_b}{p'_e} = \left(\frac{s'}{p'_e} - \frac{t'}{p'_e}\right) + \frac{\left(\frac{t'}{p'_e} - \frac{\mathbb{V}}{p'_e}\right)^2}{\left(\frac{s'}{p'_e} + \frac{t'}{p'_e}\right)}\left[1 + \frac{\sqrt{\left(\frac{s'}{p'_e}\right)^2 + \left(\frac{\mathbb{V}}{p'_e}\right)^2 - \frac{2\mathbb{V}t'}{p'^2_e}}}{\left(\frac{t'}{p'_e} - \frac{\mathbb{V}}{p'_e}\right)}\right] \quad (100)$$

Replacing $\mathbb{V} / p'_e$ by $C_\eta\left(\dot{\varepsilon}_t\right)$ in Equation 100, Equation 101 is obtained:

$$\frac{s'_b}{p'_e} = \left(\frac{s'}{p'_e} - \frac{t'}{p'_e}\right) + \frac{\left(\frac{t'}{p'_e} - C_\eta\left(\dot{\varepsilon}_t\right)\right)^2}{\left(\frac{s'}{p'_e} + \frac{t'}{p'_e}\right)}\left[1 + \frac{\sqrt{\frac{s'^2}{p'^2_e} + \left[C_\eta\left(\dot{\varepsilon}_t\right)\right]^2 - 2\frac{t'}{p'_e}C_\eta\left(\dot{\varepsilon}_t\right)}}{\left(\frac{t'}{p'_e} - C_\eta\left(\dot{\varepsilon}_t\right)\right)}\right] \quad (101)$$

Still recalling that $s' / p'_e - t' / p'_e = s / p'_e - \Delta u / p'_e - t' / p'_e$ and that $s / p'_e - t' / p'_e = 1$, thus $\left(s' / p'_e - t' / p'_e\right) = 1 - \Delta u / p'_e$. Hence, a simple way of determining $\left(s'_b / p'_e\right)$ is given by Equation 102

$$\frac{s'_b}{p'_e} = 1 - \frac{\Delta u}{p'_e} + \frac{t'_b}{p'_e} \quad (102)$$

By plotting the ordered pairs $\left(s'_b / p'_e, t'_b / p'_e\right)$, one can then obtain the normalized basic effective stress path (bESPn), which is presented in Figure 61. Except for the points corresponding to the beginning of tests FP-13, FP-23, FP-32 and FP-42, which are not plotted in Figure 61 for being suspected of having been affected by bedding errors, as already discussed, all points of the remaining tests can be assumed as lying on a single line. This line is the bESPn (normalized basic effective stress path) for normally consolidated San Francisco Bay Mud. For being associated with the strain rate $\dot{\varepsilon}_t = 0$, the bESPn shown in Figure 61 only represents the mobilization of the frictional part of shear resistance.

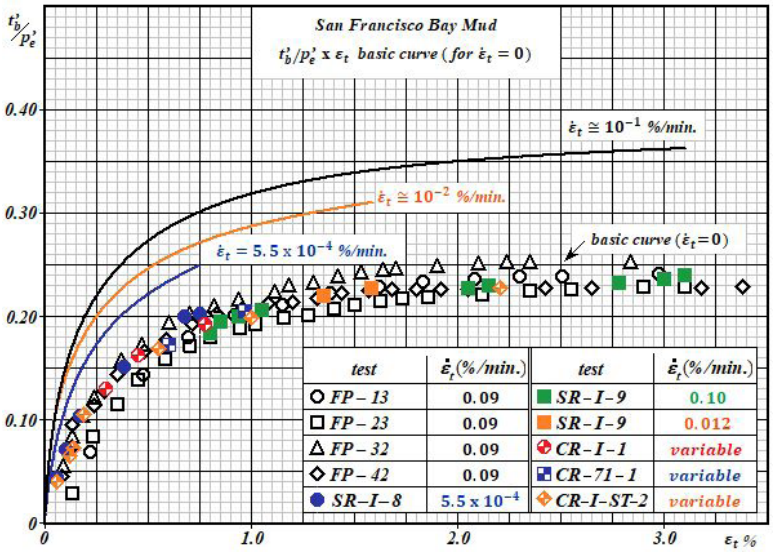

Figure 60. Normalized basic curve $t'_b / p'_e \times \varepsilon_t$ for normally consolidated specimens of San Francisco Bay Mud [data from Lacerda (1976)].

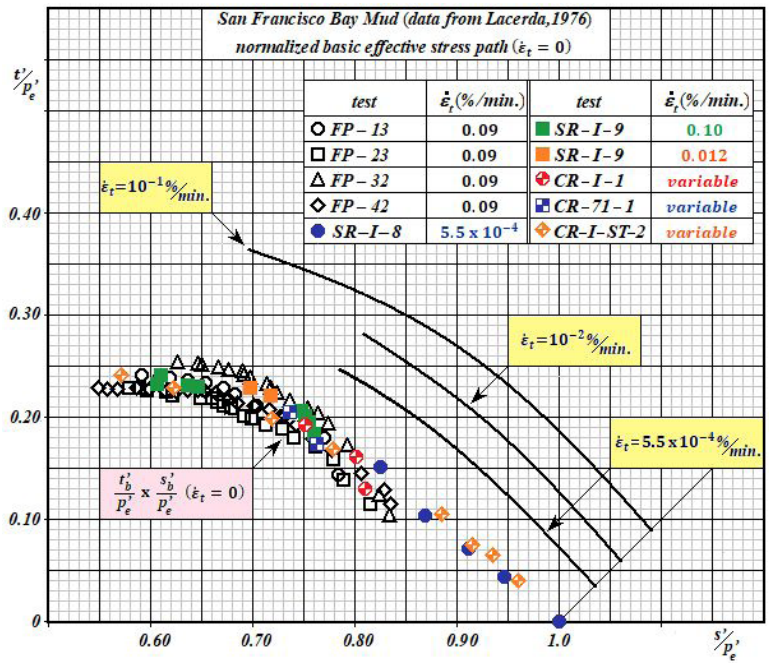

Figure 61. bESPn – normalized basic effective stress path $\left(\dot{\varepsilon}_t = 0\right)$ for normally consolidated San Francisco Bay Mud [data from Lacerda (1976)].

An interesting and remarkable aspect which should not escape from observation is that the ESPs shown in Figures 58 and 61 would represent Roscoe Surfaces sections, each one corresponding to a fixed shear strain rate $\dot{\varepsilon}_t$, as suggested by Leroueil et al. cited by Jamiolkowski et al. (1991).

Finally, it will be shown that normally consolidated San Francisco Bay Mud also satisfies *corollary 3*, whose statement is rewritten below.

Corollary 3: $\overline{CIUCL}$ ***tests carried out on a normally consolidated clay showing homothetic ESPs for any fixed*** $\dot{\varepsilon}_t$ ***and a unique curve*** $\Delta u / p'_e \times \varepsilon_t$***, regardless of*** $\dot{\varepsilon}_t$***, will show a unique curve*** $tan\,\phi'_{emob} \times \varepsilon_t$***, whatever*** $\dot{\varepsilon}_t$ ***is.***

Curve $tan\,\phi'_{emob} \times \varepsilon_t$ can be plotted taking s', t' and $\mathbb{V}$ values corresponding to each ε_t value and computing $tan\,\phi'_{emob}$ for each test, via Equation 56, reproduced below.

$$tan\,\phi'_{emob} = \frac{\left(\frac{\sigma'_1 - \sigma'_3}{2} - \mathbb{V}\right)}{\sqrt{\sigma'_1 \sigma'_3}} = \frac{\left(t' - \mathbb{V}\right)}{\sqrt{s'^2 - t'^2}} \tag{56}$$

$tan\,\phi'_{emob}$ values can also be determined rewriting Equation 56 in a normalized way relative to p'_e as

$$tan\,\phi'_{emob} = \frac{\left(\frac{t'}{p'_e} - \frac{\mathbb{V}}{p'_e}\right)}{\sqrt{\left(\frac{s'}{p'_e}\right)^2 - \left(\frac{t'}{p'_e}\right)^2}} = \frac{\frac{t'}{p'_e} - C_\eta\left(\dot{\varepsilon}_t\right)}{\sqrt{\left(\frac{s'}{p'_e}\right)^2 - \left(\frac{t'}{p'_e}\right)^2}} \tag{103}$$

Equation 103 can be potentially applied to each and every point of all tests presented in this article. However, only values of $C_\eta\left(\dot{\varepsilon}_t\right)$ for the shear strain rates $\dot{\varepsilon}_t$ equal to 5.5×10^{-4}% / min., 10^{-2}% / min. and 10^{-1}% / min. could be determined, which provided values of C_η equal to 0.035, 0.06 and 0.09, respectively. These values of C_η allowed the curves shown in Figure 62 to be drawn.

It can be observed from Figure 62 that, to fully mobilize the true angle of friction $\left(\phi'_e \cong 24°\right)$ of normally consolidated San Francisco Bay Mud in $\overline{\text{CIUCL}}$ tests type, it is necessary a shear strain at failure $\varepsilon_{tf} \cong 3\%$ corresponding to an axial strain at failure $\varepsilon_{af} \cong 4\%$.

9. Special undrained tests

9.1 Undrained creep tests

Undrained creep is meant in this article as the phenomenon by which a soil specimen is deformed over time when subjected to a constant state of total stress under undrained conditions.

The undrained creep studied in this article will be restricted to those cases where the specimens are of cylindrical shape, subjected to an axysimmetric state of stress, with the axial (vertical) total stress, denoted by σ_a, being the major principal stress and the radial (horizontal) total stress, denoted by σ_r, being the minor principal stress. The study will be also restricted to normally consolidated, saturated plastic clays with no cementation between grains.

To understand the undrained creep under the light of the concepts presented in this article and how it can be related to

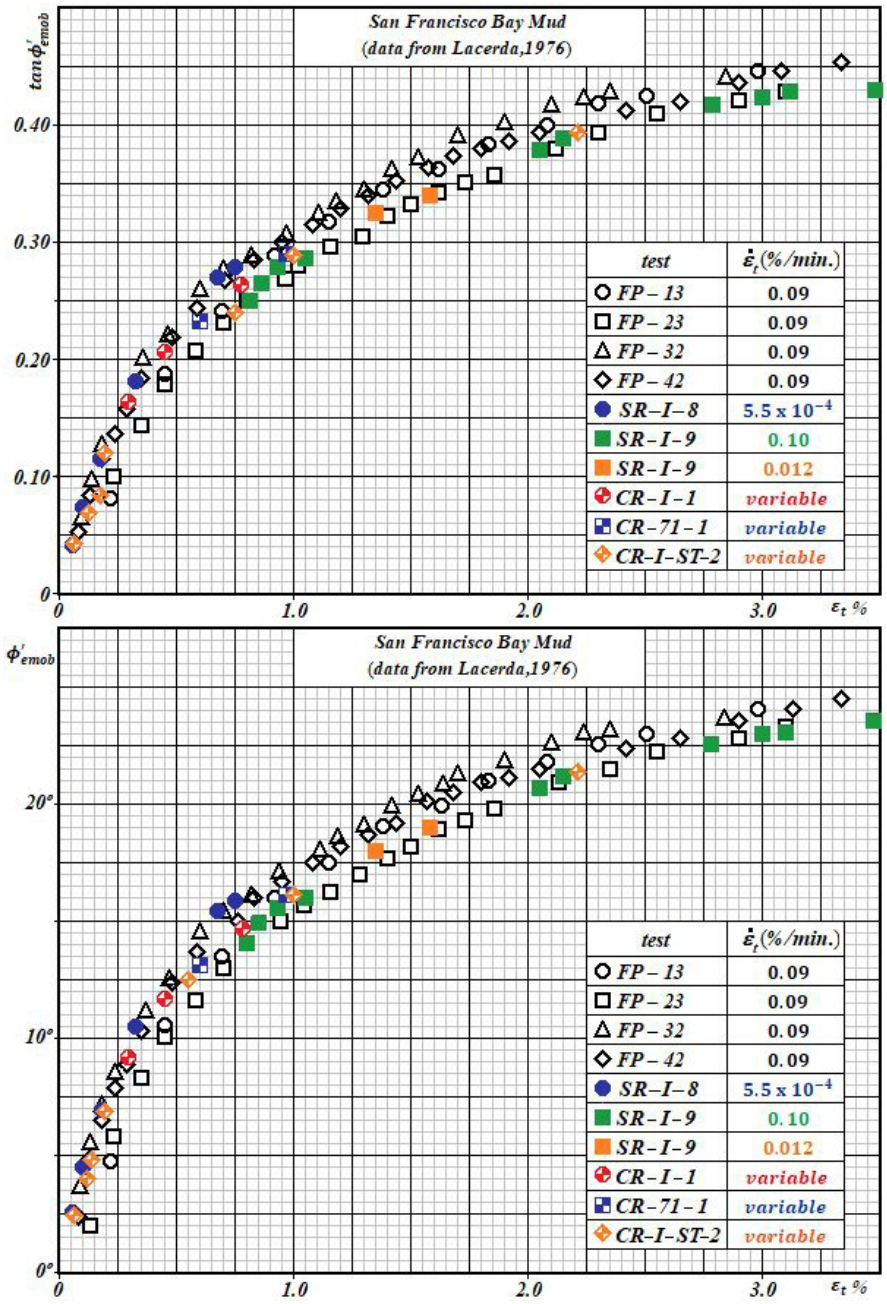

Figure 62. Curves $tan\,\phi'_{emob} \times \varepsilon_t$ and $\phi'_{emob} \times \varepsilon_t$ for normally consolidated San Francisco Bay Mud [data from Lacerda (1976)].

$\overline{\text{CIUCL}}$ tests, consider Figure 63. This figure shows several $\overline{\text{CIUCL}}$ ESPs, each one corresponding to a different shear strain rate $\dot{\varepsilon}_t$ as, for instance, ESP ***ABCDEFG*** associated with $\dot{\varepsilon}_t \quad \dot{\varepsilon}_{t1}$. Figure 63 also shows several 45º sloped straight lines, which, according to the *generalized complementary principle 1*, are the loci in which ε_t, $\left(\Delta u / p'_e\right)$ and $\tan\phi'_{emob}$ values are constant. As an example, for the straight line given by ***YFTL***, $\varepsilon_t = \varepsilon_{t4}$, $\Delta u\left(\boldsymbol{Y}\right) = \Delta u\left(\boldsymbol{F}\right) = \Delta u\left(\boldsymbol{T}\right) = \Delta u\left(\boldsymbol{L}\right)$ and $\tan\phi'_{emob}\left(\boldsymbol{Y}\right) = \tan\phi'_{emob}\left(\boldsymbol{F}\right) = \tan\phi'_{emob}\left(\boldsymbol{T}\right) = \tan\phi'_{emob}\left(\boldsymbol{L}\right)$.

During the undrained shear phase of a $\overline{\text{CIUCL}}$ test starting from point ***A*** in Figure 63 with a strain rate of $\dot{\varepsilon}_{t3}$, there is an instantaneous jump from point ***A*** to point ***H*** corresponding to the viscous resistance mobilization $\mathbb{V}\left(\boldsymbol{H}\right)$. At point ***H***, where $\varepsilon_t = 0$, shear strains start taking place and, consequently, frictional resistance begins to be mobilized and pore pressure generated. As soil deforms, the ESP to be followed is ***HIJKLM***. According to *corollary 3*, when point ***M*** is reached, the shear strain $\varepsilon_t = \varepsilon_{tf}$, corresponding to failure, and, therefore, $\phi'_{emob} = \phi'_e$.

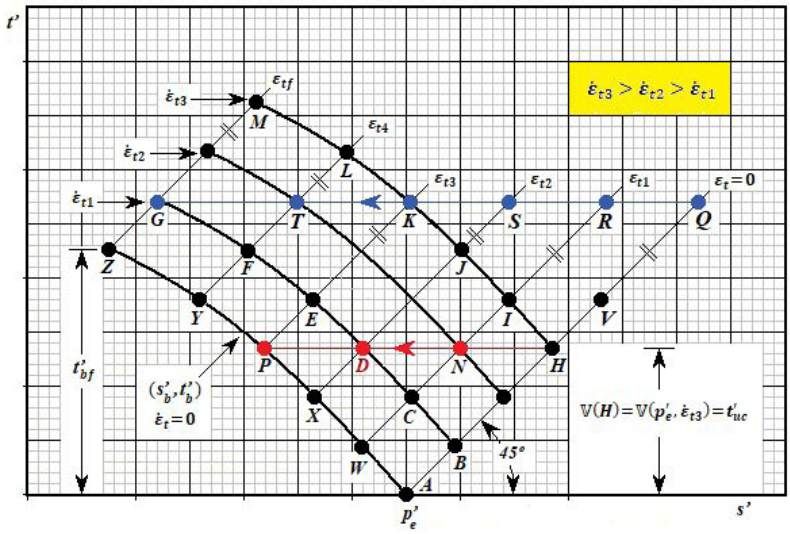

Figure 63. Effective stress paths during undrained creep tests.

Consider now another specimen from the same normally consolidated, saturated clay subjected to the same isotropic effective stress p'_e (point ***A*** in Figure 63). Such specimen will be subjected to an undrained creep test under $t' = t'_{uc}$ (subscript *uc* standing for undrained creep) corresponding to the ordinate of point ***H***, whose value will be kept constant throughout the whole test.

Immediately after applying t'_{uc}, the shear strain at $t = 0^+$ is still $\varepsilon_t = 0$, which means that there is no mobilization of frictional resistance yet, and hence the entire mobilized shear resistance is due to viscosity. Thus, at point ***H***, the shear stress $\tau_{45°} = t'_{uc} = \mathbb{V}(\boldsymbol{H}) = \mathbb{V}(p'_e, \dot{\varepsilon}_{t3})$. At $t = 0^+$, even with $\varepsilon_t = 0$, there is mobilization of viscous resistance, which means that $\dot{\varepsilon}_t \neq 0$ at point ***H***.

Turning on the load frame motor at the beginning of the undrained shear phase of a conventional $\overline{\text{CIUCL}}$ test, making the shear strain rate to be $\dot{\varepsilon}_{t3}$, mobilizes instantaneously the viscous resistance $\mathbb{V}(\boldsymbol{H}) = C_\eta(\dot{\varepsilon}_{t3})\, p'_e$. Conversely, if in an undrained creep test a $t'_{uc} = \mathbb{V}(\boldsymbol{H})$ is applied, the specimen will start to deform with a shear strain rate $\dot{\varepsilon}_t = \dot{\varepsilon}_{t3}$. This is due to the hypothesis that at any instant and on each and every plane given by α the shear stress τ_α is made up of the sum of two components: the frictional resistance component $\tau_{\phi\alpha}$ and the viscous resistance component $\tau_{\eta\alpha}$. As at point ***H*** the frictional resistance component $\tau_{\phi\alpha} = 0$ (since $\varepsilon_t = 0$), all the shear resistance must exclusively be assigned to the viscous component. Conversely, if the viscous resistance component $\tau_{\eta\alpha} = 0$, which occurs whenever $\dot{\varepsilon}_t = 0$, then the applied shear stress must entirely be resisted by friction.

Based on the above discussion, in the undrained creep test, after applying t'_{uc} as shown in Figure 63, the specimen begins to deform at point ***H*** with a shear strain rate $\dot{\varepsilon}_t = \dot{\varepsilon}_{t3}$ and the ESP to be followed is ***HNDP***. At point ***N***, where $\varepsilon_t = \varepsilon_{t1}$, there is some frictional resistance already mobilized. Considering that $t'_{uc} = \tau_{45°}$ is kept constant, the increasing mobilization of frictional resistance over time causes a decrease of equal magnitude in the mobilized viscous resistance, which in its turn is $\mathbb{V} = \eta(e) f(\dot{\varepsilon}_t)$. As the creep is undrained, $\eta(e) =$ constant. Therefore, if $\mathbb{V}$ decreases over time, so does $f(\dot{\varepsilon}_t)$, making $\dot{\varepsilon}_t$ decreases over time. Moreover, since ε_t increases over time, pore pressure Δu also increases.

It should be noted that, during undrained creep, the effective stress path ***HNDP*** crosses several ESPs from conventional $\overline{\text{CIUCL}}$ tests of decreasing strain rates, each ESP corresponding to a conventional $\overline{\text{CIUCL}}$ test carried out with $\dot{\varepsilon}_t =$ constant.

The process of transference from viscous shear resistance to frictional shear resistance continues until the ESP reaches point ***P*** on the basic ESP (see Figure 63). When point ***P*** is reached, the undrained creep comes to its end because all the viscous resistance will have been transferred to frictional resistance.

This process holds valid for each and every plane given by α. This happens because the diameter of the Mohr's circle of effective stress does not change during undrained creep. Therefore, for a fixed plane α, the shear stress τ_α, which is the sum of the viscous resistance component $(\tau_{\eta\alpha})$ and the frictional resistance component $(\tau_{\phi\alpha})$, is kept constant throughout the whole process.

The previous paragraph also leads to the following discussion: during undrained creep shown in Figure 63 the Mohr's circle of effective stress has a constant diameter equal to $2t'_{uc}$. At point ***H*** one has: $\mathbb{V}(\boldsymbol{H}) = \mathbb{V}(p'_e, \dot{\varepsilon}_{t3}) = \eta(e) f(\dot{\varepsilon}_{t3}) = t'_{uc}$, $\varepsilon_t = 0$, $\dot{\varepsilon}_t = \dot{\varepsilon}_{t3}$, $\Delta u = 0$ and the mobilized frictional resistance is equal to zero, whatever the plane may be. Thus, the viscosity ellipse and the Mohr's circle of effective stress coincide and

the friction ellipse collapses into the segment of magnitude $(\sigma'_a - \sigma'_r)$, as shown in Figure 64a.

At point ***N*** in Figures 63 and 64, the shear strain $\varepsilon_t = \varepsilon_{t1}$. Thus, according to *corollary 3*, there is some mobilized frictional resistance. This makes the mobilized viscous resistance $\mathbb{V}(\boldsymbol{N})$ to be lower than $\mathbb{V}(\boldsymbol{H})$. Thus, at point ***N***, $\varepsilon_t = \varepsilon_{t1}$, and $\dot{\varepsilon}_t = \dot{\varepsilon}_{t2} < \dot{\varepsilon}_{t3}$. Therefore, $\mathbb{V}(\boldsymbol{N}) = \eta(e) f(\dot{\varepsilon}_{t2})$ and $\Delta u(\boldsymbol{N}) = \boldsymbol{NH}$. In brief, as undrained creep goes on, the minor axis of the viscosity ellipse decreases, making the minor axis of the friction ellipse increases. This is what is shown in Figure 64b.

At point ***D*** in Figure 63, the shear strain $\varepsilon_t = \varepsilon_{t2}$. The shear strain rate $\dot{\varepsilon}_t = \dot{\varepsilon}_{t1} < \dot{\varepsilon}_{t2}$, $\mathbb{V}(\boldsymbol{D}) = \eta(e) f(\dot{\varepsilon}_{t1}) < \mathbb{V}(\boldsymbol{N})$ and the pore pressure $\Delta u(\boldsymbol{D}) = \boldsymbol{DH}$. At point ***D*** the minor axis of the viscosity ellipse becomes smaller than it was at point ***N***, whereas the minor axis of the friction ellipse at point ***D*** becomes larger than it was at point ***N***, as shown in Figure 64c.

Finally, at point ***P*** in Figure 63, $\varepsilon_t = \varepsilon_{t3}$ and $\dot{\varepsilon}_t = 0$, indicating that all viscous resistance has entirely been transferred to frictional resistance. Thus, at point ***P***, $\mathbb{V}(\boldsymbol{P}) = 0$ and the viscosity ellipse collapses into the segment of magnitude $(\sigma'_a - \sigma'_r)$. On the other hand, the friction ellipse becomes coincident to the Mohr's circle of effective stress as shown in Figure 64d and pore pressure magnitude is given by ***PH*** in Figure 63.

If another undrained creep test was carried out with a t' value corresponding to point ***V*** in Figure 63, the same mechanism of transference from viscous resistance to frictional resistance would take place. In this case, however, the ESP to be followed in Figure 63 would be ***VIEY*** and undrained creep would come to an end at point ***Y*** on the basic bESP. As t'_{uc} in this test would be higher than t'_{uc} corresponding to the test whose ESP is ***HNDP***, the shear strain ε_t at the end of undrained creep would be $\varepsilon_t = \varepsilon_{t4} > \varepsilon_{t3}$. The final excess pore pressure would be higher than that observed in the previous test, being represented by ***YV*** in Figure 63.

It is worth observing that, except for a particular but important feature to be discussed further, undrained creep phenomenon is analogous to isotropic consolidation. During isotropic consolidation, the state of total stress is kept constant and there is an increase in effective stress equal to the dissipation of the excess pore pressure along time. During undrained creep, the state of total stress is also kept constant and there is an increase in the mobilized frictional resistance equal to the decrease in the mobilized viscous resistance along time.

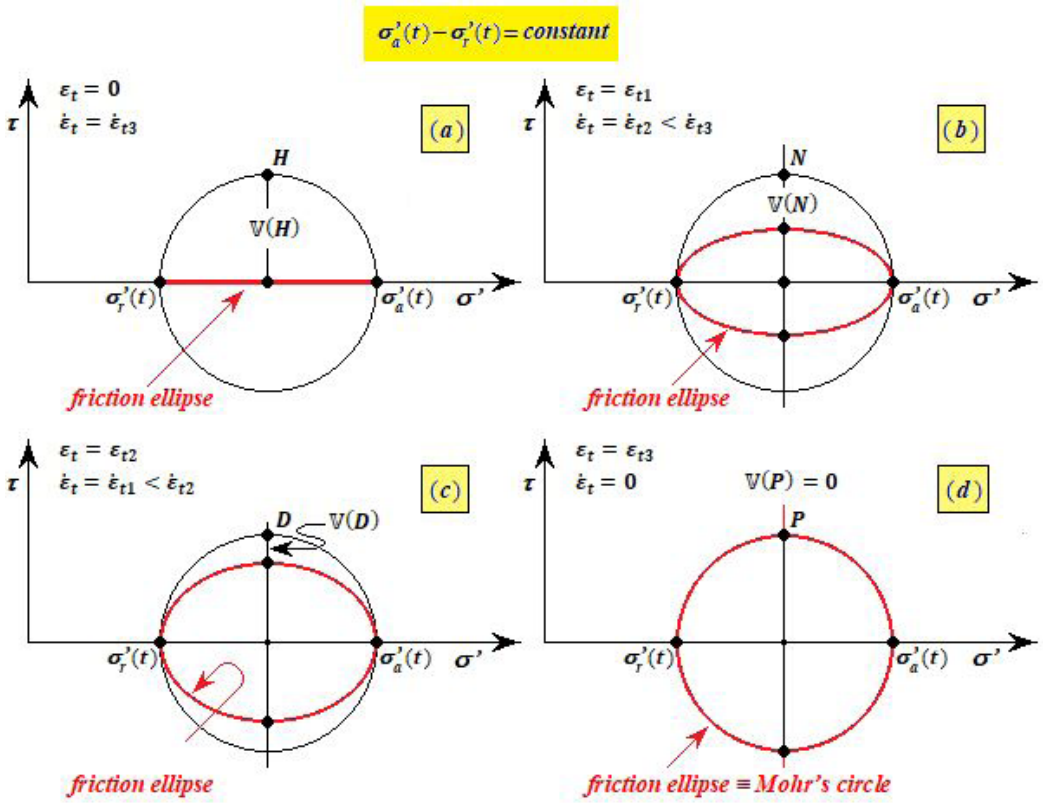

Figure 64. Mohr's circles of effective stress, friction elipses and mobilized states of friction during undrained creep ESP ***HNDP***. (a) At point ***H*** – no friction mobilized (b) Mobilized state of friction at point ***N*** (c) Mobilized state of friction at point ***D*** (d) At point ***P*** – friction fully mobilized.

The only feature that makes such analogy not be "perfect" is explained next. This explanation can be made going back to Figure 63 to analyse the undrained creep test carried out with a t'_{uc} value corresponding to the ordinate of point ***Q*** in Figure 63.

The ESP of an undrained creep test starting at point ***Q*** in Figure 63 is ***QRSKTG***. Such an ESP crosses several ESPs of conventional $\overline{\text{CIUCL}}$ tests of decreasing strain rates. Each ESP corresponds to a conventional $\overline{\text{CIUCL}}$ test carried out with a constant $\dot{\varepsilon}_t$. Such ESPs can be viewed as Roscoe's surfaces sections, each one associated with a given $\dot{\varepsilon}_t$. On its way from the right to the left an undrained creep ESP crosses several ESPs of decreasing $\dot{\varepsilon}_t$ values, transferring mobilized viscous resistance to mobilized frictional resistance until reaching point ***G***, whose shear strain is ε_{tf} and whose shear strain rate is $\dot{\varepsilon}_{t1}$. At point ***G***, all the available resistance provided by friction, given by t'_{bf}, has already been fully mobilized. However, the value of t'_{uc} applied is now $t'\left(\boldsymbol{Q}\right) > t'_{bf}$. Thus, in order to meet equilibrium conditions after reaching point ***G***, the specimen needs to make use of an additional resistance corresponding to the difference $t'\left(\boldsymbol{Q}\right) - t'_{bf}$. This difference is supplied by the mobilized viscous resistance given at point ***G*** by $\mathbb{V}\left(\boldsymbol{G}\right) = \eta\left(e\right) f\left(\dot{\varepsilon}_{t1}\right)$. However, to keep this viscous resistance active so that the equilibrium is satisfied, the specimen must continue to deform with a shear strain rate equal to $\dot{\varepsilon}_{t1}$, that is, shear strains will continue to take place indefinitely with a rate $\dot{\varepsilon}_{t1}$. This is the so-called undrained creep failure.

The undrained creep mechanism described above could be illustrated, without loss of generalization, replacing the axes s' and t' in Figure 63 by the axes s'/p'_e and t'/p'_e and plotting the normalized effective stress paths $(s'/p'_e) \times (t'/p'_e)$. Now, even without not being able to evaluate ε_t and $\dot{\varepsilon}_t$ along time, one can come to some conclusions of remarkable theoretical and practical importance concerning undrained creep. Such conclusions encompass the two cases listed below:

(a) $t'_{uc}/p'_e \leq t'_{bf}/p'_e$

(b) $t'_{uc}/p'_e > t'_{bf}/p'_e$

In case (a), if $\left(t'_{uc}/p'_e\right) < \left(t'_{bf}/p'_e\right)$, there will be no failure by creep. Shear strain ε_t will approach a definite value over time, shear strain rate will approach zero and creep will come to an end. The ε_t value at which creep will cease can be found entering the basic curve $t'_b/p'_e \times \varepsilon_t$ with the value $t'_b/p'_e = t'_{uc}/p'_e$, thus determining the ε_t value with which t'_{uc}/p'_e is associated.

In case (b), if $\left(t'_{uc}/p'_e\right) > \left(t'_{bf}/p'_e\right)$, there will be failure by undrained creep in a finite time period, no matter how long it takes. In this case, the higher the ratio $\left(t'_{uc}/p'_e\right)$, the shorter the time period to failure (and the higher the strain rate at failure). In this case, failure will occur as soon as $\varepsilon_t = \varepsilon_{tf}$ and the strain rate at failure can be predicted.

Before going on with the study of undrained creep, it is adequate to recall the excerpt from Taylor (1948, pp. 379-380), reproduced at the end of section 4, which reveals his ideas about the action of adsorbed water. Most of these ideas have inspired the author to develop the model presented in this article.

The undrained creep mechanism was also clearly depicted by Bjerrum (1973) in an excerpt of his classic state-of-the-art report, which is reproduced below to avoid loss of fidelity to the original:

> "*In general, in a natural clay an applied shear stress will be carried partly as cohesion in the semi-rigid water-film type contact points and partly as friction in contact points with mineral contact. However, as demonstrated by Schmertmann and Hall (1961), with time the effect of the interparticle creep will be a tendency to transfer loads from the cohesive to the more rigid and stable frictional contact points with the result that the mobilized cohesion decreases and a correspondingly greater part of the available friction becomes mobilized. As this process will lead to a reduction in shear stress in the cohesive contact points, the result is a reduction in the rate of failure of contact points, and thus in the rate of creep deformation. If the shear stress acting on the clay element is smaller than the available friction, the cohesive contact points will ultimately be relieved and the creep deformations will come to a halt. If the shear stresses exceed the available frictional resistance, the difference will have to be carried by the cohesive-type contact points. The rate of creep will therefore decrease until this condition is reached, and from then on it will remain constant*." (Bjerrum, 1973, p. 125).

With the reproduction of the above excerpts, there is no doubt that both Taylor (1948) and Bjerrum (1973) captured the mechanism the author tried to quantify in this article using the concept of viscous resistance, improperly called cohesion, as already discussed.

After discussing undrained creep and its consequences under the light of the model presented in section 7, one can now check its validity when applied to normally consolidated samples of San Francisco Bay Mud.

9.2 Undrained creep tests on normally consolidated San Francisco Bay Mud specimens

In order to check whether or not the proposed model applies to the undrained creep tests carried out on normally consolidated specimens of San Francisco Bay Mud, the following Lacerda's (1976) undrained creep tests listed in Table 2 are available: CR–I–1, CR–I–2, CR–71–1 and CR–I–ST–2.

According to section 9.1, in order to distinguish among the undrained creep tests listed above those that would fail from those in which creep would cease, one must know the t'_{bf}/p'_e value for normally consolidated San Francisco Bay

Mud as well as the t'_{uc} / p'_e value corresponding to each of the undrained creep tests to be analyzed.

Test CR–71–1 was interrupted after about 100 minutes. Therefore, the available data are so scarce that they are not useful. As test CR–I–2 specimen seemed to be slightly overconsolidated (with an $OCR \cong 1.3$), it has been decided not to include its data in the analyses presented in section 8. However, as test CR–I–2 lasted more than 10000 minutes and the specimen failed, it was decided to take it into account in this section due to the data scarcity concerning Lacerda's (1976) undrained creep tests. Due to such scarcity, to better analyze the model's ability in predicting soil behaviour during undrained creep, two additional tests carried out by Lacerda (1976) have been selected. Although these additional tests data are not entirely available in Lacerda's (1976) PhD thesis dissertation, the available data can provide valuable information to be considered in this section. Such additional tests, denoted by S–I–3 and CR–I–5, are both undrained creep tests.

It would also be interesting to analyze the step creep test CR–I–ST–2 carried out in seven steps. However, among these seven steps, only the last one is of interest for this section. So, it was decided to only make a brief comment about the last step of test CR–I–ST–2. The undrained creep tests to be analyzed will then be those whose data are summarized in Table 5.

In order to identify among the tests listed in Table 5 those that would fail and those in which creep would cease, one must compare their t'_{uc} / p'_e values with the t'_{bf} / p'_e value of normally consolidated San Francisco Bay Mud.

Based on Figures 61 and 63 and on what has been discussed in section 9.1, Figure 65 can be drawn showing the normalized ESPs corresponding to $\dot{\varepsilon}_t = 5.5\times10^{-4}\%/\text{min.}$, $\dot{\varepsilon}_t = 10^{-2}\%/\text{min.}$ and $\dot{\varepsilon}_t = 10^{-1}\%/\text{min.}$and the bESPn that corresponds to $\dot{\varepsilon}_t = 0$. Point $\boldsymbol{M}$ of coordinates $\left(s'_f / p'_e, t'_f / p'_e\right) = (0.70, 0.36)$, shown in Figure 65, corresponds to failure of $\overline{\text{CIUCL}}$ tests carried out with $\dot{\varepsilon}_t = 10^{-1}\%/\text{min.}$. Point $\boldsymbol{Z}$ coordinates $\left(s'_{bf} / p'_e, t'_{bf} / p'_e\right)$ can easily be computed. Firstly, one determines t'_{bf} / p'_e by entering Equation 99 with $\phi'_{emob} \cong 24°$ and with point $\boldsymbol{M}$ coordinates $(0.70,\ 0.36)$to obtain $t'_{bf} / p'_e = 0.24$ Then, by entering Equation 102 with $t'_{bf} / p'_e = 0.24$ and $\Delta u / p'_e$ corresponding to $\varepsilon_t = \varepsilon_{tf}$, one obtains $s'_{bf} / p'_e = 0.59$. Thus, point $\boldsymbol{Z}$ coordinates $\left(s'_{bf} / p'_e, t'_{bf} / p'_e\right) = (0.59, 0.24)$ correspond to failure of $\overline{\text{CIUCL}}$ tests "carried out" with $\dot{\varepsilon}_t = 0$. At points $\boldsymbol{M}$ and $\boldsymbol{Z}$, $\phi'_{emob} = \phi'_e = 24°$ and, according to *corollary 3*, the shear strain value $\left(\varepsilon_t\right)$ at both points is the same, corresponding to the shear strain at failure $\varepsilon_t = \varepsilon_{tf} = 3\%$. Besides, points $\boldsymbol{M}$ and $\boldsymbol{Z}$ lie on the same 45º sloped straight line. This 45º sloped straight line, defined by points $\boldsymbol{M}$ and $\boldsymbol{Z}$, is the locus of all points on the plane $\left(s' / p'_e\right)\times\left(t' / p'_e\right)$ representing failure of San Francisco Bay Mud normally consolidated specimens, subjected to $\overline{\text{CIUCL}}$ tests, irrespective of the shear strain rate $\dot{\varepsilon}_t$ applied during the test.

In order to analyze the tests listed in Table 5 under the light of the model presented in section 7, the t'_{uc} / p'_e value of each undrained creep test must be compared with the t'_{bf} / p'_e value of 0.24.

For test CR–I–1, $t'_{uc} / p'_e = 0.234$. In this case, according to the model, the undrained creep would cease. In order to evaluate the shear strain ε_t at which the creep is expected to cease, one should enter into the basic curve $t'_b / p'_e \times \varepsilon_t$ in Figure 60 with the value $t'_b / p'_e = t'_{uc} / p'_e = 0.234$, thus determining the ε_t value with which t'_{uc} / p'_e is associated. Following this procedure, an $\boldsymbol{\varepsilon_t}$ value from 2% to 3% is found. The $\varepsilon_t \times \dot{\varepsilon}_t$ plot corresponding to test CR–I–1 is shown in Figure 66. Such a test lasted about 20000 minutes, during which the shear strain rate $\dot{\varepsilon}_t$ decreased, reaching

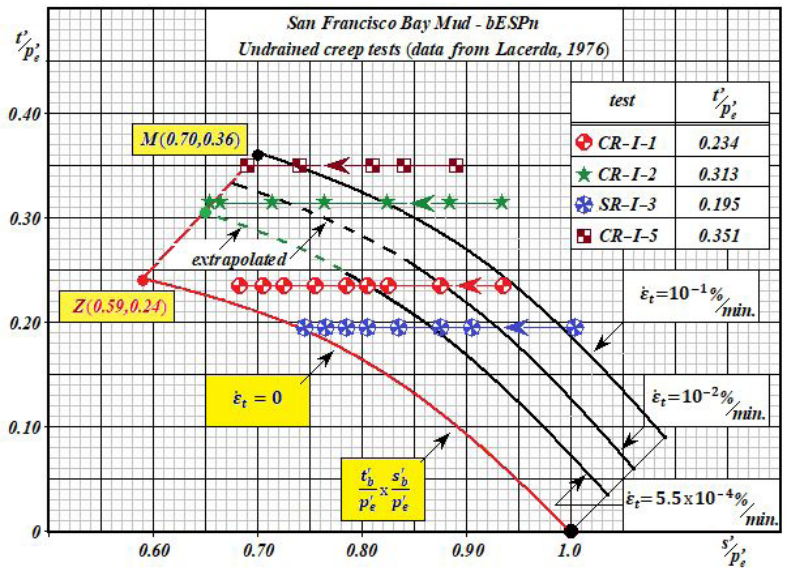

Figure 65. Normalized ESPs corresponding to different $\dot{\varepsilon}_t$ values and the normalized basic effective stress path (bESPn).

Table 5. Undrained creep tests on normally consolidated San Francisco Bay Mud carried out by Lacerda (1976), analyzed in this article.

Test	Stage	p'_e (kPa)	t'_{uc} (kPa)	t'_{uc} / p'_e
CR–I–1	unique	78.4	18.4	0.234
CR–I–2	unique	78.4	24.5	0.313
SR–I–3	unique	78.4	15.3	0.195
CR–I–5	unique	78.4	27.6	0.351

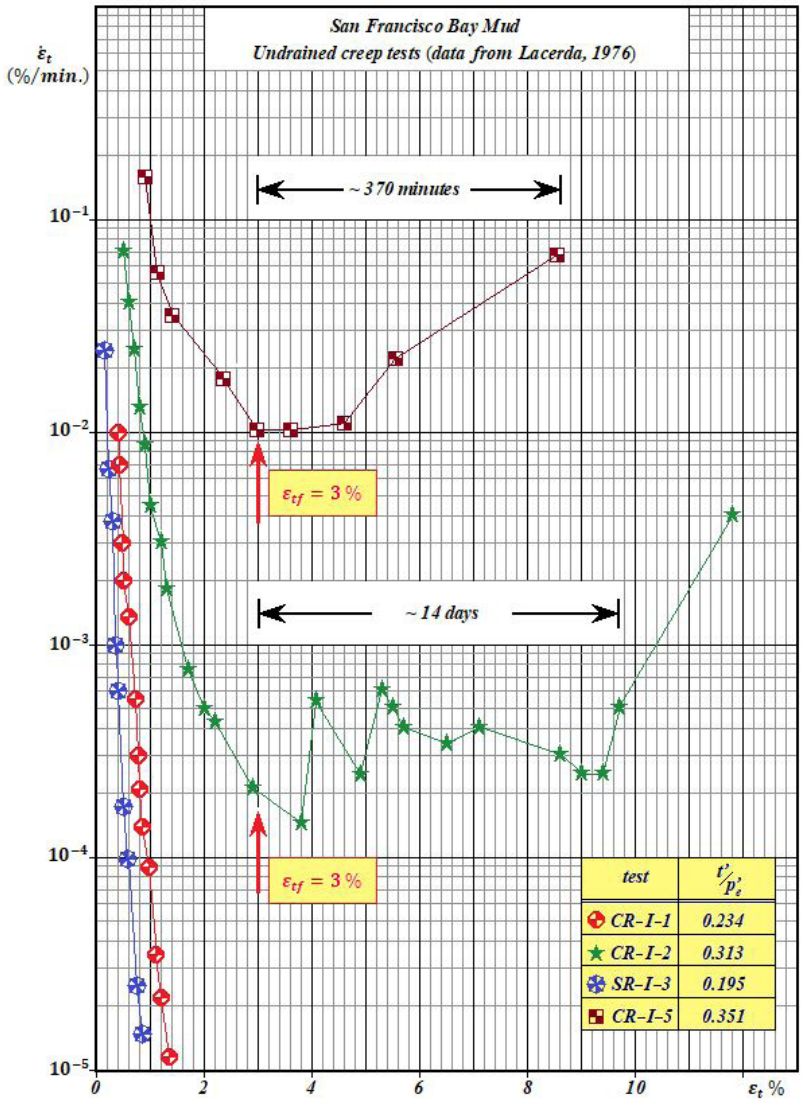

Figure 66. $\varepsilon_t \times \dot{\varepsilon}_t$ plots for undrained creep tests on normally consolidated San Francisco bay Mud specimens [data from Lacerda (1976)].

10^{-5}% / min., after which the test was ended. Such result is in agreement with the model predictions.

In test SR–I–3, $t'_{uc} / p'_e = 0.195$. In this case, since $t'_{uc} / p'_e < t'_{bf} / p'_e = 0.24$, undrained creep should also cease. By entering into the basic curve $t'_b / p'_e \times \varepsilon_t$ of Figure 60 with the value $t'_b / p'_e = t'_{uc} / p'_e = 0.195$, an $\varepsilon_t \cong 1\%$ is obtained. This is the expected value towards which ε_t should tend along time. The ε_t $\dot{\varepsilon}_t$ plot of test SR–I–3 is shown in Figure 66. Such a figure shows that $\dot{\varepsilon}_t$ decreases all test long. After about 10000 minutes, when $\dot{\varepsilon}_t = 1.4 \times 10^{-5}$% / min. and $_t = 0.87$ %, test SR–I–3 was finished. These results are also in agreement with the model predictions.

In test CR–I–2, $t'_{uc} / p'_e = 0.313$. Since $t'_{uc} / p'_e > t'_{bf} / p'_e = 0.24$, a failure by undrained creep should be expected. By making (by feeling) an extrapolation of the ESP corresponding to $\dot{\varepsilon}_t = 5.5 \times 10^{-4}\% / min.$ shown in Figure 65, one can estimate, for this $\dot{\varepsilon}_t$ value, a $t'_f / p'_e = 0.305$, which is very close to $t'_{uc} / p'_e = 0.313$ corresponding to test CR–I–2. Therefore, it is expected that failure occurs with a shear strain rate $\dot{\varepsilon}_t$ close to $5.5 \times 10^{-4}\%$ / min.. This is indeed the case observing the $\varepsilon_t \times \dot{\varepsilon}_t$ plot for test CR–I–2 in Figure 66. The shear strain rate continuously decreases up to $\varepsilon_t = 3.8\%$, reaching a minimum shear strain rate of $\dot{\varepsilon}_t = 1.5 \times 10^{-4}\%$ / min.. From then on, along 14 days, the specimen was deformed during failure, with a shear strain rate $2 \times 10^{-4}\% / \text{min.} \leq \dot{\varepsilon}_t \leq 6 \times 10^{-4}\% / \text{min.}$, with an average value of $3.4 \times 10^{-4}\%$ / min. In spite of making use of an extrapolation of the ESP corresponding to the shear strain rate $\dot{\varepsilon}_t = 5.5 \times 10^{-4}\%$ / min., the prediction is fairly good and illustrates the validity of the model.

A similar analysis can be carried out for test CR–I–5, whose value of $t'_{uc} / p'_e = 0.351$. Since $t'_{uc} / p'_e > t'_{bf} / p'_e$, a failure by undrained creep is also expected. However, as $t'_{uc} / p'_e = 0.351$, the shear strain rate at failure for test CR–I–5 is expected to be higher than that observed for test CR–I–2. By extrapolating (by feeling) the ESP corresponding to an $\dot{\varepsilon}_t = 1.0 \times 10^{-2}\% / min.$ in Figure 65, one can estimate, for this $\dot{\varepsilon}_t$ value, a $t'_f / p'_e \cong 0.33$. The value of $t'_{uc} / p'_e = 0.351$ is only 6% higher than 0.33. This suggests that for test CR–I–5 one can expect a shear strain rate at failure close to $10^{-2}\% / min.$. As shown in Figure 66, the $\varepsilon_t \times \dot{\varepsilon}_t$ plot corresponding to test CR–I–5 shows a decreasing shear strain rate up to $\varepsilon_t = 3.0$ %, when $\dot{\varepsilon}_t$ reaches a minimum value of 1.0×10^{-2} % / *min.*. From then on, strain rate increases with time, probably due to soil structure degradation, but this discussion is beyond the scope of this article.

A similar analysis could also be carried out for the last stage of the test CR–I–ST–2 (step creep test), for which $t'_{uc} / p'_e = 0.365$. In this case, according to Figure 65, failure would take place with a shear strain rate $\dot{\varepsilon}_t = 10^{-1}\%$ / min., which is ratified by Lacerda's (1976) data.

In summary, regarding undrained creep tests performed on normally consolidated specimens of San Francisco Bay Mud, the presented model is able to make the following predictions:

a) If $t'_{uc} / p'_e < t'_{bf} / p'_e$, undrained creep will cease. The ε_t value at which undrained creep will cease can be found by entering into the basic curve $t'_b / p'_e \times \varepsilon_t$ with the value $t'_b / p'_e = t'_{uc} / p'_e$, thus determining the ε_t value associated with t'_{uc} / p'_e.

b) If $t'_{uc} / p'_e > t'_{bf} / p'_e$, there will be failure by undrained creep as soon as ε_t reaches $\cong 3\%$ (which means that $\phi'_{emob} = \phi'_e$). In these cases, the shear strain rate at failure can be predicted.

Thus, the presented model has shown to be a powerful tool to make predictions concerning the behaviour of normally consolidated specimens of San Francisco Bay Mud when subjected to undrained creep.

9.3 Stress relaxation tests

In this article, undrained stress relaxation means the phenomenon in which a soil specimen is kept under a constant state of strain while the state of stress is observed over time.

The undrained stress relaxation tests studied in this article are restricted to those cases where specimens are of cylindrical shape, subjected to an axysimmetric state of stress, the axial (vertical) total stress, denoted by σ_a, being the major principal stress and the radial (horizontal) total stress, denoted by σ_r, the minor principal stress. The study is also restricted to normally consolidated, saturated plastic clays with no cementation between grains.

To understand undrained stress relaxation under the light of the concepts presented in this article and its connection with $\overline{\text{CIUCL}}$ tests, consider Figure 67.

Suppose that a $\overline{\text{CIUCL}}$ test will be carried out with a shear strain rate $\dot{\varepsilon}_t = \dot{\varepsilon}_{t3}$. The ESP to be followed in Figure 67 is ***AHIJKLM***. Initially, there will be a "viscosity jump" ***AH*** and from then on shear strains will become to occur. Failure will take place when the ESP reaches point ***M***.

Suppose now that the $\overline{\text{CIUCL}}$ test previously described will be repeated, except for a detail: at point ***I***, the load frame motor is turned off, starting a stress relaxation stage. From then on, what does the model predict?

Since the soil is saturated and the test is undrained, $\varepsilon_v = 0$. In addition, from the moment the load frame motor is switched off, $\dot{\varepsilon}_t = 0$. Thus, during an undrained stress relaxation stage shear strain does not change with time.

According to the model, since $\dot{\varepsilon}_t = 0$, the viscous resistance will vanish. Besides, since ε_t = constant, according to the *generalized complementary principle 1*, Δu and ϕ'_{emob} are expected to have constant values during undrained stress relaxation. As a consequence, the ESP to be followed during undrained stress relaxation is ***IQCW***, a 45º sloped straight line, as shown in Figure 67. Point ***W*** is expected to be the end of the stress relaxation effective stress path ***IQCW***, since at point ***W*** the specimen would already have got rid off all viscous resistance and would become to resist to the remaining shear stress only by friction.

If the load frame motor is turned on during a stress relaxation stage, the viscous resistance will instantaneously be reactivated and the $\overline{\text{CIUCL}}$ test will continue following the ESP associated with the shear strain rate $\dot{\varepsilon}_t$ applied. For instance: suppose that during the stress relaxation ***IQCW*** in Figure 67 the load frame motor is turned on again at point ***C***, with a shear strain rate $\dot{\varepsilon}_t = \dot{\varepsilon}_{t2}$. Thus, there will be an instantaneous jump, represented by ***CQ***, corresponding to the viscous resistance reactivation and the test will continue following the effective stress path ***QRSTV***.

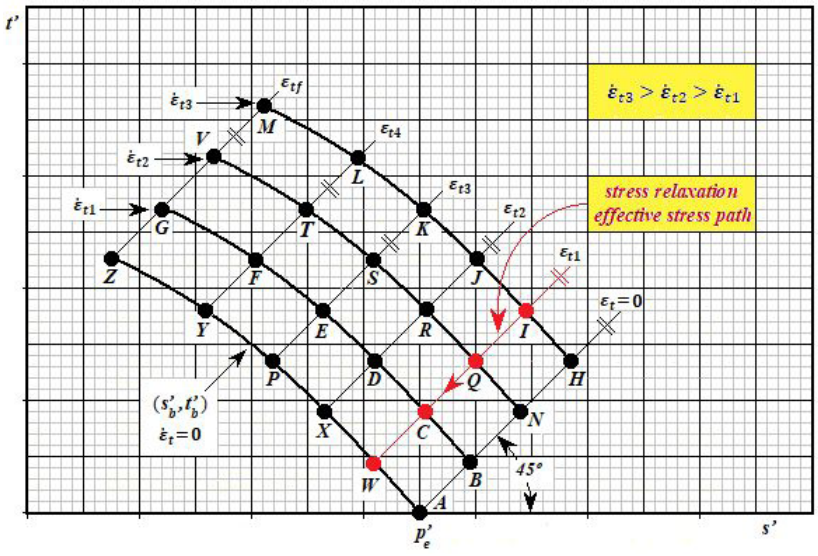

Figure 67. Effective stress paths for $\overline{\text{CIUCL}}$ tests with stress relaxation stages.

Table 6. Summary of data from stress relaxation tests carried out by Lacerda (1976) on normally consolidated specimens of San Francisco Bay Mud.

Test	Stress relaxation stage	s'/p'_e initial value	t'/p'_e initial value	s'/p'_e final value	t'/p'_e final value	Stage duration (minutes)
SR–I–5	1	1.00	0.278	0.850	0.075	3070
$p'_e = 78.4$ (kPa)	2	0.888	0.463	0.700	0.213	1320
	3	0.725	0.388	0.581	0.244	2700
	4	0.568	0.356	0.534	0.234	8370
SR–I–8	1	0.781	0.244	0.751	0.151	4530
$p'_e = 78.4$ (kPa)	2	0.830	0.400	0.741	0.201	1660
	3	0.819	0.444	0.612	0.237	365
	4	0.745	0.425	0.528	0.208	1000
SR–I–9	1	0.979	0.323	0.831	0.128	1250
$p'_e = 314$ (kPa)	2	0.844	0.313	0.775	0.173	1250
	3	0.758	0.303	0.712	0.196	1280
	4	0.764	0.347	0.671	0.249	100

However, if at point ***T*** the load frame motor is turned off again, another stress relaxation stage will start following the effective stress path ***TFY***.

9.4 Stress relaxation tests on normally consolidated San Francisco Bay Mud samples

To illustrate what was discussed in the previous section, three stress relaxation tests carried out by Lacerda (1976) on normally consolidated specimens of San Francisco Bay Mud will be presented. The main features of these tests, denoted by SR–I–5, SR–I–8 and SR–I–9, are summarized in Table 6.

What was presented in section 9.3 for the ESPs can be extended, without loss of generality, to the normalized ESPs $(s'/p'_e) \times (t'/p'_e)$. So, it is expected that normalized effective stress paths corresponding to stress relaxation stages are represented in a $(s'/p'_e) \times (t'/p'_e)$ plane by 45º sloped straight lines with descending direction.

Four stress relaxation stages have been carried out in each of the three tests listed in Table 6. The normalized ESPs for these stages are shown in Figure 68. These ESPs show that stress relaxation is also in agreement with the proposed model.

The discussions and experimental results presented in this article concerning undrained creep and undrained stress relaxation suggest that Taylor's and Bjerrum's ideas can be gathered in another general principle, which should be tested for other soils and which will be called *generalized*

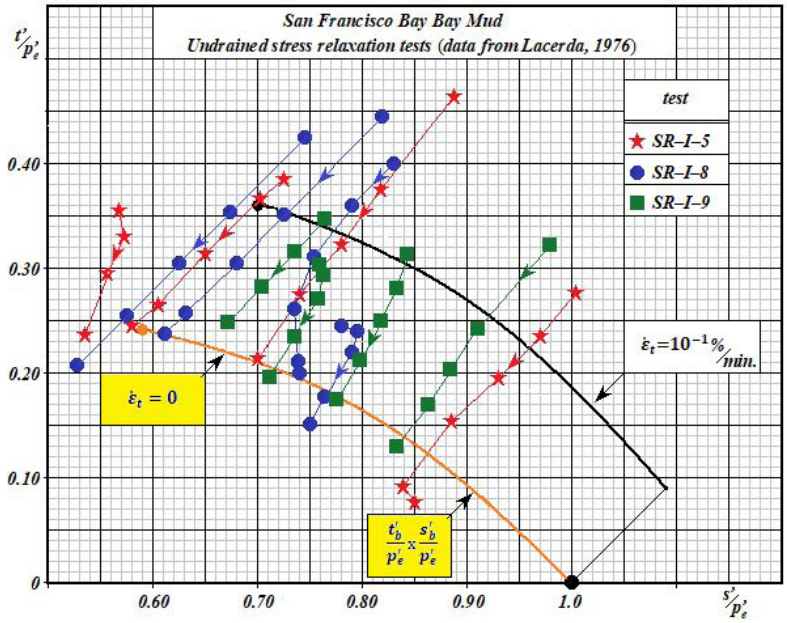

Figure 68. Normalized effective stress paths during stress relaxation stages for normally consolidated specimens of San Francisco Bay Mud [data from Lacerda (1976)].

complementary principle 2 or Taylor's and Bjerrum's law, whose statement is written below:

Generalized complementary principle 2 or Taylor's – Bjerrum's law

A normally consolidated plastic soil subjected to a given state of stress, in which the shear stresses are resisted partially by frictional resistance and partially by viscous resistance, will tend to get rid off the viscous resistance over time and will try to resist the remaining shear stresses only by friction.

In a clearer and more direct way, the *generalized complementary principle 2* states that a normally consolidated plastic soil under a normalized state of effective stresses given by $(s'/p'_e, t'/p'_e)$ will always move over time towards the normalized basic effective stress path $(s'_b/p'_e\ ,\ t'_b/p'_e)$, which is the Roscoe's surface for $\dot{\varepsilon}_t = 0$.

10. Summary and conclusions

What has been presented and discussed throughout the article can be summarized as listed below:

1. Phenomena that do not obey Terzaghi's principle of effective stress (PES) are related to strain rate and time effects (such as creep and stress relaxation).
2. The usual approach to deal with phenomena which do not obey the PES is to preserve the PES essence and develop tools to tackle each of these particular phenomena as being outside the PES validity domain. The approach followed in this article is different: the original PES is extended to encompass strain rate and time effects in such a way that these effects become natural consequences of the extended PES version. Concepts that allow such PES extension are presented in some classical texts from the beginning of soil mechanics.
3. The word "*cohesion*" has been used in soil mechanics with different meanings, bringing misunderstanding and conceptual confusion. Concerning earth natural materials, the term "cohesion" should be understood as a resistance coming from cementation between soil grains. This "*cohesion*" provides a tensile strength under tensile effective stress which makes the difference between rocks and soils.
4. The word "*cohesion*" is also often used to describe a sticky earthy material that is soft to the touch when moistened. Earth materials that show such a feature are also called "*cohesive soils*". To avoid misunderstanding, these materials would more properly be called plastic soils. For the sake of conceptual clearness and objectivity, the expression "*plastic soil*" should be used for all soils that present liquid and plastic limits.
5. When plastic soils are sheared, there is a component of shear resistance that comes from the action (distortion) of the highly viscous adsorbed water layers surrounding particles in contact. The closer the adsorbed water is to the particles surface, the higher its viscosity. Thus, it is expected that the lower the void ratio, the higher the shear resistance

component due to the action of the adsorbed water, which is of viscous nature.

6. Hvorslev (1960) showed it is possible to express the shear strength of a clay as: $\tau_{ff} = c_e(e) + \sigma'_{ff} \tan\phi'_e$, where $c_e(e)$ was called "*true cohesion*", a function of void ratio (e), and ϕ'_e a constant, called the true angle of internal friction. Since the soil tested by Hvorslev was a remoulded clay, it could have no cementation. Thus, the Hvorslev's "*true cohesion*" could not have the same nature of Coulomb's "*cohesion*". Hvorslev (1960) assumed that the "*true cohesion*" c_e of a saturated clay depends not only on void ratio but also on strain rate and clay structure.
7. Since normally consolidated, saturated clays have straight line strength envelopes passing through the origin in a $\sigma' \times \tau$ plot, they do not have "*cohesion*" in the sense used by Coulomb but they do have plasticity. In other words: normally consolidated clays do not have "*cohesion*" in the sense used by Coulomb but do have "*true cohesion*" in the sense used by Hvorslev. Furthermore, when normally consolidated specimens of a given clay, with the same void ratio, are subjected to undrained shear, the higher the strain rates, the higher their strengths. These features suggest that Hvorslev's "*true cohesion*" should more properly be called viscous resistance and expressed by the product of the coefficient of viscosity and a function of the shear strain rate.
8. The model presented herein assumes that, in plastic soils, the shear stress τ_α acting on a plane whose normal makes an angle α with the direction of σ_1 is expressed, at any instant, as the sum of a viscous resistance component $\tau_{\eta\alpha}$ and a frictional resistance component $\tau_{\phi\alpha}$, that is, $\tau_\alpha = \tau_{\phi\alpha} + \tau_{\eta\alpha}$.
9. $\tau_{\eta\alpha} = \eta(e) f\left[d(\varepsilon_1 - \varepsilon_3)/dt\right]\sin 2\alpha$, i.e. the viscous resistance component in a plane given by α is a function of the clay structure and of the product of the soil viscosity $\eta(e)$ by a function f of the distortion rate. Therefore, $\tau_{\eta\alpha}$ is similar to Hvorslev's true cohesion c_e (see conclusion 6).
10. Denoting by σ'_α the normal effective stress acting on the plane whose normal makes an angle with the direction of σ_1, the locus of the ordered pairs $(\sigma'_\alpha, \tau_{\eta\alpha})$ is the viscosity ellipse, whose centre has coordinates $\left[(\sigma'_1 + \sigma'_3)/2, 0\right]$ and whose major and minor axes are respectively $(\sigma'_1 - \sigma'_3)$ and $2\eta(e)d(\varepsilon_1 - \varepsilon_3)/dt = 2\mathbb{V}$.
11. $\tau_{\phi\alpha} = \sigma'_\alpha \tan\phi'_{mob\alpha}$ and thus $\tan\phi'_{mob\alpha} = (\tau_{\phi\alpha}/\sigma'_\alpha)$. The locus of the ordered pairs $(\sigma'_\alpha, \tau_{\phi\alpha})$ is the friction ellipse, whose centre has coordinates $\left[(\sigma'_1 + \sigma'_3)/2, 0\right]$ and whose major and minor axes are respectively $(\sigma'_1 - \sigma'_3)$ and $\left[(\sigma'_1 - \sigma'_3) - 2\mathbb{V}\right]$. (There is a difference between $\tan\phi'_{mob\alpha}$ and $\tan\phi'_{emob}$. For a fixed state of stress, $\tan\phi'_{mob\alpha} = (\tau_{\phi\alpha}/\sigma'_\alpha)$ and $\tan\phi'_{emob}$ is the maximum value of $\tan\phi'_{mob\alpha}$, i.e. maximum obliquity).
12. At any instant $\tan\phi'_{emob}$ can be computed by
$$\tan\phi'_{emob} = \frac{\left(\frac{\sigma'_1 - \sigma'_3}{2} - \mathbb{V}\right)}{\sqrt{\sigma'_1\sigma'_3}} = \frac{(t' - \mathbb{V})}{\sqrt{s'^2 - t'^2}}$$
13. The sum of the viscosity and friction ellipses gives the Mohr's circle of effective stress. The two ellipses cannot exist separately since only the Mohr's circle of stress satisfies equilibrium.
14. Since $\tau_{\eta\alpha} = \eta(e)\dot{\gamma}\sin 2\alpha$, for $\alpha = 45°$, $\tau_{\eta\alpha} = t'$. In the case of an ideal conventional CIUCL test, as soon as the load frame motor is switched on, the viscous resistance is fully mobilized instantaneously. Thus, the ESP shows an immediate "viscosity jump" along a 45º sloped straight line corresponding to a $t' = \mathbb{V}$. From then on, as there is neither volume change nor strain rate change, the viscous resistance remains constant throughout the shear phase. But since t' continues to increase as shear strain ε_t increases, this means the frictional resistance is mobilized throughout the shear phase, which leads to two remarkable conclusions: frictional resistance mobilization is associated to shear strain development and failure is governed by friction, i.e. when the available frictional resistance is totally mobilized, failure takes place.
15. Since failure is governed by friction mobilization, failure takes place whenever $\tan\phi'_{emob}$ reaches its maximum available value, which is $\tan\phi'_e$. Geometrically, this means that failure takes place when the friction ellipse touches the ϕ'_e sloped straight line passing through the origin.
16. To compute the undrained shear strength of a plastic soil, the viscous and frictional resistance components must be summed up. As the viscous resistance component depends on the shear strain rate, the greater the shear strain rate, the higher the viscous resistance component and, therefore, the higher the undrained strength.
17. CIUCL test results have been showing that the viscous resistance $\mathbb{V}$ is not a linear function of $\dot{\gamma}$. Thus, it should be rewritten as $\mathbb{V} = \eta(e) f(\dot{\gamma})$, where f is a non-linear function of $\dot{\gamma}$. On the other hand, for normally consolidated, saturated clays, $\mathbb{V}$ is a linear function of the isotropic consolidation stress p'_e, i.e. $\eta(e) f(\dot{\gamma}) = C_\eta(\dot{\gamma}) p'_e$.
18. In section 7.1 ten hypotheses are listed as the basis for the development of a behavioural model for normally consolidated, saturated clays. Part of these hypotheses comes from experimental evidence and part is working hypotheses of theoretical nature. In section 7.2 it was added another hypothesis that came from experimental evidence, which is: during

the undrained shear phase of $\overline{\text{CIUCL}}$ tests starting from the same p'_e, the pore-pressure Δu is the same regardless of the shear strain rate $\dot{\varepsilon}_t$. The set of these eleven hypotheses lead to the *complementary principle 1* which states that *points of intersection between a given 45° sloped straight line and* ESPs *starting from the same* p'_e *and corresponding to different shear strain rates* $\dot{\varepsilon}_t$ *have the same* ε_t, Δu and ϕ'_{emob}.

19. (s', t') are the coordinates of a point on the ESP of a $\overline{\text{CIUCL}}$ test carried out under a given p'_e and with an $\dot{\varepsilon}_t \neq 0$, whereas (s'_b, t'_b) are the coordinates of a point on the ESP of a idealized $\overline{\text{CIUCL}}$ test carried out under the same p'_e but with $\dot{\varepsilon}_t = 0$. Obviously, it is not possible to carry out a $\overline{\text{CIUCL}}$ test with $\dot{\varepsilon}_t = 0$, whose results would be free from the viscous resistance component. However, based on the *complementary principle 1*, it is possible to derive expressions relating s'_b to s' and t'_b to t', provided they correspond to the same ε_t. Then, for this fixed p'_e, one can plot the basic curves $\Delta u \times \varepsilon_t$, $t'_b \times \varepsilon_t$ and the basic effective stress path (s'_b, t'_b), which are all free from the viscous resistance component.
20. The $t' \times \varepsilon_t$ curves and the ESPs of $\overline{\text{CIUCL}}$ tests carried out with a fixed $\dot{\varepsilon}_t$ but under different values of isotropic consolidation stress p'_e on a given normally consolidated clay are similar. Thus, for a given $\dot{\varepsilon}_t$, there is a unique $(t' / p'_e) \times \varepsilon_t$ curve and a unique ESP on the plane $(s' / p'_e) \times (t' / p'_e)$. Although limited, the experimental evidence presented by Lacerda's (1976) test results show that the $\Delta u \times \varepsilon_t$ curves obtained from $\overline{\text{CIUCL}}$ tests carried out under different values of p'_e are similar, regardless of the $\dot{\varepsilon}_t$ value. Thus, the $(\Delta u / p'_e) \times \varepsilon_t$ plot can be represented by a unique curve regardless of the $\dot{\varepsilon}_t$ value. This means that the complementary principle 1 can be generalized to all p'_e values. Thus, it was renamed as the *generalized complementary principle 1: During undrained shear of* $\overline{\text{CIUCL}}$ *tests carried out on normally consolidated specimens of a given clay, points on the plane* $(s' / p'_e) \times (t' / p'_e)$ *corresponding to the intersections of any given 45° sloped straight line and the several ESPs, each one associated with a different* $\dot{\varepsilon}_t$ *value, will show the same values of* ε_t, $(\Delta u / p'_e)$, *and* $\tan\phi'_{emob}$, *whatever the shear strain rate* $\dot{\varepsilon}_t$ *may be.*
21. The *generalized complementary principle 1* leads to the three corollaries below:
    Corollary 1: $\overline{\text{CIUCL}}$ *tests carried out on a normally consolidated clay showing homothetic* ESPs *for any fixed* $\dot{\varepsilon}_t$ *and a unique curve* $\Delta u / p'_e \times \varepsilon_t$, *regardless of* $\dot{\varepsilon}_t$, *will show a unique basic curve* $t'_b / p'_e \times \varepsilon_t$, *whatever* $\dot{\varepsilon}_t$ *is.*
    Corollary 2: $\overline{\text{CIUCL}}$ *tests carried out on a normally consolidated clay showing homothetic* ESPs *for any fixed* $\dot{\varepsilon}_t$ *and a unique curve* $\Delta u / p'_e \times \varepsilon_t$, *regardless of* $\dot{\varepsilon}_t$, *will show a unique normalized basic effective stress path* $(s'_b / p'_e, t'_b / p'_e)$, *whatever* $\dot{\varepsilon}_t$ *is.*
    Corollary 3: $\overline{\text{CIUCL}}$ *tests carried out on a normally consolidated clay showing homothetic* ESPs *for any fixed* $\dot{\varepsilon}_t$ *and a unique curve* $\Delta u / p'_e \times \varepsilon_t$ *regardless of* $\dot{\varepsilon}_t$, *will show a unique curve* $\tan\phi'_{emob} \times \varepsilon_t$, *whatever* $\dot{\varepsilon}_t$ *is.*
22. The results from $\overline{\text{CIUCL}}$ tests carried out on normally consolidated specimens of San Francisco Bay Mud are in fair agreement with the *generalized complementary principle 1* (see Table 4) as well as with corollaries 1, 2 and 3. Although there is some scattering, considering that soil specimens were trimmed from natural undisturbed samples, it can be concluded that the experimental data follow the proposed model.
23. During undrained creep of a normally consolidated specimen compressed to p'_e, $t' / p'_e = t'_{uc} / p'_e =$ constant, where t'_{uc} corresponds to half of the deviator stress applied. As time goes by, shear strain increases, mobilizing frictional resistance and demobilizing viscous resistance, which makes the strain rate decreases over time. During the undrained creep process, the ESP crosses successive normalized ESPs of $\overline{\text{CIUCL}}$ tests corresponding to decreasing $\dot{\varepsilon}_t$ values (see Figures 63 and 65). Each of these normalized ESPs of $\overline{\text{CIUCL}}$ tests can be seen as a Roscoe's surface associated with a constant $\dot{\varepsilon}_t$, and the normalized basic effective stress path (bESPn) can be viewed as the Roscoe's surface corresponding to $\dot{\varepsilon}_t = 0$.
    Recalling that t'_{bf} / p'_e corresponds to the failure condition for $\dot{\varepsilon}_t = 0$, two cases may occur:
    (a) $t'_{uc} / p'_e \leq t'_{bf} / p'_e$
    (b) $t'_{uc} / p'_e > t'_{bf} / p'_e$
    In case *(a)*, there will be no failure by undrained creep. Shear strain ε_t will approach a definite value over time, shear strain rate will approach zero and creep will come to an end, at the normalized basic effective stress path (bESPn).
    In case *(b)*, there will be failure by undrained creep in a finite time, no matter how long it takes. In this case, the higher the ratio (t'_{uc} / p'_e), the shorter the time to failure and the higher the strain rate at failure. For normally consolidated San Francisco Bay Mud, $t'_{bf} / p'_e = 0.24$. Since for tests CR–I–1 and SR–I–3 the t'_{uc} / p'_e values were respectively 0.234 and 0.195, both tests belong to case *(a)* and, hence, there would be no undrained creep failure. This is suggested by the results obtained from both tests shown in Figure 66. On the other hand, since for tests CR–I–2 and CR–I–5 the t'_{uc} / p'_e values were respectively 0.313 and 0.351, both tests belong to case *(b)* and, thereby, there was failure by creep, as shown in Figure 66.

Although it has been applied to a few tests, the presented model has shown to be a powerful tool to make predictions concerning the behaviour of normally consolidated specimens of San Francisco Bay Mud when subjected to undrained creep.

24. During an undrained stress relaxation stage, $\varepsilon_v = 0, \dot{\varepsilon}_t = 0$ and thus $\varepsilon_t =$ constant. According to the presented model, since $\dot{\varepsilon}_t = 0$, the viscous resistance must vanish. Since ε_t = constant, according to the generalized complementary principle 1, Δu and ϕ'_{emob} are expected to keep constant values during undrained stress relaxation. Moreover, since the viscous resistance is demobilized (due to $\dot{\varepsilon}_t = 0$) and the mobilized frictional resistance remains constant (due to ε_t = constant), the deviator stress decreases. As a consequence, the ESP to be followed during the undrained stress relaxation is a downward 45º sloped straight line towards the bESPn, which would correspond to Roscoe's surface for $\dot{\varepsilon}_t = 0$. When the ESP touches the bESPn, the shear stress is free from its viscous component, the stress relaxation ceases and the remaining shear stress is exclusively of frictional nature.
The ESPs of the undrained stress relaxation stages carried out by Lacerda (1976), during $\overline{\text{CIUCL}}$ tests on normally consolidated specimens of San Francisco Bay Mud, show that undrained stress relaxation is also in agreement with the proposed model (see Figure 68).
25. The discussion and experimental results presented in this article concerning undrained creep and undrained stress relaxation suggest that Taylor's and Bjerrum's ideas can be gathered into another general principle (which deserves a deeper study) called *generalized complementary principle 2* or *Taylor's and Bjerrum's law*, whose formal statement is presented in section 9.4.
In a more direct way, the *generalized complementary principle 2* states that a normally consolidated plastic soil under a normalized state of effective stresses given by $(s'/p'_e, t'/p'_e)$ will always move over time towards the normalized basic effective stress path $(s'_b/p'_e\ ,\ t'_b/p'_e)$, which would be the Roscoe's surface for $\dot{\varepsilon}_t = 0$.

Acknowledgements

The author is indebted to Prof. Robson Palhas Saramago for his support in organizing the powerpoint slides, to Dr. Gustavo Santos Domingos for his help in improving the figures in the text, to Prof. Vitor Nascimento Aguiar for his contribution in reading the manuscripts and making valuable suggestions which made the article more readable, to Prof. Luiz Guilherme de Mello for his kindness in sharing with the author interesting aspects of Prof. Victor F. B. de Mello's life, which increased the author's motivation to do his best and to his wife Claudia for her support, patience and love.

Declaration of interest

The author has no conflicts of interest to declare. The author has observed and affirmed the contents of the paper and there is no financial interest to report.

Data availability

All experimental data referring to San Francisco Bay Mud examined in the course of the current study have come from Lacerda's PhD thesis research, the major part of which is available in his PhD thesis dissertation (Lacerda, 1976). Some part of these experimental data has directly been obtained from Lacerda in the form of raw data, which are not available in his PhD thesis dissertation.

List of symbols

bESP	Basic effective stress path
bESPn	Normalized basic effective stress path
c'	Cohesion
c_e	Hvorslev's true cohesion
e	Void ratio
h_0	Initial height of a triaxial specimen
r_0	Initial radius of triaxial specimen
q'_f	Deviator stress at failure
p'_e	Isotropic effective stress
p'_f	Octahedral stress at failure
s	$(\sigma_v + \sigma_h)/2$
s'	$(\sigma'_v + \sigma'_h)/2$
s'_b	Value of s' when $\dot{\varepsilon}_t = 0$
t	$(\sigma_v - \sigma_h)/2$ or time
t'	$(\sigma'_v - \sigma'_h)/2$
t'_b	Value of t' when $\dot{\varepsilon}_t = 0$
t'_{bf}	Value of t'_b at failure
t'_{uc}	Value of t' during undrained creep
u	Pore pressure
v	Specific volume $(v = 1 + e)$
w	Water content
w_L	Liquid limit
w_P	Plastic limit
bESP	Basic effective stress path
bESPn	Normalized basic effective stress path
C_c	Compression index
$\overline{\text{CIU}}$	Consolidated isotropically undrained triaxial test
$\overline{\text{CIUCL}}$	Consolidated isotropically undrained compression loading triaxial test
CSL	Critical state line
C_α	Coefficient of secondary consolidation

ESP	Effective stress path
G	Specific gravity
I_P	Plasticity index
K_0	Coefficient of earth pressure at rest
M	Slope of CSL projection on a $p' \times q'$ plane ($M = q'_f / p'_f$)
PES	Principle of effective stress
S_u	Undrained shear strength
TSP	Total stress path
VICL	Virgin isotropic compression line
γ	Distortion ($\varepsilon_a - \varepsilon_r$)
$\dot{\gamma}$	Distortion rate ($d\gamma / dt$)
ε_a	Axial (vertical) strain
ε_1	Major principal strain
ε_3	Minor principal strain
ε_r	Radial (horizontal) strain
ε_v	Volumetric strain
ε_t	Shear strain ($\varepsilon_t = \gamma / 2$)
$\dot{\varepsilon}_t$	Shear strain rate ($\dot{\varepsilon}_t = \dot{\gamma} / 2$)
$\dot{\varepsilon}_a$	Axial (vertical) strain rate $\left(d\varepsilon_a / dt\right)$
$\varepsilon_{l\alpha}$	Longitudinal strain of an element on the vertical plane of a triaxial specimen that makes an angle α with the direction of ε_1
$\varepsilon_{s\alpha}$	Shear strain on the vertical plane associated to the angle α
ϕ'	Angle of friction
ϕ'_e	Hvorslev's true angle of internal friction
$\phi'_{mob\alpha}$	$\tan^{-1}\left(\tau_{\phi\alpha} / \sigma'_\alpha\right)$
ϕ'_{emob}	$\tan^{-1}\left(\tau_{\phi\alpha} / \sigma'_\alpha\right)_{max}$
η	Viscosity of a plastic soil
μ	Newton's coefficient of viscosity or Bjerrum's vane test correction factor
σ	Normal total stress
σ'	Normal effective stress
σ_1	Major total principal stress
σ_2	Intermediate total principal stress
σ_3	Minor total principal stress
σ'_1	Major effective principal stress
σ'_2	Intermediate effective principal stress
σ'_3	Minor effective principal stress
σ_a	Total axial stress (equal to σ_1 in a $\overline{\text{CIUCL}}$ test)
σ'_e	Equivalent stress
σ_v	Total vertical stress (equal to σ_1 in a $\overline{\text{CIUCL}}$ test)
σ_r	Total radial stress (equal to $\sigma_2 = \sigma_3$ in a $\overline{\text{CIUCL}}$ test)
σ'_a	Effective axial stress (equal to σ'_1 in a $\overline{\text{CIUCL}}$ test)
σ'_{af}	Effective axial stress at failure
σ'_{ff}	Effective stress on failure plane at failure
σ'_i	Intrinsic pressure
σ'_{rf}	Effective radial stress at failure
σ'_t	Tensile effective stress
σ'_v	Effective vertical stress (equal to σ'_1 in a $\overline{\text{CIUCL}}$ test)
σ'_r	Effective radial stress (equal to $\sigma'_2 = \sigma'_3$ in a $\overline{\text{CIUCL}}$ test)
σ'_α	Effective stress on a plane whose normal makes an angle α with the direction of σ_1
τ	Shear stress
τ_{ff}	Shear stress on failure plane at failure
τ_α	Shear stress on a plane whose normal makes an angle α with the direction of σ_1
$\tau_{\eta\alpha}$	Viscous component of τ_α
$\tau_{\phi\alpha}$	Frictional component of τ_α
Δu	Excess pore pressure
$\mathbb{V}$	Viscous resistance on a plane whose normal makes 45º with the direction of σ_1

References

Aguiar, V.N. (2014). *Contribution to the study of the stress-stress-strength-time of soft clays* [Doctoral thesis, Federal University of Rio de Janeiro]. Federal University of Rio de Janeiro's repository (in Portuguese).

Andrade, M.E.A. (2014). *One-dimensional consolidation accounting for viscous resistance to compression* [Doctoral thesis, Federal University of Rio de Janeiro]. Federal University of Rio de Janeiro's repository (in Portuguese).

Atkinson, J.H., & Bransby, P.L. (1978). *The mechanics of soils – an introduction to critical state soil mechanics*. McGraw-Hill Book Company.

Berre, T., & Bjerrum, L. (August 6-11, 1973). Shear strength of normally consolidated clays. In Organizing Comittee of the ICSMFE (Ed.), *Proceedings of 8th International Conference on Soil Mechanics and Foundation Engineering* (Vol. 1, pp. 39-49). Moscow: ICSMFE.

Bishop, A.W., & Henkel, D.J. (1962). *The measurement of soil properties in the triaxial test*. London: Edward Arnold Ltd..

Bjerrum, L. (August 6-11, 1973). Problems of soil mechanics and construction on soft clays – State-of-the-Art report to session IV. In Organizing Comittee of the ICSMFE (Ed.), *Proceedings of 8th International Conference on Soil Mechanics and Foundation Engineering* (Vol. 3, pp. 111-159). Moscow: ICSMFE.

Burland, J.B. (1990). On the compressibility and shear strength of natural clays. *Geotechnique*, 40(3), 329-378. http://dx.doi.org/10.1680/geot.1990.40.3.329.

Burland, J.B. (2008). Reflections on Victor de Mello, Friend, Engineer and Philosopher. *Soils and Rocks,* 31(3), 111-123. https://doi.org/10.28927/sr.313111.

Carneiro, F.L.L.B., & Battista, R.C. (1975). *Mechanics of materials* [Lecture notes]. Retrieved in March-November, 1975, Lecture notes taken by Martins, I.S.M.

Christian, J.T., & Baecher, G.B. (2015). D.W. Taylor and the foundations of modern soil mechanics. *Journal of Geotechnical and Geoenvironmental Engineering*, 141(2), 02514001.

Costa, T. (2005) *Engineering of transparency – life and oeuvre of Lobo Carneiro*. COPPE/UFRJ (in Portuguese).

Danziger, F.A.B., Jannuzzi, G.F., & Martins, I.S.M. (2019). The relationship between sea-level change, soil formation and stress history of a very soft clay deposit. *AIMS Geosciences*, 5(3), 461-479. https://doi.org./10.3934/geosci.2019.3.461.

de Mello, V.F.B. (2014). *Geotechnics of subsoil and of earth and stone used as construction materials: Primordia, questions, updates*. Oficina de Textos. (unfinished book – in Portuguese).

de Mello, L.G. (2021). Personal communication.

Fonseca, A.P. (2000). *Compressibility and shear strength of a gully soil from Ouro Preto-MG* [Master's dissertation, Federal University of Rio de Janeiro]. Federal University of Rio de Janeiro's repository (in Portuguese).

Gibson, R.E. (August 16-27, 1953). Experimental determination of the true cohesion and true angle of internal friction in clays. In Organizing Comittee (Ed.), *Proceedings of the 3rd International Conference on Soil Mechanics and Foundation Engineering* (Vol. 1, pp. 126-130). Zurich.

Graham, J., Crooks, J.H.A., & Bell, A.L. (1983). Time effects on the stress-strain behavior of natural soft clays. *Geotechnique*, 33(3), 327-340. http://dx.doi.org/10.1680/geot.1983.33.3.327.

Holtz, R.D., & Jamiolkowski, M.B. (1985). Discussion of "Time dependence of lateral earth pressure". *Journal of Geotechnical Engineering*, 111(10), 1239-1242. http://dx.doi.org/10.1061/(ASCE)0733-9410(1985)111:10(1239).

Hvorslev, M.J. (1937). Über die festigkeitseigenschaften gestörter bindiger böden. Ingeniörvidenskabelige Skrifter.

Hvorslev, M.J. (June, 1960). Physical components of the shear strength of saturated clays. In American Society of Civil Engineers (Org.), *Research Conference on Shear Strength of Cohesive Soils* (pp. 169-273). Boulder, United States: University of Colorado.

Jamiolkowski, M. (2012). Role of Geophysical Testing in Geotechnical Site Characterization. *Soils and Rocks*, 35(2), 117-137. https://doi.org/10.28927/SR.352117.

Jamiolkowski, M., Leroueil, S., & Lo Presti D.C.F. (1991). Theme lecture: design parameters from theory to practice. In Coastal Development Institute of Technology (Ed.), *Procceedings of the International Conference on Geotechnical Engineering for Coastal Development* (Vol. 91, pp. 877-917). Yokohama: Geo-Coast.

Kavazanjian Junior, E., & Mitchell, J.K. (1984). Time dependence of lateral earth pressure. *Journal of Geotechnical Engineering*, 110(04), 530-533. http://dx.doi.org/10.1061/(ASCE)0733-9410(1984)110:4(530).

Kavazanjian Junior, E., & Mitchell, J.K. (1985). Closure to time dependence of lateral earth pressure. *Journal of Geotechnical Engineering*, 111(10), 1246-1248. http://dx.doi.org/10.1061/(ASCE)0733-9410(1985)111:10(1246).

Lacerda, W.A. (1976). *Stress-relaxation and creep effects on soil deformation* [PhD thesis dissertation]. University of California at Berkeley.

Lacerda, W.A. (1977). Discussion on the evaluation of K_0 during the drained creep in one-dimensional compression tests. In Publications Sub-Committee of the Organizing Comittee Organizing Comittee (Ed.), *Proceedings of the 8th International Conference on Soil Mechanics and Foundation Engineering* (Vol. 3, pp. 347-348). Tokyo.

Lacerda, W.A., & Houston, W.N. (1973). Stress relaxation in soils. In Organizing Committee (Ed.), *8th International Conference on Soil Mechanics and Foundation Engineering* (pp. 221-227). Moscow.

Lacerda, W.A., & Martins, I.S.M. (1985). Discussion of "Time dependence of lateral earth pressure". *Journal of Geotechnical Engineering*, 111(10), 1242-1244. http://dx.doi.org/10.1061/(ASCE)0733-9410(1985)111:10(1242).

Lambe, T.W. (1951). *Soil testing for engineers*. John Wiley & Sons.

Lambe, T.W. (1981). Geotechnical engineering at the Massachusetts Institute of Technology, 1925-1981. In Massachusetts Institute of Technology (Ed.), *Past, present and future of geotechnical engineering symposium*. (pp. 48-60). Massachusetts Institute of Technology.

Leonards, G.A. (1985) Discussion of "Time dependence of lateral earth pressure". *Journal of Geotechnical Engineering*, 111(10), 1244-1246. https://doi.org/10.1061/(ASCE)0733-9410(1985)111:10(1244).

Leroueil, S., Kabbaj, M., Tavenas, F., & Bouchard, R. (1985). Stress-strain-strain rate relation for the compressibility of sensitive natural clays. *Geotechnique*, 35(2), 159-180. http://dx.doi.org/10.1680/geot.1985.35.2.159.

Lira, E.N.S. (1988). *Automatic data acquisition system for triaxial tests* [Master's dissertation, Federal University of Rio de Janeiro]. Federal University of Rio de Janeiro's repository (in Portuguese).

Martins, I.S.M. (1983). *Sobre uma nova relação índice de vazios tensão em solos* [Master's dissertation, Federal University of Rio de Janeiro]. Federal University of Rio de Janeiro's repository (in Portuguese).

Martins, I.S.M. (1992). *Fundamentals for a model of saturated clay behaviour* [Doctoral thesis, Federal University of Rio de Janeiro]. Federal University of Rio de Janeiro's repository (in Portuguese).

Martins, I.S.M., & Lacerda, W.L. (1994). On the relationship void ratio – vertical effective stress in one-dimensional compression. *Soils & Rocks – Brazilian Journal of Geotechnics. ABMS, V.17, n.3, December, P.155-166. Brazilian Society for Soil Mechanics and Geotechnical Engineering* (in Portuguese).

Marzionna, J.D. (2014). *Foreword to Geotechnics of subsoil and of earth and stone used as construction materials: primordia, questions, updates* ABMS/Oficina de Textos (unfinished book) (in Portuguese).

Mesri, G., & Castro, A. (1987). C_α/C_c concept and K_0 during secondary compression. *Journal of Geotechnical Engineering*, 113(3), 230-247. http://dx.doi.org/10.1061/(ASCE)0733-9410(1987)113:3(230).

Mesri, G., & Castro, A. (1989). Closure to C_α/C_c concept and K_0 during secondary compression. *Journal of Geotechnical Engineering*, 115(2), 273-277. http://dx.doi.org/10.1061/(ASCE)0733-9410(1989)115:2(273).

Mesri, G., & Godlewski, P.M. (1977). Time and stress-compressibility interrelationship : Mesri, G; Godlewski, P M J Geotech Engng Div ASCE, V103, NGT5, 1977, P417–430. *International Journal of Rock Mechanics and Mining Sciences & Geomechanics Abstracts*, 14(4), 60. https://doi.org/10.1016/0148-9062(77)91005-1.

Moreira, J.E., & Décourt, L. (1989). Biographical notes. In V.F.B. De Mello (Ed.), *De Mello volume* (pp. XI-XV). Editora Edgar Blücher Ltda.

Rodriguez, T.T. (2005). *Pourpose of getechnical classification for brazilian colluvium* [Doctoral thesis, Federal University of Rio de Janeiro]. Federal University of Rio de Janeiro's repository (in Portuguese).

Rouse, H., & Howe, J.W. (1953). *Basic mechanics of fluids* (pp. 114-127). John Wiley & Sons.

Santa Maria, P.E.L. (2000). Personal communication.

Saramago, R.P. (2021). Personal communication.

Schmertmann, J.H. (1983). A simple question about consolidation. *Journal of Geotechnical Engineering*, 109(1), 119-122.

Schnaid, F., Martins, I.S.M., Delgado, B.G., & Odebrecht, E. (2021). Strain rates effects in the prediction of geotechnical parameters. *Geotecnia*, 152, 405-434 (in Portuguese). https://doi.org/10.14195/2184-8394_152_12.

Schofield, A.N. (1999). A note on Taylor's interlocking and Terzaghi's "true cohesion" error. *Geotechnical News*, 17(4), 1-6.

Schofield, A.N. (August 27-31, 2001). Re-appraisal of Terzaghi's soil mechanics. In C.S. Desai (Ed.), *Proceedings of the 15th International Conference on Soil Mechanics and Foundation Engineering* (Vol. 1, pp. 2473-2480). Istanbul.

Sheahan, T.C., Ladd, C.C., & Germaine, J.T. (1996). Rate-dependent undrained shear behavior of saturated clay. *Journal of Geotechnical Engineering*, 122(2), 99-108. http://dx.doi.org/10.1061/(ASCE)0733-9410(1996)122:2(99).

Tatsuoka, F., Ishihara, M., Di Benedetto, H., & Kuwano, R. (2002). Time-dependent shear deformation characteristics of geomaterials and their simulation. *Soil and Foundation*, 42(2), 103-129.

Taylor, D.W. (1942). *Research on consolidation of clays*. Massachusetts Institute of Technology/Department of Civil and Sanitary Engineering. Serial 82.

Taylor, D.W. (1948). *Fundamentals of soil mechanics*. John Wiley & Sons.

Taylor, D.W. (1955). *Review of research on shearing strength of clay – 1948 to 1953*. Vicksburg, Mississipi: Waterways Experiment Station.

Terzaghi, K. (1936). The shearing resistance of saturated soil and the angle between the planes of shear. In *Proceedings of the 1st International Conference on Soil Mechanics and Foundation Engineering* (Vol. 1, pp. 54-56). Cambridge, Massachussets: Harvard Printing Office.

Terzaghi, K. (1938). The Coulomb equation for the shear strength of cohesive soils. In *From theory to practice in soil mechanics – selections from the writings of Karl Terzaghi* (pp.174-180). John Wiley & Sons.

Terzaghi, K. (1941). Undisturbed clay samples and undisturbed clays. *Journal of the Boston Society of Civil Engineers*, 28(3), 45-65.

Terzaghi, K., & Frölich, O.K. (1936). *Théorie du tassement des couches argileuses*. Dunod.

Thomasi, L. (2000). *On the existence of a viscous component on the normal effective stress* [Master's dissertation, Federal University of Rio de Janeiro]. Federal University of Rio de Janeiro's repository (in Portuguese).